December 2019

Surface Alloying of Mild Steel During Casting Process: Microstructural Evolution, Phase Development and Heat Treatment

Kaustubh Kishore Rane
University of Wisconsin-Milwaukee

SURFACE ALLOYING OF MILD STEEL DURING CASTING PROCESS: MICROSTRUCTURAL EVOLUTION, PHASE DEVELOPMENT AND HEAT TREATMENT

by

Kaustubh Kishore Rane

A Thesis Submitted in

Partial Fulfillment of the

Requirements for the Degree of

Master of Science

in Engineering

at

The University of Wisconsin-Milwaukee

December 2019

ABSTRACT

SURFACE ALLOYING OF MILD STEEL DURING CASTING PROCESS: MICROSTRUCTURAL EVOLUTION, PHASE DEVELOPMENT AND HEAT TREATMENT

by

Kaustubh Kishore Rane

The University of Wisconsin-Milwaukee,2019
Under the Supervision of Professor Pradeep Rohatgi.

Casting is one of the oldest manufacturing processes in practice and the growth of casting industry through the ages has led to scientific leaps in the field of metallurgy. As we look into the history of metal castings, it is prominent that a steady growth in the knowledge leading to rise of newer casting techniques has caused an exponential increase in the way we can use metal castings to improve our lives. The surface alloying of mild steel to compositions targeted towards stainless steel compositions was performed in this study by sand casting process. Sand casting is one of the cheapest methods of production of components used in industries ranging for kitchen utensils, automobile to the water and piping industry. All of the industries require superior castings with a surface that would resist corrosion and wear and at the same time would be available at low production costs.

This study focuses on development of a surface alloying technique for WCB steel castings to impart superior properties on the outer surface. The gravity sand casting technique is explored in this study for in-situ surface alloying of WCB steel to a targeted composition that can be compared to that of stainless-steel alloys currently available in the industry specifically focusing on 316L stainless steel and 2205 duplex stainless steel (DSS). The process developed in this study focuses on improving the WCB steel.

The experiments were performed at Maynard Steel, Badger Alloys and the UWM Foundry Lab with samples and prototypes being cast using WCB steel as base metal and Ni, Cr, Fe-Mn, Fe-Si, and Mo being used as the surface alloying elements. REFCOHOL 1010 and REFCOBAR Gel were the binders used in this process for preparing the slurry which was applied to the mold cavity prior to casting for surface alloying of WCB steel. The objective of the study was to improve selected properties of the surface of cast WCB steel components as compared to the base metal. This was done by controlling the composition and quantities of the alloying elements used in the slurry. All samples and prototypes after sectioning showed clear formation of a surface alloyed layer ranging from 100 μm to 4000 μ in depth in all samples made at UWM, Maynard Steel and Badger Alloys. The surface alloyed layer has increased amounts of Ni, Cr and other elements depending up on the slurry applied on the mold prior to casting.

The samples showed an increase in the hardness of the surface alloyed layer as high as 54% as compared

to the base metal over the range of the four trials performed at three different locations. Austenite and ferrite were the primary phases identified in the surface alloyed layer using XRD. Pearlite colonies were observed at the interface between the surface alloyed layer and base metal. The formation of σ phase was observed at the grain boundaries in the surface alloyed layer which was rich in Cr. The depth of the surface alloyed layer was controlled in the samples which were cast at the UWM Foundry Lab and the highest depth of surface alloyed layer was 4000 μ.

Industrial trials of the surface alloying process to successfully cast surface alloyed butterfly valve prototypes proves the feasibility of the process on an industrial scale. The heat treatment of the surface alloyed layer by solution annealing at 1000 ˚C for 10 minutes led to dissolving of the σ phase, diffusion of carbon from the interface layer into the base metal, and promotion of a dual phase in the surface alloyed layer for samples with the targeted composition of 2205 DSS. The process leads to reduction of the overall costs of the components while imparting superior properties as compared to WCB steel.

To,

Seema Rane, Kishore Rane, and Pratiksha Rane

TABLE OF CONTENTS

LIST OF FIGURES

LIST OF TABLES

ACKNOWLEDGEMENTS

Through the period of the last five semesters, I am thankful to have the company of colleagues who have been a pleasure to work with and guidance of my advisor who ushered me into the world of metallurgical research to the point that this has become my life. The research experience I have gained during this period has been immensely helpful and has laid a strong foundation stone for my career in academia.

First and foremost, I would like to thank Dr. Rohatgi for my time at the University of Wisconsin - Milwaukee. I never would have thought that metallurgy would become my life and Dr. Rohatgi had a major role in making me fall in love with this field. The decision I made to attend this school back in Fall 2017 has paid off with great rewards. I want to acknowledge Water Equipment Policy I/UCRC for providing the funding necessary to execute the project over the period of my five semesters. The industrial expertise provided by the board of I/UCRC gave insights on what the industry demands and how lab research can be transferred to the industry. I want to acknowledge the department of mechanical engineering for appointing me as a TA which gave me experience in teaching.

Finally, I want to acknowledge the effort put in by the undergraduate students under the SURF program into this project. Swaroop and Justin were constant pillars I could lean on whenever there was as issue which required out of the box thinking as well as for winding down after a long day. Dr. Ajay Kumar has been a research influence during this period. Finally, I want to thank the faculty and staff at the University of Wisconsin-Milwaukee for making this one of the best times of my life.

Bhagavad Geeta 2.23

नैनं छिन्दन्ति शस्त्राणि नैनं दहति पावकः।
न चैनं क्लेदयन्त्यापो न शोषयति मारुतः॥

No weapon can cut the soul into pieces, nor can it be burned by fire,
nor moistened by water, nor withered by the wind.

Chapter 1

Introduction

he objective of this research is to surface alloy mild steel using alloying elements such as Ni, Cr, Fe-Mn, Fe-Si, and Mo during the casting process to impart superior surface properties thus eliminating the need for post-processing treatments such as nitriding or carburizing. Components used in applications involving constant exposure to the atmospheric conditions can cause degradation of the surface. This degradation can result in the corrosion of the sample or wear of the surface during its term of operation. This can be considered in the case of castings which are utilized in the water or pumping industry. Such components including pumps, butterfly valves, valve seats, faucets, and flanges that are cast tend to be cast of stainless steel on account of its corrosion resistant properties. The oxide layer formed on the surface of stainless steel leads to formation of a barrier between the environment and the sample surface (Davis et al., 1994).

Casting highly alloyed melt leads to components with superior properties as compared to mild-steel but this also leads to a significant rise in costs. The applications for which these components are generally cast for tend to require higher surface properties as compared to bulk properties. For example, in the case of butterfly valves, the surface coming in contact with water needs to be corrosion resistant as compared to the core of the valve. Thus, if the core is made of a different material and the outside provides sufficient corrosion resistant, the surface alloyed component would perform on a similar level as a stainless steel component. This can stand true for any application including conditions requiring high wear resistance or variable alloying compositions through the component.

The primary technique explored in this thesis is gravity sand casting as it is the preferred casting technique in foundries producing such components. As metal molds would cool the melt at a rate faster than required for the dissolution of the alloying powders into the surface, sand

molds provide the necessary surface texture to apply an alloying powder slurry and the rate of heat transfer is lower than that of metal molds. WCB steel is a mild-steel which does not have corrosion resistance or wear resistance as high as alloys such as 316L SS, 304 SS, 2205 DSS, 410L SS or 434L SS but it is cheaper when compared to the said alloys. By adding controlled quantities of alloying elements to the steel, an outer surface can be created which has higher corrosion resistance or wear resistance as compared to mild steel but the bulk of the material remains as WCB steel. This leads to savings in the manufacturing cost of the final component by reducing the cost of raw material and any other post processing techniques as well as allows for a variation in the surface chemistry depending on the application.

The focus of this research is to develop a technique which can be readily implemented in the casting industry. Discussions with industry partners Maynard Steel and Badger Alloys lead to the understanding that this process can help to reduce the cost of the final component by a margin of up to but not limited to 55% on average. The costs change depending on the bulk metal, alloying powders used and the post-processing treatments.

The study starts with discussing the currently available surface alloying techniques as well as having a prior look at the work done on this method. This is done to understand what currently is available and being practiced to produce a novelty out of the study. The components used in the slurry such as binder medium, alloying elements, application technique of the slurry and curing of the slurry is discussed further in the experimental section along with the metallographic preparation techniques. The study focuses on two sets of primary experiments which were conducted at the UWM Foundry Lab, quartz tube and open pour experiments. Quartz tube experiments took place under vacuum which prevented any oxidation of the melt as well as formation of an oxide layer on the sample during cooling. The samples were cast in sodium silicate bound sand molds provided by Maynard Steel. The open pour experiments were conducted to replicate the industrial pouring conditions as closely as possible. Though the melt size was approximately 1.5 lbs, the melt went through roughly the same conditions of facing issues such as oxidation and working through a sprue, runner and gate system.

Maynard Steel pours were large size pours wherein the sand cores provided by them were coated with the slurry and sent back for casting. The samples were heat treated by normalizing and tempering before being sent back. Badger Alloys sent the molds from their facility to the UWM Foundry Lab for slurry application. The slurry was applied and cured and the molds were shut-off before being returned to the facility. One heat was performed at Badger Alloys, conducted

for surface alloying butterfly valves which are used in the water equipment industry. The thesis focuses on butterfly valve samples only as the base metal was WCB steel.

Microstructural characterization is a critical aspect in the study of surface alloyed components. In the case of surface alloying as the base metal is poured over the alloying powders, the diffusion reaction will occur as in the case of producing a melt of alloyed steel on account of a steady cooling rate of the melt inside the mold cavity. Thus, as the base metal is solidifying, the alloying process is taking place in the mold surface. The carbon from the base metal would infiltrate the alloying surface leading to higher carbon content in the surface alloyed layer.

Phase formation would be altered as well on account of varied composition on the surface. Residual stresses are another aspect to be considered in the component. As the final component is composed of two separate alloys, the stresses which are developed in the crystals need to be quantified in the surface alloyed layer. Highly compressive or tensile stresses can cause damage to machinery during post-processing as well as lead to sample damage. The commonly used technique of center bore drilling is not explored in this study with the stresses being quantified by XRD. The primary reason being that the base metal would be penetrated by the drill as soon as the surface alloyed layer is drilled. This will lead to measurements being picked up from the base metal which is not required in this study. XRD eliminates this problem and acts as a non-destructive technique for measurements. There are portable XRD machines developed by Bruker which are finding use as residual stress testers in the field.

An increased wear resistance is one of the applications which can be implemented in mild steel using this technique. The quantification of hardness of the surface alloyed layer and its comparison with the base metal would provide an accurate perspective of the improvement in wear resistance. It has been previously reported that hardness and wear resistance can be related in some materials. The general trend shows an increase in wear resistance as hardness increases (Luyckx & Love, 2004). The hardness for these samples has been measured using Vicker's Microhardness test and Nanoindentation. The macrohardness tests such as Rockwell A, B, C or the Brinell hardness test would not accurately isolate and indent the surface alloyed layer thus impairing the readings. Microhardness and nanoindentation allows to mitigate that issue and indentation of particular phases in the microstructure.

The section on heat treatment discusses the various technique which are explored in this study. As mentioned above, the microstucture which is formed may not be the same as contemporary stainless steels and performing the same heat treatment cycles can lead to formation of

unwanted phases, intermetallics or carbides in the alloyed layer. Trials of currently defined heat treatment cycles test the applicability in the current samples. The goal for heat treatment cycles is to promote the growth of oxide layers and inhibit the formation of intermetallics σ and χ phases in the grain boundaries and avoid the formation of carbides.

The study is largely experimental with emphasis on casting samples, developing technique to control the depth of surface alloying and control the composition in the surface alloyed layer. Characterization of the surface alloyed layer was conducted extensively to understand the effects of varying quantities of alloying powders on the mechanical properties of the layer. A system has been developed to provide a method of developing a calculated quantity of slurry to obtain a certain depth of surface alloying. While the mechanics of that technique have not been investigated in this study, experimental analysis shows positive results which confirm that the depth of surface alloying can be controlled by measuring the quantity of alloying powders. The variation in the slurry composition has been covered over the range of samples extensively. This variation proves that the process can be applied to any number of compositional variations as long as the melting point of the alloying powders and the pouring temperature of the melt are in accordance with the desired alloy.

Chapter 2

Literature Review

2.1 Surface Alloying

One of the patents regarding the surface alloying of mild steel was filed in 1969 by the International Nickel Company. The process was developed to surface alloy gray iron, alloy cast iron, alloy ductile iron or ductile iron with Ni, Cr, Ni-Cu alloy powders, stainless steel powders and other nickel alloy powders. The process explores the use of methyl cellulose as a binding agent with a high quantity of water. The inventors utilized methyl cellulose on account of its capacity to suspend heavy metal particles for a longer periods of time (Macdonald, 1969). The process allowed for surface alloying of base metal but the drawbacks were in the curing time for the slurry as well as the need for slurry to be applied to a consumable pattern. This is one of the points addressed in the study with curing times reduced from 24 hours to 1 hour or less as well as removing the need for a consumable pattern. Another patent by Yoshiwara, et.al., utilizes high-density energy beam to surface alloy metal using localized melting. The energy beam with an intensity greater than 10^3 W/cm^2 is used on areas requiring alloying. The alloying element is added to the local region to form a surface alloyed area. While the technique can be used for selective alloying, the charges as well as preparation time for the sample and costs to run the machine can be higher as compared to the casting process (Yoshiwara & Kawanami, 1988). A prior attempt has been made at surface alloying of stainless steel by Elhamid, et.al., to increase the quantity of chromium in the surface layer by removing iron and then additionally nitriding or plasma nitriding the surface from which iron has been removed. This would lead to creation of a surface which has low iron and high chromium alloyed layer which is approximately in the range of 1 nm to 1 μm in thickness. The process is two fold with passivation being the primary

step to remove iron from the surface followed by nitriding to further enrich the surface. The inventors aimed to achieve 20% higher quantity of chromium in the surface alloyed layer as compared to the initial quantity of chromium (Elhamid & Dadheech, 2014).

Another patent discusses the technique of surface coating steel using zinc alloy plating layer, chromate plating layer and an organic coating to create a composite component surface to improve its corrosion resistance. While the process adds another layer to the base metal, the components will face issues regarding long term adhesion. The process of producing the composite surface is conducted using a form press (Suzuki et al., 1994). Revankar (Revankar, 1999) patented a technique for hard facing castings using wear resistant sheets. Though the term sheets has been used, it refers to application of a slurry of alloying powders and binder on a polystyrene pattern and left for curing to harden and form into a sheet. This sheet is then placed inside the mold cavity after which molten metal is poured. The metal of choice in this patent was ductile iron though it has been mentioned the process can be applied to other metals as well. An organic binder is used and the powders used are preferably wear resistant materials such as tungsten carbide, chromium carbide, etc. This layer of slurry and powders needs to be sintered to a high temperature and then placed in the mold cavity. While the process would lead to increased wear resistance, the time required to complete the coating as well as the high temperatures involved in sintering and requirement of resources such as high temperature adhesive can make the process tedious. This was one of the issues which was addressed in the research and the process was built in a way to be implemented into the casting industry without the need for a significant change in the production line.

Mazumder and Singh (Mazumder & Singh, 1986) conducted laser alloying and lase cladding of AISI 1016 using various mixtures of Ni, Mn and Cr as the alloying elements. The tests helped to produce samples wherein the quantity of Cr was 58% and the quantity of Ni was 26%, which is highly superior to that of cast stainless steel. Considering 316L SS, the weight percentage of chromium can be as high as 18% and nickel can be as high as 8%. A comparison between the two compositions makes it clear on how surface alloying can essentially help to improve the surface composition. Though it is not necessary to enrich the samples up to 58% Cr as a low concentration would be applicable in applications demanding an improved WCB as-cast component. Tomlinson and Bransden (Tomlinson & Bransden, 1990) laser surface alloyed grey cast iron with Cr, Ni, Co and Cr-Co. The concentration of alloying elements starts fairly low with what is approximately observed in regular stainless steels but attempts were made to enrich

the surface up to 40% Cr and 52% Ni. The high quantities of Ni and Cr would provide good properties to the surface but it may increase the cost of alloying the surface. It is necessary to identify the correct quantities of alloying elements necessary to provide the required properties but also maintain the economics of the process.

Surface enrichment by ball milling is an alternate technique used to improve the pitting corrosion resistance of stainless steel. 316L stainless steel are enriched with approximately 18% Cr which helps to prevent surface corrosion but the addition of Mo can help to prevent pitting corrosion as well (Jinlong, Tongxiang, & Chen, 2016). The process involved ball milling a plate of solution annealed plate of 316L stainless steel with Mo nanopowders. As in the case of 316L stainless steel, 304 stainless steel has also been previously laser alloyed with FeCoCrAlNi high-entropy alloy to improve its corrosion and cavitation erosion resistance. The process lead to formation of a surface alloyed layer up to 1 mm in depth after using alloying powders which formed approximately 500 μm to 600 μm of a coating on the 304 stainless steel coupon (Zhang, Wu, Zhang, Guan, & Tan, 2016). One of the important factors to observe is the low quantity of alloying powders required and the depth of surface alloying achieved. Depth control is an important factor in the process of surface alloying as it leads to optimization of the slurry composition as well as does not alter the entire bulk composition of the casting. In the process of metal casting, as the melt is continuously moving through the mold cavity on account of convection flow. This can lead to erosion of the dried slurry causing enriched pockets inside the melt or uneven alloying elements distribution.

Nicard, et.al., (Nicard, Allély, & Volovitch, 2019) used the hot dipping process on high strength steels with samples containing Al-Si coating and Zn and Mg as alloying elements. The process leads to a formation of a consistent coating but is a part of post-treatment. The surface alloying process during casting removes this excess step necessary for providing improved properties. Grey cast iron has been surface alloyed using laser alloying process with 75Ni25Cr composition alloying powder. The process lead to increase in the corrosion resistance in diluted H_2SO_4 and NaOH. A powder feeder distributed the alloying mixture as the laser continuously alloys the surface (Zhong, Liu, & Zhang, 2006). Surface melting of austempered ductile iron using TIG process and alloying with molybdenum and chromium as alloying elements leads to formation of a hardened alloyed layer. The alloyed layer was found to have reduced wear rate and increase in the hardness up to 3 times the original value of austempered ductile iron on account of formation of ledeburite structure in the alloyed layer (Amirsadeghi & Sohi, 2008).

Szajnar, et.al., created a composite with different properties by using a high carbon ferrochrome pad as an alloying mount. The molten cast steel was poured over the pad which lead to diffusion in the solid state leading to interstitital diffusion of carbon and crucial diffusion of chromium. This leads to formation of an alloyed layer enriched in chromium with a high content of carbon and a transition zone (Szajnar, Dulska, Wróbel, & Baron, 2015). Surface alloying of G25CrSiMnMoNi 4-4-4-2,5-4 was performed during the casting process with High speed steel HS 18-0-1. The reinforcement HS 18-0-1 was used as a plate for the enrichment process and not as a powder (Szajnar, Wróbel, & Wróbel, 2007). Ductile iron has been alloyed with ferrochromium powder having a concentration of 63% chromium using tungsten inert gas arc process. A layer of ferrochrome powder was applied on the ductile iron sample using sodium silicate as a binder followed by surface melting using the ITG. This lead to formation of martensites, transformed austenite, cementites, and ledeburites which are high in carbon content. The microhardness of ductile iron increased from 242 HV in as-cast stage to 816 HV with an upper limit of 1176 HV after the surface enrichment process (Sohi, Ebrahimi, Ghasemi, & Shahripour, 2012). Shielded metal arc welding was used to form a chromium enriched iron layer on top of 70% nodular graphite ductile iron using an E309L stainless steel electrode. The arc heating process lead to diffusion of carbon towards coating and chromium towards iron. Carbide formations were observed in the interface between the arc welded surface and the base metal and austenite was observed in XRD plots. The hardness peaked in the coating and was approximately 5 times the microhardness of the substrate. This increase in hardness helped to reduce the weight loss on account of wear in the sample (Shamanian, Abarghouie, & Pour, 2010). Tantalum has been used for enrichment of mild steel due to its affinity of forming carbides. Laser alloying process was used for surface enrichment wherein Ta powder was applied on the surface of mild steel using organic paint as binders. Martensite and austenite were the primary phases formed in the alloyed layer and the microhardness was the highest close to the surface reaching higher than 1700 HV. The wear resistance was found to be improving by increasing the power of the laser alloying beam (Radziszewska & Kusiński, 2008). Hot dip galvanizing was used for coating multiple grades of steel and ductile iron forming intermetallic Fe-Zn phases. It was found that the coating of zinc was maximum after 3 seconds of hot dipping while it becomes lowest at 6 seconds (Kopyciński & Guzik, 2007). Fuzuli and Agil surface alloyed white cast iron during the casting process using alloying powders on the mold to produce a CrNi80Si2B2 and LACrNi white cast iron coating on the cast iron surface. It was found that the infiltration of cast iron

with the alloying powders was affected by the superheating temperature of the melt as it allows for the melt to remain liquid for longer period of time thus facilitating dissolution. The microhardness of the sample increased by increasing the thickness of the alloying powder putty. The hardness peaked for a coating of 5 mm and decreased as the thickness increased while the wear was significantly reduced for alloyed samples. The corrosion rate also decreased significantly in the case of alloyed samples (Fuzuli & Agil, 2018).

2.2 Alloying Elements Properties

Sriram and Tromans studied that pitting corrosion of duplex stainless steels can be improved by the addition of nitrogen in the γ phase. It was concluded that the presence of Cr and Mo in the α phase leads to higher corrosion resistance than that of the γ phase containing low quantities of nitrogen but the corrosion resistance of γ phase can be increased by alloying nitrogen. The enrichment on account of nitrogen is due to the metal ions dissolving on the surface thus enriching the metal with nitrogen (Sriram & Tromans, 1989). Modifications to the 304 stainless steel composition specimens were made with Cr, Mo, Si, Mn, S and Ni content of the original composition. Macroscopic segregation absence was confirmed using spark spectroscopy and the samples were tested for their tensile strength. The addition of Ni, Si, Cr, and Mn lead to increase in the relative yield strength as compared with the reference while there was a decrease in the relative tensile strength, relative elongation to rupture, and relative reduction of area on addition of alloying elements (Martin, Weber, Theisen, Michler, & Naumann, 2011). Potentiodynamic tests and capacitance tests were performed on multiple alloyed steels with varying Cr, Ni, and Mo to study the effect of compositional variation on electrochemical properties of austenitic stainless steel in LiBr solution. The corrosion resistance of stainless steels was highest for high levels of Cr and Mo and Ni did not have any effect on the same (Fernández-Domene, Blasco-Tamarit, García-García, & García-Antón, 2014).

Ohkubo, et.al., studied the effects of C, N, and Mo on solid solution hardening while Si, Mn, Ni, Cr, and Cu were varied to study the effect of work hardening. The addition of Mo, Si, Cr, N, and C lead to an increase in the hardness of the alloy, addition of Si, Cr, Mo, N, and C lead to increase in the 0.2% proof stress and increase in Si, Cr, Mo, C, and N lead to an increase in the tensile strength of the alloy. It was also observed that flow stress increased as the cell size decreased which is in relation with the Hall-Petch relation on addition of C

and N (Ohkubo, Miyakusu, Uematsu, & Kimura, 1994). Townsend used the ASTM G101 corrosion test to analyze how the variation in elemental composition will lead to changes in the corrosion resistance. Sulfur has a highly detrimental effect on corrosion while phosphorous has a very low effect on the corrosion resistance. Copper is beneficial at lower compositions in steel. (Townsend, 2001). The elemental composition of centrifugally cast high speed steel was varied to study the changes in hardness and fracture toughness. The alloying elements formed multiple forms of carbides in the microstructure with the sample with lowest quantity of W_{eq} had the highest carbide percentage among the five variable samples while it was the highest for Ni-grain samples at 31.8%. The hardness peaked at the maximum of 756 HV while the fracture toughness was highest for Adamite at 67.3 Mpa$\sqrt{m}$ which also had the lowest hardness (Kim et al., 2005).

2.3 Phase Formation and Residual Stress Analysis

Residual stress measurements can be performed using multiple techniques such as x-ray diffraction, neutron diffraction, and center hole drilling technique. The hole drilling technique is defined as an ASTM E837-13a standard (ASTM, 2008). This method measures the changes in strain as the sample is drilled through the section. Depending on the fluctuations in the strain through the depth the stresses can be considered uniform or non-uniform. As the removal of material during drilling leads to relieving of strain in the sample, the residual stress can be quantified. Though the technique can be applied readily, its would not be applicable in case of surface alloyed samples. As the alloy system changes through the depth, the strain in the material would vary once the alloyed layer is penetrated and the drill starts relieving stresses from the base metal. A study by Rendler and Vigness (Rendler & Vigness, 1966) talks about the use of hole-drilling technique to determine the magnitude and the principal direction of residual stresses. The comparison between hole-drilling technique and XRD for measuring residual stresses revealed that the hold-drilling method would not be the most effective technique to measure surface residual stresses (Kolařík, Pala, Ganev, & Fojtik, 2014). As the samples have a surface alloyed layer with a maximum depth of 4000 μm, the residual stress need not be quantified in the bulk metal. Thus, XRD was utilized as the residual stress quantification technique on account of higher surface measurement accuracy and its non-destructive capability.

P. S Prevey detailed the techniques for measurement of residual stresses using XRD. A plane

stress elastic model was used for deriving a formula to measure the residual stress. Some of the techniques described in the previous literature include the single-angle technique, two-angle technique, the $\sin^2\psi$, the Marion-Cohen technique, and the full-tensor determination. As the x-ray radiation in case of ferrous alloys gets diffracted at a depth of 0.005 mm by a margin of 50%, the technique fits the application of surface alloying (Prevey et al., 1986). Asymmetric x-ray diffraction has been used to measure the residual stresses in epitaxial thin films and found that the theoretical stresses measured using differences in the thermal expansion coefficients are in accordance with the experimentally measured values (Uchida et al., 1999). A patent by Takano, et.al., was filed for the development of a 'rule' or 'scale' which is used to directly measure the residual stresses in samples. The process is highly manual and works with using α as the driving angle with plotting I vs 2θ as α is varied. The technique also requires the value of ψ under no stress conditions thus requiring the samples to undergo annealing to be stress free (Takano, Tsutsui, Kifune, & Miyoshi, 1971). An alternate technique is to quantify the residual stresses using finite element analysis by comparing plastic strains and nodal displacements (Metzger, New, & Dantzig, 2001). Cullity's work on x-ray diffraction talks about the strain gauge as being the spacing between the lattice planes. The work deals with using the spacing of a stressed and unstressed sample to measure the residual stresses in the sample. The technique requires the use of an unstressed sample which would lead to annealing of the sample. As the annealing is to be performed for the surface alloyed layer and not the base metal, the cycle is difficult to predict on account of variations in the composition. The equation for measuring the residual stresses is given as,

$$\sigma_{\mathrm{y}} = \frac{-E}{\nu}\left(\frac{d_{\mathrm{n}} - d_{\mathrm{o}}}{d_{\mathrm{o}}}\right) \tag{2.1}$$

Where,

$\mathrm{d_n}$ = Lattice plane spacing in stressed specimen

$\mathrm{d_o}$ = Lattice plane spacing in unstressed specimen

E = Young's Modulus of the specimen

ν = Poisson's Ratio of the specimen

There are two underlying conditions which have to be satisfied according to Cullity,

1. The specimen surface must lie on the diffractometer axis and remain there as ψ is changed.
2. The radial motion of the counter must be truly radial.

A rough sample surface should be avoided along with excess machining of the samples. This

machining can lead to generation of further macrostresses in the specimen. The deformation which is caused on account of grinding the sample would also lead to production of macrostresses which can be quantified by XRD but the technique may not reveal the true macrostresses in specimens that have been plastically deformed be tension, compression bending, rolling, or die drawing (Cullity & Stock, 2001).

LaFontaine, et.al., measured the stress relaxations occurring in aluminium metallizations during thermal relaxation cycles. The aluminium films deposited on oxide silicone substrates were measured using x-ray diffraction and continuous indentation test showed uniformity (LaFontaine, Paszkiet, Korhonen, & Li, 1991). While discussing the elastic constants required for measuring the residual stresses, Prevey found out that the use of incorrect elastic constants can lead to errors as high as 80% (Prevey, 1976). Surface treated Ti-6Al-4V was measured for compressive residual stresses generated during the laser shot peening process. The measurements were conducted using a mobile x-ray diffractometer and the Dolle-Haulk method was used for quantifying the residual stresses(Martinez, Sathish, Blodgett, & Shepard, 2003). Gaussian peak fitting x-ray diffraction data had been previously used by Korsunsky, et.al., for mapping strain in Al2124 alloy matrix composites. A reference sample without strain and a sample with strain were evaluated for calculating the strain in the samples (Korsunsky, Wells, & Withers, 1998). As the strain measurements are used for residual stress measurements, Gaussian peak fitting was used for analyzing the peak data of the samples.

2.4 Heat Treatment

The heat treatment of duplex stainless steels to improve its corrosion resistance was performed by solution treatment at 1150 °C for 15 minutes followed by aging at 900 °C for 2 minutes. The heat treatment did not give rise to sigma phase while the corrosion resistance increased as the aging temperature increased. The average value of hardness was observed to reduce over the increase in temperature of the heat treatment cycle (Hammood, Noor, & Alkhafagy, 2017). Another study performed over a range of primary cycle temperature from 1000 °C to 1200 °C followed by secondary heat treatment at 1200 °C for four hours gave rise to an austenitic microstructure in 316L stainless steels. There was an increase in the UTS and the yield strength of the samples after the first heat treatment cycle while the corrosion resistance increased after the second cycle after the formation of a completely austenitic phase. The reason for necessity

of development of the austenitic phase is to dissolve the σ phase which leads to regions without any Cr concentration leaving it open for aggravated corrosion (Chen, Li, Cheng, Wang, & Huang, 2018). Heat treatment of 2205 DSS was performed by inserting nano Nd2FeB14 by hot isostatic pressing. The forged 2205 DSS Samples underwent initial annealing 1050 °C for 30 minutes and then quenched in water which were then aged later at 475 °C for 64 hours. The aging lead to formation of spinodal nanostructure in the δ-ferrite. The final component post the treatment cycle had superior mechanical properties and increased impact energy (Gebril, n.d.). Kashivar, et.al., solution annealed 2205 DSS at 1050 °C and 1100 °C for 2 hours and then aged the samples in a muffle furnace at 700 °C for periods in the range of 15 minutes to 6 hours. It was found that the solution annealing temperature has an effect on the formation of σ or χ phases during the aging treatment with both phases being formed after high periods of aging (Kashiwar, Vennela, Kamath, & Khatirkar, 2012). As the formation intermetallics such as σ or χ phase can cause a detrimental effect on the properties of the surface alloyed layer, long term aging was not performed on the surface alloyed samples.

Selective Laser Melting has been used as a heat treatment technique for 316L stainless steel with cycles temperatures selected as 600 °C, 950 °C, and 1095 °C for a period of 2 hours. It was found that while the Vicker's hardness of the sample heat treated at 600 °C increased over the original sample, there was a decrease in the elongation of the sample. The opposite was observed for samples which were heat treated at higher temperatures in case of hardness and elongation (Montero Sistiaga, Nardone, Hautfenne, & Van Humbeeck, 2016). Tan, et.al., annealed 2205 DSS at multiple temperatures in the range of 1030 °C to 1200 °C for a period of 2 hours followed by water quenching. The annealing lead to a change in the microstructure of the samples with an approximate 50% ferrite 50% austenite phase being observed after 1080 °C of annealing. The balance of the two element enriched phases increases the corrosion resistance of the samples which decreases after increasing or decreasing the annealing temperature (Tan et al., 2009). Badji, et.al., annealed welded 2205 DSS for a period of 1 hour in the temperature range of 800 °C to 1200 °C and then quenched in water. The volume fraction of σ phase was highest after annealing at 850 °C while it was the lowest at 1050 °C. The impact energy peaked at 1050 °C and 1100 °C annealing treatment while the elongation peaked at 1050 °C (Badji et al., 2008). A 40 μm powder layer was deposited using selective lase melting to develop a martensitic structure using AISI 420 powder. While after annealing the steel contains carbides, this was not observed in laser melted microstructure. It was also observed that there was

partitioning and austenite reversion after selective laser melting as compared to quenching and partitioning heat treatment (Krakhmalev, Yadroitsava, Fredriksson, & Yadroitsev, 2015).

Sieurin, et.al., studied the effects of σ phase precipitation in 2205 DSS showing a comparison of time, temperature and volume fraction reporting that the volume fraction of σ phase increases when held at 850 °C for longer periods of time (Sieurin & Sandström, 2007). High temperature sensitization of 304L and 304LN at 675 °C for 1 hour and 24 hours respectively followed by low temperature sensitization at 500 °C for 11 hours. The treatments showed that 304LN is more resistant to 304L to sensitization and both alloys are prone to intergranular stress corrosion cracking. After low temperature sensitization, 304LN is more resistant to to intergranular stress corrosion cracking as compared to 304L. The mechanical properties did not change on account of the sensitization treatment and nitrogen helps in improving the stress corrosion cracking resistance up to 0.16% (Bali, Kain, & Raja, 2009).

Chapter 3

Experimental Procedure

3.1 Casting of Samples

The three sets of samples used in this study have been cast at:

1. UWM Foundry Lab
2. Maynard Steel
3. Badger Alloys

All the samples had a variation in their alloying element chemistry but the target was to achieve a chemistry of the surface alloyed layer as close as possible to a current grade of stainless steel. Two of the most important objectives of this study were to improve the wear resistance and corrosion resistance of the surface alloyed samples. Corrosion resistance is heavily dependent on the heat treatment performed after casting and this will be further discussed in section 3.5. The chemical composition of WCB steel, 316L SS and 2205 DSS are mentioned in tables 3.1, 3.2, and 3.3 respectively.

Element	C	Mn	P	S	Si	Fe
Weight %	0.3 Max	1	0.04	0.045	0.6	Balance

Table 3.1: Chemical composition of WCB Steel.

Element	Cr	Ni	C	Mn	P	S	Si	Mo	Fe
Weight %	16-18	10-14	0.03	2.00	0.045	0.03	1	2-3	Balance

Table 3.2: Chemical composition of 316L Stainless Steel.

Element	Cr	Ni	C	Mn	P	S	Si	Mo	Fe
Weight %	22-23	4.5-6.5	0.03	2.00	0.03	0.02	1	3-3.5	Balance

Table 3.3: Chemical composition of 2205 Super Duplex Stainless Steel.

Wear resistance can be directly correlated to the hardness of a material with higher hardness implying improved wear resistance. Ni is a good solid-solution strengthener and is used along with Cr in stainless steels such as 316L and 2205 DSS. Cr is used to create a passivation layer of Cr_2O_3 in stainless steels. Cr is also an austenite stabilizer and is required to achieve dual-phase structure in 2205 DSS. As previous literature suggests, stainless steel has better corrosion and wear resistance as compared to mild steel and hence, 316L SS and 2205 DSS were the alloy compositions targeted in the surface alloyed layer.

The casting technique used was gravity sand casting with the molds being made out of no-bake sand. UWM Foundry Lab 3D printed the patterns with a PLA polymer and the castings made were 1-1.5 lbs. The model of the pattern is shown in figures 3.1 and 3.2. The experiments were aimed at understanding the effect of various alloying elements before conducting industrial sized experiments. Quartz sand in a three part mixture were used to make the cope and drag sections of the mold. Sprue, sprue basin, runners, gates, risers and pouring basin were all designed into the CAD model of the pattern and simulated in SolidCAST. Degassing vents were drilled into the cope of the mold to ensure there was enough permeability and to help release the gases released during casting.

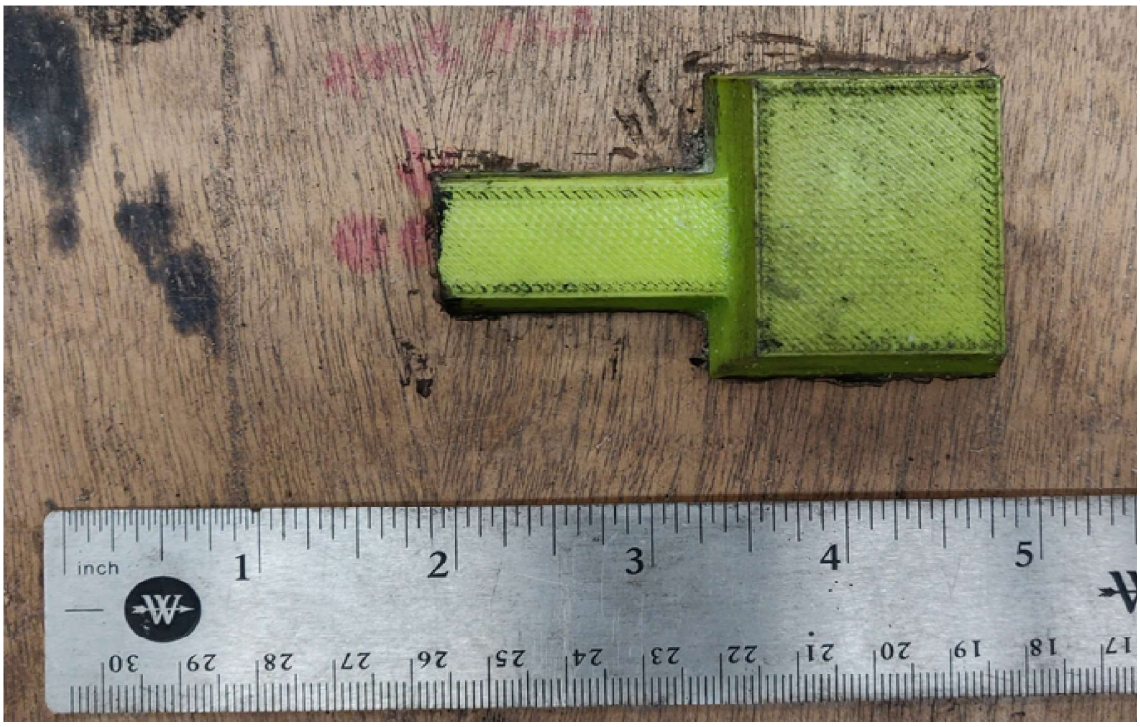

Figure 3.1: Top view of 3D printed PLA pattern made at UWM Foundry Lab.

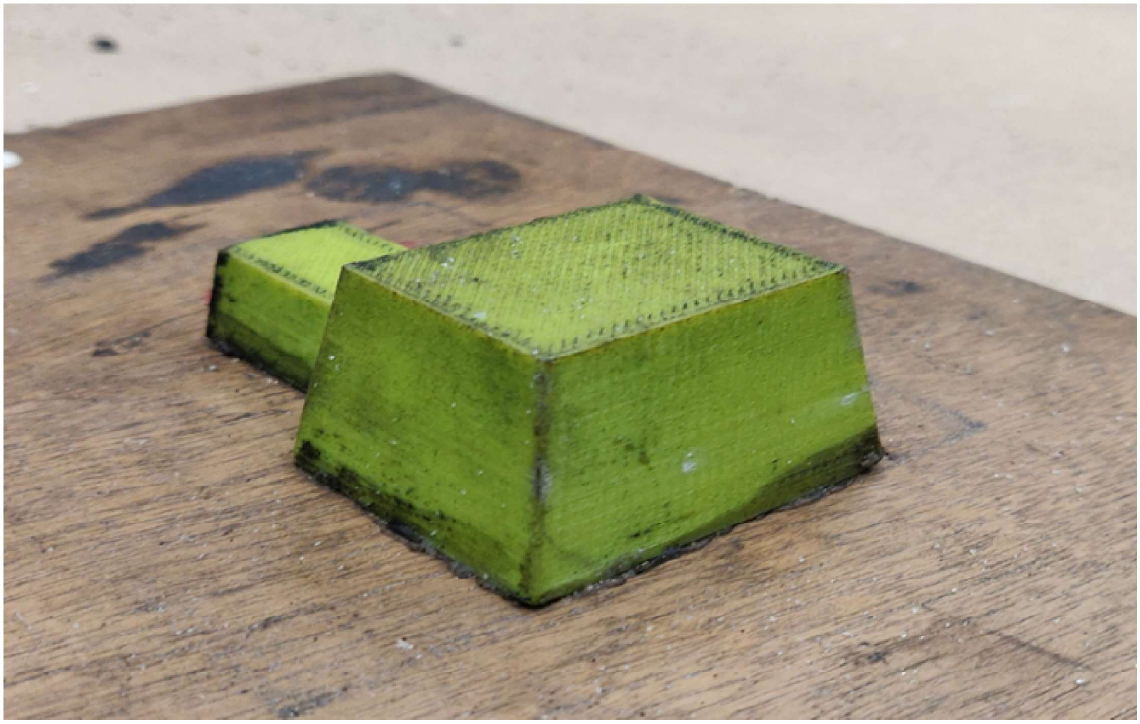

Figure 3.2: 3D printed PLA pattern made at UWM Foundry Lab.

Maynard Steel experiments included sodium silicate cores bonded with CO_2 gas. The cores

were coated with a slurry of binder and metal powders, and then sent back to Maynard Steel for metal pour. The cores were placed in sand molds and molten WCB steel was poured. Each heat at Maynard Steel produced an average of 30-40 samples weighing 10,000 lbs. The samples were steel ingots with a centrally depressed area having a surface alloyed circular cross-section. Figures 3.3 and 3.4 are obtained from Maynard Steel where the surface alloyed samples were cast.

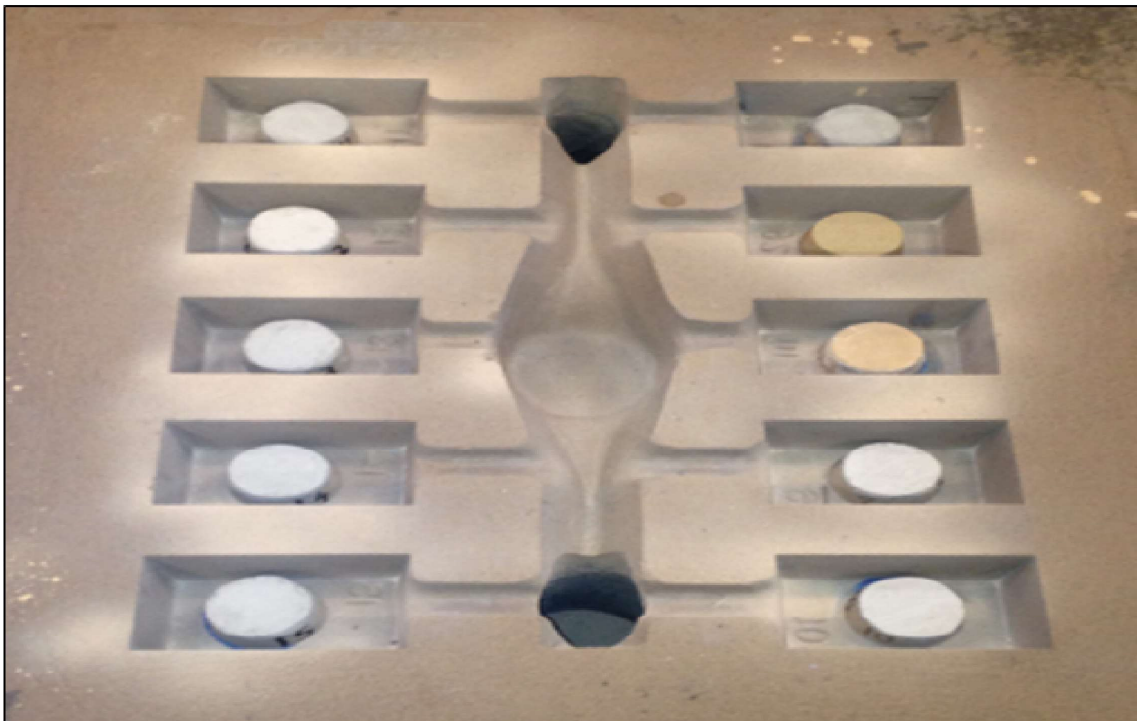

Figure 3.3: Mold and slurry coated sand cores for castings made at Maynard Steel.

Figure 3.4: 50 units of 10-lbs castings poured at Maynard Steel.

Badger Alloys heats were aimed at producing an industrial butterfly valve prototype having a surface alloyed layer as shown in figure 3.5. As this technique is aimed at replacing expensive alloys such as standard grade stainless steels with cheaper alternatives, a chemistry containing alloying elements similar in weight percentage to 2205 DSS was selected. The sand molds were provided by Badger Alloys and sent to UWM. The prepared slurry (discussed in section 2.1.1) was applied to the cores and the molds closed, shown in figure 3.6, were sent back to Badger Alloys for casting. Three surface alloyed butterfly valves were cast with 40 micron particle size of Ni-Cr powders, 80 micron particle size Ni-Cr powders, and 200 micron particle size 316L stainless steel powders.

Figure 3.5: Surface alloyed butterfly valve prototypes cast at Badger Alloys. Ni, Cr, Fe-Mn and Fe-Si were used as alloying powders. REFCOHOL 1010 and Sodium Polyacrylate were used as separate binders.

Figure 3.6: Molds for butterfly valve made at Badger Alloys for casting an industrial surface alloyed prototype.

3.1.1 Slurry Preparation

One of the challenges faced in this study included designing a technique to ensure the alloying metal powders would stay adhered to the mold surface. While this was necessary, it was also important to consider the effect of flowing molten steel through the mold cavity. As the alloying is only desired on the surface, a method had to be developed and studied to ensure the metal powders adhered to the mold cavity walls without falling off and without causing any detrimental effect on the chemical composition of the surface alloyed layer or steel.

The first set of samples were made using a commercially available refractory wash REFCOHOL 1010. REFCOHOL 1010 is manufactured by REFCOTEC and is used by casting industries as a coating for the mold cavities. The wash primarily contains high quantities of Zirconia powder along with iso-propyl alcohol, Naptha and other proprietary binding agents. The role of Zirconia powder is to act as a refractory layer between the molten steel and sand mold. As two of the required aims for selecting a binder, i.e., preventing reaction with sand and being commercially available were satisfied, REFCOHOL 1010 was selected as the initial binder. The

composition of REFCOHOL 1010 can be seen in table 3.4.

Chemical Name	Weight %Range
Isopropanol	15-16
Solvent Naptha	7-9
Zirconia (Zirconiaium Silicate)	65-75
Crystalline Silica (Quartz)	1 Max
Proprietary Binding/Suspending Agents	1-5

Table 3.4: Chemical composition of REFCOHOL 1010 as provided in SDS.

The binder was be applied to mold cavity surfaces and metal powders would be sprinkled onto the applied layer before drying. The layer would then be ignited by a blow torch to evaporate the excess alcohol and any other hydrocarbons present in the binding agents. Though the adhesive bond of metal powders with the binder layer was not extremely strong, it was enough to be utilized for experimenting the process. This technique was applied to castings made at UWM, Maynard Steel, and Badger Alloys.

The second binder was utilized in the second stage of the study. This binder was obtained from REFCOTEC but is not commercially available and is still in development phase. The binder, REFCOBAR 1010 Gel, does not contain any refractory powder and can be directly mixed with metal powders. This is one important aspect of change as previously, with REFCOHOL 1010, it was found that mixing the refractory wash with metal powders and then using the same in casting experiments did not lead to any surface alloying. The use of new binder without any refractory powders in it also lead to possibilities of adding higher quantities of metal alloying powders.

The powders were measured accurately and mixed together for uniform distribution in the mold casting. The binder was added along with similar quantities of water. The addition of water was a recommendation by Dr. Seibel from REFCOTEC as the binder was a water based binder. The resulting slurry was painted on the surface of the molds and left to dry. Initially, the drying process was conducted in a low temperature furnace at a temperature of 100 °C for a period of 20 minutes. This was later found to be detrimental as the development of water vapor would be trapped in the slurry leading to bubbles being formed in the hardened slurry. When molten metal would come in contact with the metal powders in the slurry, such bubbles had the highest probability of turning into porosities, blow holes or other casting defects. To avoid such

defects, the slurry was air dried for the second set of experiments in the UWM Foundry Lab experiments. The time used for drying in open air was approximately 45 minutes to 1 hour. Though there was an increase in the time requirement before pouring molten metal, it ensured there was no moisture to cause any hazards and the samples did not show signs of porosities or other defects seen in the earlier samples.

This new water based binder was used for experiments at the UWM Foundry Lab and Badger Alloys valve disk castings for industrial prototypes. The binder was not ignited for the drying process as in case of REFCOHOL 1010. The slurry, on hardening, adhered strongly to the sand molds and did not fall off even when the mold was turned up-side down or moved in any direction. This ensured the slurry would not run off from the vertical walls of mold cavity and can be used to coat the mold cavity of castings with complex geometries, something that was not possible with REFCOHOL 1010.

For the experiments with REFCOBAR 1010, the slurry preparation technique was modified to ensure a desired thickness of surface alloying was achieved. This would be an advantage for applications requiring a 100 micron thickness of surface alloying or 4000 microns of surface alloying. The control over surface alloying thickness is desirable to ensure minimum wastage of the alloying elements which helps to reduce the overall costs of the castings.

The thickness of the surface alloying should be fixed and multiplied by 1 sq cm area to calculate the total volume which will be occupied by steel. The density of steel then is used along with this volume to calculate the mass of steel occupying that space. Depending on that mass, the quantities of alloying elements can be determined according to the weight percentages of the alloy for 1 sq cm of area. This can be scaled up to the total surface area of the mold cavity to provide an accurate measurement of the quantities of powders required for surface alloying. The binder, REFCOBAR 1010, is added after mixing the powders and is approximately 20-30% by weight of the total weight of powders. Water is finally added approximately the same weight as the binder to provide added fluidity. This mixture has been applied using a brush as well as swabbed on the mold cavity and has provided good results with consistent surface alloyed layer. This will be further discussed in the experimental results of samples made using REFCOBAR 1010.

3.1.2 Maynard Steel Ni-Cr Pour

The first heat of samples was cast at Maynard Steel using REFCOHOL 1010 as binder and Ni and Cr powders as alloying elements. The powders used for this set of trials was lab grade, i.e., it was 99.9999% pure. If we compare this to further heats and trials, the purity of those powders was lower to accommodate the increase in costs on account of lab grade powders. The powders were sprinkled on top of the coated mold core on account of the nature of the binder. As the binder contains high quantity of refractory in form of Zr powder

Sample	Ni (grams)	Cr (grams)
95	1.64	1.64
96	1.9	2
97	2	2
111	15	15
112	15	15

Table 3.5: Composition of the alloying powders for the Maynard Steel samples.

3.1.3 Stainless Steel Alloying

One of the changes made to the composition of the surface alloyed layer included the use of 316L stainless steel powder as the alloying powder in the mold cavity. The concept was to enrich the surface of mild steel to a composition which was targeted towards 316L stainless steel. In the previous attempts, the samples were alloyed using Ni and Cr powders in an attempt to target compositions which would improve properties such as corrosion resistance higher than that of WCB steel. In an industrial environment, such as in the manufacture of flanges, this would provide increased life while cutting down costs. One of the major errors which was identified during those tests was the uneven distribution of the alloying elements. In order to mitigate this issue and provide a balance of alloying elements, stainless steel powder was identified as possible alloying powder.

The trials were conducted using 316L stainless steel powders having a variation in particle sizes. The powders were 95% pure and were purchased at low costs in an attempt to lower the final production costs. The binder used was REFCOHOL 1010 and the technique to coat the mold surface was the same as in the case of trial 1 samples. The binder was applied on to the mold surface and the alloying powder was sprinkled on top to cover the binder applied surface. After

curing the binder, the mold cores were sent to Maynard Steel and WCB was used as the base metal for the pour. The experiments were planned on the basis of two major variables, weight of the alloying powder and the particle size. The variation in weight was brought in to understand the depth up to which surface alloying could take place while the variation in particle size was done to observe how different particle sizes would lead to variation in the consistency of the surface alloyed layer.

The melt was successful in surface alloying of the WCB melt but the consistency in the depth of surface alloying was not observable in the samples. As the binder was a base for the alloying powders to lay on and not as a mixer, some portion of the coating could have been lost in the process. During the melt pour, some of the samples were lost on account of coated mold core damage. The remaining were normalized, tempered, shot blasted and sent back for processing. The samples represented in this study exhibited a consistency in the surface alloyed layer through the mold core surface. The list of castings is given below:

Sample	Particle Size (μm)	Weight (grams)
305	1000	4
309	800	2
317	600	2
319	600	2
321	600	4
322	600	4

Table 3.6: List of castings made at Maynard Steel using 316L Stainless Steel powder as alloying powder.

3.1.4 Badger Alloys Experiments

The Badger Alloys experiments were aimed at testing the feasibility of the surface alloying technique for casting prototypes of components which are used in the water industry. For this set of experiments, Badger Alloys provided the molds for casting butterfly valves which are used in the water industry and are made of through section stainless steel to prevent corrosion of the surface over the working period. The objective was to quantify the levels of enrichment which could be achieved in an industrial setting for casting a components which requires high quantities of Ni and Cr on the surface.

The binder selected for this set of trials was REFCOTEC Refcohol 1010 which is the same binder that was used in the first two Maynard Steel trials. As the powders cannot be mixed with the binder on account of high quantities of refractory Zirconia present in the binder, the sprinkling technique was used for coating the mold surface with the slurry. The quantities of alloying powder was determined according to the composition that was desired in the surface alloyed layer after casting. A mixture of Ni and Cr powders was used with the objective of enriching the surface alloyed layer to a composition that was targeted to 18/8 stainless steel. Approximately 100 grams of such powder was made with the 18/8 measurements being converted to form 100 grams together. Thus, it was anticipated that the composition of the alloying powder on the slurry would surface alloy the WCB steel to a composition similar to 18/8 stainless steel.
Three particle sizes were used in this set of experiments. Ni and Cr powders were tested with 40 micron and 80 micron sizes and 316L stainless steel powders were used with 200 micron particle sizes. In case of 316L stainless steel, there was no need for measuring out the powder in terms of a specific composition as the alloying composition is already present in the powders.

Particle Size (micron)	Ni (grams)	Cr (grams)	Powder/Area (grams/cm^2)
40	0.8	1.84	0.165
80	0.51	1.19	0.106
200	316L Powder	316L Powder	0.137

Table 3.7: List of castings made at Badger Alloys using Ni, Cr, and 316L Stainless Steel powder as alloying powders.

3.1.5 Quartz Tube Experiments

Quartz tube experiments were the first stage of experimentation at the UWM Foundry Lab. The aim of the experiments was to test the performance of a binder and new alloying powders before moving on towards the open pour experiments. The open pour experiments consumed one crucible per pour as compared to quartz tube experiments where in the same equipment could be used multiple times. Another factor to be considered in quartz tube experiments is the use of a vacuum pump to ensure absence of oxygen in the system which leads to formation of oxides. Though the experiment produced samples of diameter 4 cm and height of 1.5 cm, the thickness of surface alloyed layer was variable. This variation was the important factor of such experiments to understand the maximum depth of surface alloying which can be achieved.

The experiments produced samples with thickness of surface alloyed layer ranging from 950 μm to 4010 μm. The complete list of open pour experiments conducted at UWM Foundry Lab along with average thickness of surface alloyed layer achieved and comparable composition of the surface alloyed layer is shown in table 3.8.

Sample	Thickness of alloyed layer (μm)	Targeted Composition in Surface Alloyed Layer
R1	950-1000	316L SS
R2	1950-2050	316L SS
R3	2900-3100	316L SS
R4	3950-4100	316L SS
R5	980-1070	2205 DSS

Table 3.8: List of castings made at UWM Foundry Lab using the quartz tube experiments. The average thickness of surface alloyed layer along with comparable composition is also shown.

As mentioned in table 3.8, the chemical composition of the surface alloyed layer is mentioned in table 3.11 to target the chemical composition of 316L SS and 2205 DSS. The castings made in the industry undergo sand blasting to remove any residual sand adhered to the casting and in some cases, the castings are machined to ensure a smoother surface finish. To ensure that machining or any post-processing steps do not affect the surface alloying of casting, an alloyed layer of average thickness 4000 μm would provide enough clearance for machining. The stereoscopic image for measurement of the thickness of the surface alloyed layer is shown in figure 3.8. The binder used for samples made in table 3.8 is the water-based binder REFCOBAR 1010 obtained from REFCOTEC.

The experimental setup for performing quartz tube experiments in UWM lab is shown in figure 3.7.

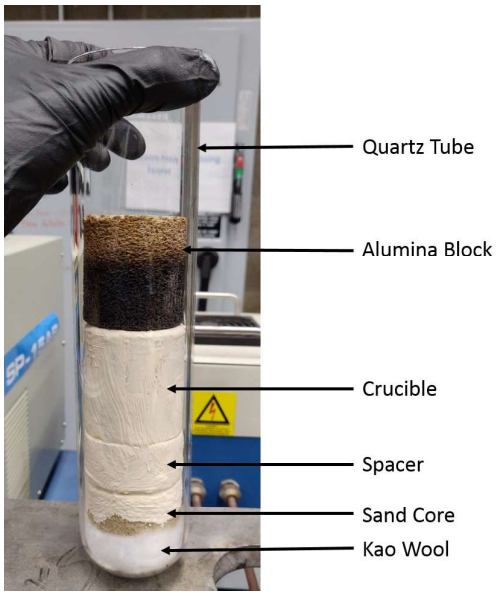

Figure 3.7: Experimental setup of quartz tube experiment with the components labeled.

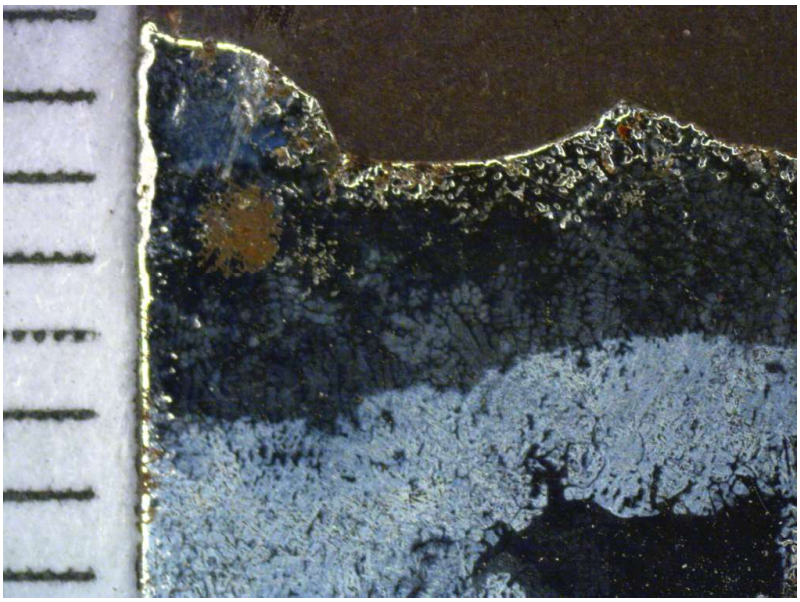

Figure 3.8: Stereoscopic image of sample R4 with a surface alloyed layer having an average thickness of 4000 μm. The composition of alloying powder is mentioned in table 3.11. Each scale division is 1 mm.

The quartz tube used for the experiments were 5 cm diameter and of 30 cm length. Kao wool was the first component placed inside the tube at the base. This wool acted as a resting stage for the sand core to be placed without getting stuck in the curved bottom of the tube. The sand core was made from sodium silicate bond sand and coated with slurry of binder and

alloying powders. The spacer was placed on top of sand core. This spacer was cut from a hollow graphite cylinder and was about 2.5 cm in height. The function of the spacer was to act as a separation between the crucible and sand core. The spacer was coated with a layer of Zirconia wash which prevented the diffusion of carbon from graphite into the molten steel. The crucible was also made of graphite and was a cylinder with the base covered and containing a hole for molten steel to flow from into the sand core. A thick coating of Zirconia wash was applied to the crucible as well to prevent graphite diffusion. Ingots of WCB steel were placed in the crucible. When the temperature would reach approximately 1700 °C, the molten steel would flow from the crucible onto the sand core. An alumina block was placed on top of the crucible to act as a refractory to prevent the silicone o-rings, used to secure the vacuum, from melting.

The setup was secured in between the induction coil with the crucible directly under the effect of heating due to the current flowing through the coil. The induction coil used in these experiments had a diameter of 7.5 cm and 7 turns of the coil. Water flowed through the coils continuously through the experiments to ensure the high temperatures generated during the heating process did not damage the induction coil. The induction coil setup was SP-15AB built by MTI Corp. The current flowing through the coils started at 55 Amp and was increased at a rate of 10 Amp every 100 seconds. The heating cycle was preset to 100 seconds cycles and change in current was a manual process. The current was increased to a maximum of 200 Amp where complete melting of mild steel was expected to occur. The coil was then shut-off and the tube along with all its components was left to cool in the coil with water flowing through the coils. Figure 3.9 shows the setup during the heating phase.

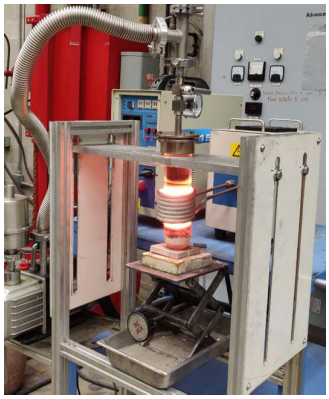

Figure 3.9: Heating phase of the quartz tube experiment. The melt was superheated to a temperature of 1700 °C.

3.1.6 Open Pour Experiments

The open pour experiments were the second stage of the experiments conducted at the UWM Foundry Lab. The aim of these experiments was to replicate the industrial metal casting environment as closely as possible. The sand molds were made using no-bake chemically bonded industrial quartz. The chemicals used in the process included Uniset Bio-Zero Part I, Uniset Bio-B57 and Accelerator 750W. The chemicals were mixed into the sand while agitating continuously to ensure the entire batch of sand was mixed with the chemicals. Uniset Part I and accelerator were mixed first and Bio-B57 was added later. The quantities of chemicals used for a 25 lbs batch of sand is mentioned in table 3.9.

Chemical	Quantity (oz)
Uniset Bio-Zero Part I	3
Uniset Bio-B57	3
Accelerator 750W	0.05

Table 3.9: Quantities of chemical binding agents added to 25 lbs of quartz mold sand.

The mixed sand would be placed over the patterns surrounded by concrete blocks to act as the flask edges for containing the sand. Similarly, the drag side would be made for the mold with the same sand. The setting time for sand was approximately 30-45 minutes. Sprue and degassing holes were cut into the drag after it had hardened. The mold cavity would be given a couple of layers of Zirconia wash as it prevented diffusion of steel with sand and provided a good surface finish to the castings. Before pouring metal, the cope and drag would be shut using an industrial bonding agent.

A graphite crucible was used for melting steel and the furnace used for the experiments was the same induction coil furnace from quartz tube experiments. The crucible would be coated with multiple layers of Zirconia wash. The crucibles were then placed in a low-temperature furnace for removing the moisture from the wash. The curing temperature was 100 °C for a period of 1 hour. This ensured that all the water from the water based Zirconia wash was evaporated from the crucibles. The metal ingots weighing approximately 1.5 lbs would be placed inside the crucible and heated to a temperature of 1700 °C or above which was enough for steel to flow easily into the mold cavity and closely resembled the industrial environment. On account of slag left behind and high temperature heating, one crucible was used per casting.

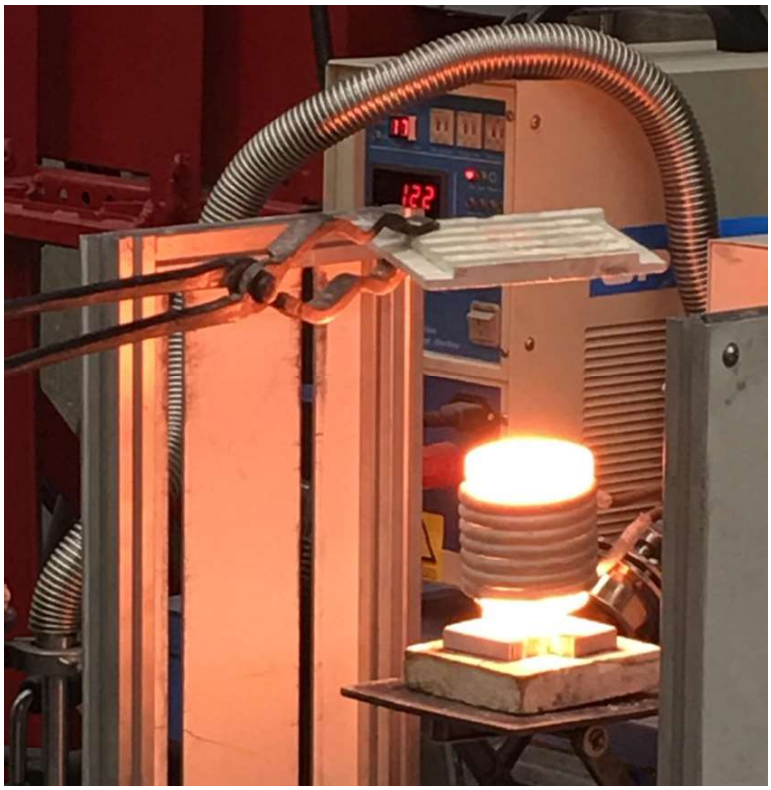

Figure 3.10: Melting steel in Zirconia coated graphite crucible for open pour experiment. The steel was superheated to a temperature of 1700 °C.

Sample	Thickness of alloyed layer (μm)	Targeted Compositions of Surface Alloyed Layer
R6	990-1070	2205 DSS
R7	1895-2050	2205 DSS
R8	1950-2080	2205 DSS
R9	900-975	2205 DSS
R10	930-1025	2205 DSS
R11	Sample Lost	2205 DSS
R12	1875-2010	2205 DSS

Table 3.10: List of castings made at UWM Foundry Lab using the open pour experiments with the average thickness of surface alloyed layer along with comparable composition.

Sample	Ni (grams)	Cr (grams)	Fe-Mn (grams)	Fe-Si (grams)
R1	0.76	1.38		
R2	1.45	2.62		
R3	2.05	3.71		
R4	2.97	5.37		
R5	0.62	1.72	0.38	0.02
R6	0.82	2.27	0.51	0.03
R7	5.85	16.26	3.64	0.23
R8	2.92	8.13	1.82	0.11
R9	2.92	8.13	1.82	0.11
R10	1.95	5.42	1.21	0.07
R12	3.9	10.84	2.42	0.156

Table 3.11: Composition of the alloying powders for the R series samples cast at the UWM Foundry Lab with WCB as the base metal. Samples R1-R4 were made with targeted composition of 316L stainless steel while R5-R12 were made with a targeted composition comparable to 2205 DSS.

Seven castings were made using this technique. The chemical composition was comparable to 2205 DSS and the highest thickness of surface alloyed layer achieved was 2080 μm. The list of castings made is shown in table 3.10 and the chemical composition of the alloying slurry used to coat the mold cavity is given in table 3.11. Figure 3.10 shows the heating process of the crucible during the melting part of the experiment. The current was set to 55 Amp for the first cycle of the induction coil and increased in increments of 10 Amp per cycle. Each heating cycle of the system was set at 100 seconds as in quartz tube experiments.

3.2 Sample Preparation

The samples were cut using a band-saw with continuous lubricant flow to ensure there was no change in the microstructure on account of heat generated during the cutting process. The sample size was under 1 in^2 so that the samples could fit inside the mounting press with enough room on the side to avoid cracking of the mount matrix. Samples used for XRD and heat treatment were cut separately as continuous cycles of mounting would damage the samples.

3.2.1 Metallographical Preparation

The sample mounting was performed on Buehler SimpliMet 3000. The heating cycle was set at 3 minutes, the cooling cycle was 4 minutes and the pressure used for compression was 4200 psi. PhenoCure Compression Mounting Compound, a phenolformaldehyde based compound, was used as the mounting resin as it is conductive and is compatible with SEM-EDS-BSE system. Figure 3.11 shows an example of a mounted sample.

Figure 3.11: Surface alloyed UWM Foundry Lab sample R2 mounted in phenolformaldehyde compound.

Polishing of the samples was performed on Buehler MetaServ 250 Grinder-Polisher. The grinding papers were Buehler CarbiMet SiC Abrasive Grinding Papers of 8 in diameter and PSA backed. This grinding paper is recommended by Buehler and is suitable for polishing steel samples. Polishing started with 120 grit grinding paper at 300 rpm for a period of 5-7 minutes to even out the surface of the samples and remove any excess mounting polymer attached to the sample surface. This is followed by 9 μm MetaDi Supreme Diamond suspension on a UltraPad surface under 27 N of force for period of 5 minutes at 150 rpm. Then 3 μm MetaDi Supreme Diamond suspension is used on a TriDent surface under a force of 27 N for a period of 3 minutes at 150 rpm. For the 9 and 3 μm suspensions, the rotation of the sample and base plate was in opposite directions and in the same direction respectively. The final polishing occurs in two stages, first with the 1 μm MasterPrep Alumina suspension and with the 0.05 μm MasterPrep Alumina suspension. Ideally, only the 0.05 μ is suggested by Buehler but on adding the 1 μm step before the 0.05 μm helps to obtain a higher surface finish. The force applied for both stages of the final polish is 27 N and the speed is set at 30 rpm for a period of 3 and 5 minutes respectively. The time is not specified by Buehler and had to be decided on a trial and error

basis. The selected times ensure a good surface fishing along with lower time consumption. A ChemoMet MicroFloc pad was used for both 1 and 0.05 μm Alumina suspensions and the rotation of the polishing pad and sample holder was in opposite directions. As the surface alloyed layer was only on the edges, care was taken to ensure no stray grinding marks were left on the edges which would affect optical microscopy and SEM imaging. The samples were immediately dried after grinding with each grit size and diamond suspension to prevent corrosion and the samples were held far enough from pressurized air gun to ensure absence of erosion marks.
The samples were cleaned using cotton balls and isopropyl alcohol and then dried using pressurized air. The samples were stored in a vacuum desiccator to avoid corrosion and other detrimental effects of the surrounding environment.

3.2.2 Etching of Samples

Etching is performed to reveal the microstructure, phases and grain boundaries of the samples. For ferrous alloys, it is important to understand the phases formed so as to ensure good mechanical properties and help in selecting a good heat treatment cycle.
As the surface alloyed layer has a different chemistry than the base metal, the first etchant selected was 3% Nital. The etchant was made using 3 ml of Nitric Acid and 97 ml Ethanol in a fume hood. The sample would be immersed in the etchant and held for 3 seconds and the surface was neutralized using isopropyl alcohol followed by air drying. The aim of this etching was to etch only the mild steel base which would keep the surface alloyed layer unetched. Thus, it was possible to understand the separation of the two metals and characterize the thickness of the surface alloyed layer. The interface would be revealed on account of the alloying elements separation.
The second phase of etching involved electro-etching using an etchant with the composition 15% HCl and 85% Ethanol. The sample was completely immersed in the solution and an electrode was placed on the surface alloyed layer. An electric current of 2 Amp would be passed through the setup for a period of 2-3 minutes to etch the surface alloyed layer. As the chemical composition of the surface alloyed layer is comparable to stainless steels, selecting the correct etchant was crucial. Kallings No. 2 reagent and Marbles reagent were also used for etching the surface alloyed layer in samples where the composition was comparable to 2205 DSS. The composition of both the etchants is given in the tables 3.13 and 3.14.

Composition	Concentration
HCL	3-5 ml
Ethanol	95-97 ml ml

Table 3.12: Composition of Nital used as etchant for the base metal to reveal the surface alloyed layer which is not affected by Nital.

Composition	Concentration
$CuCl_2$	5 grams
Hydrochloric Acid	100 ml
Ethanol	100 ml

Table 3.13: Composition of Kallings No. 2 Reagent used as etchant for the surface alloyed layer.

Composition	Concentration
$CuSO_4$	10 grams
Hydrochloric Acid	50 ml
Water	50 ml

Table 3.14: Composition of Marbles Reagent used as etchant for the surface alloyed layer.

As compared to Nital, Kalling's No. 2 is used for etching duplex stainless steels and Marble's Reagent is used for etching superalloys. It is recommended to use Nital for the initial etch to observe the thickness of the surface alloyed layer. The optical micrographs are used for quantification of average thickness of the surface alloyed layer. Kalling's No. 2 and Marble's Reagent are used for etching the surface alloyed layer but as the composition of the surface alloyed layer is comparable to stainless steels and not the same, the etched microstructure may or may not be the same.

3.3 Characterization of Samples

Characterization of the samples was performed to understand the composition of the alloyed surface and the effect of the micro-alloying elements on mechanical properties and phase formation. The mechanism of surface alloying and the solidification behavior of steel, movement

of the solidification front, effect of the plane front on particle pushing considering the alloying elements are powders, and Brownian motion on account of powders mixing with molten steel in initial stages of pouring have been mentioned in further chapters.

Advanced characterization of samples was conducted at the Advanced Analysis Facility at UWM under the guidance of Dr. Steven Hardcastle. Experiments for quantifying residual stress were performed at University of Wisconsin-Madison at their Engineering Research Building using a Panalytical Emperyan. The samples used for optical microscopy, SEM-EDS-BSE, and hardness tests were mounted samples. The samples used for XRD and heat treatment were unmounted samples. After each heat treatment cycle, the sample went through XRD testing to understand the changes in phases.

3.3.1 Optical Microscopy

Optical microscopy is a technique used for understanding the morphology of the surface alloyed layer and quantification of the thickness of the surface alloyed layer. The grain structure of the surface alloyed layer is expected to differ as compared to traditional stainless steel alloys. This is attributed to the difference in compositions as well as the heat treatment cycles performed on the casting. All of this changes the microstructure of the surface alloyed layer as well as the base metal. Further, the interface between the surface alloyed layer and base metal should be examined for presence of defects such as cracks and porosities. A defective interface can lead to bonding issues and high temperature heat treatment cycles could initiate cracks in the surface alloyed layer.

The hardness tests conducted on the surface alloyed layer and base metal are examined on the optical microscope post indentation. This is done for both Vicker's Microhardness and Nanoindentation tests. The morphology of the indent and the surrounding area shows the impact of the post-processing treatment on the mechanical properties. The metallographically prepared samples were micrographed after being etched with all three etchants. This was done to study the microstructure of not just the alloyed layer but of the base metal as well. As we will see ahead, some of the industrial samples were obtained heat treated according to WCB standard and were later heat treated according to 316L or 2205 DSS standards. This would change the microstructure of the alloyed layer but will also affect the already heat treated base metal. As mentioned in section 2.2.2, Nital helps to etch the base metal while the other two etchants work on the alloyed layer.

The microscopy was performed on Nikon Eclipse TS100 with magnifications of 50X, 100X and 200X. Higher magnifications upto 2000X was possible but avoided due to poor image quality and performing SEM at higher magnifications provides better images for analysis as compared to optical microscopy. Primary features observed during optical microscopy included grain boundaries, phases, defects, pitting corrosion, and physical aspect of the interface between the alloyed layer and the base metal.

3.3.2 SEM-EDS-BSE

This is a characterization technique intended for high resolution and high magnification imaging as well as for the quantification of chemical composition of the material. The magnifications can be obtained as high as 100,000X and have a better image resolution as compared to the optical microscope. The higher magnification allows for a detailed look at the grain boundaries, where intermetallics form during heat treatment cycles. It also allows for understanding the morphology of the interface between the alloyed layer and the base metal and reveals details about the interface microstructure which are not visible using an optical microscope.

The characterization is divided into three sections in total, scanning electron microscopy, back-scatter electron spectroscopy and energy dispersive spectroscopy. The first two are used for imaging the sample surface while the third one is used to quantify the chemical composition of the sample. The quantification is limited to individual elements and does not provide details on the phase in which the elements are present. For example, in case of steel alloys such as WCB, EDS will quantify the weight and atomic percentages of elements such as Fe, C, O, Si, etc. but it won't provide details on the phases in which the elements are present, such as ferrite or pearlite. The primary mode of imaging works on the principle of high energy electrons impacting the sample and capture of the reflected electrons leading to the formation of an image. The electron gun is used for delivering high energy electrons to the sample. Some of the electrons pass through the sample but the ones which are deflected on impact are collected by the detector. These electrons get converted into signals which are processed to form an image. The beam moves over the sample scanning the surface and the resolution of the image depends on the scanning time. This translates to higher the scanning time, higher is the resolution of the image. The images obtained using SEM are monochrome and thus performing optical microscopy helps in obtaining color micrographs specifically in the cases of coloring etchants such as Marble's Reagent.

The SEM imaging was performed on JOEL JSM-6460 LV fitted with an Energy Dispersive Spectroscopy setup. The working distance for the samples was set at 15 mm, accelerating voltage was 15 - 19 kV and spotsize was set to 55. For BSE analysis, composition and topography modes were used. As mentioned in prior literature, BSE is useful for identification of phases specially austenite and ferrite in the surface alloyed layer as well as for identifying intermetallics σ and χ phases formed in the surface alloyed layer post heat treatment. The composition mode helps to detect differences in the changes in composition as it shows a variation in the contrast of the different compositions present on the sample surface. This is useful as austenite and ferrite have different compositions and can be detected as contrasting spots on the image.

Energy Dispersive Spectroscopy is a technique which utilizes the kα_1 radiation emitted by the sample when an electron from the incoming beam impacts an electron from the atoms of the sample in the k orbit. This impact leads to the orbital electron to jump out creating a vacancy. An electron from the higher L orbit jumps onto the lower energy state and release a packet of energy in the transition. This packet of energy differs for every element and acts as a fingerprint for element identification. Depending on the total intensity of the radiation output from the sample surface, the weight percentage and atomic percentages of the elements in the sample are quantified. The different modes available in EDS include:

1. Point and ID
2. Area X-Ray Maps
3. Line Scans

Point and ID is used for quantification of the elemental composition at a certain point in the sample surface. This is important to identify the composition inside the microstructure, grain boundaries, and interface before and after heat treatment. In a dual phase stainless steel such as 2205 DSS, the differences between austenite and ferrite can be observed by performing the point and ID test on the microstructure and separating the carbon rich ferrite from the nitrogen rich austenite. The point and ID scan was performed on the surface alloyed layer as well as the interface and the base metal over multiple sections of the sample.

Area X-Ray Maps are used for mapping the elemental distribution over an area as opposed to selected points. The maps produced as a result display the elements present in the sample scattered over the selected area. A wide area can be scanned over time allowing for better

quantification results and observing pockets which contain higher quantities of alloying elements. These pockets can be generated on account of the plane front movement, convection flows set up by the molten metal flowing through the mold cavity or due to the uneven distribution of the elements before application of the slurry.

Line scans are done for observing the elemental distribution and change in composition over a length of the sample. In this case, as there will be drastic change in the composition of the metal as we move from the surface alloyed layer to the base metal, it is crucial to understand the distribution of the elements as well as their quantification. Line scans produce graphical results where the x-axis is the length over which the scan was performed and the y-axis is the counts/second of radiation emitted by the sample surface for that particular element. Considering there is an interface present, the sudden drop is expected in that region and detailed line scans have been performed of the magnified view of the interface. The results have been discussed in further sections. Multiple line scans were performed over the sample surface.

All of the above tests were performed at the same time as the SEM and BSE imaging took place. Care was taken to ensure the IR camera did not interfere with the radiation detection. The time was set to 5 minutes for each test except the Point and ID as it sets it's scanning time by itself. The line scan graphs, x-ray maps and elemental quantification tables were referred for making recordings of the composition of the surface alloyed layer.

3.3.3 XRD

The characterization of coating on cast samples is necessary to identify the phases which are produced during the casting process. Each phase formed in steel and the surface alloyed layer has a definite crystal structure. Atoms arranged in a specific order form the crystal structures such as FCC, BCC, HCP among others. Austenite is a BCC phase where as ferrite is a FCC phase and they can be identified in the steel sample by using XRD. One of the factors which helps identify the phases is d-spacing. D-spacing is the distance between two planes in a crystal structure. X- Ray Diffraction (XRD) is a characterization technique which utilizes x-rays for identifying the phases present. The setup consists of an x-ray gun and a detector which may or may not move at the same rate. In case of Bragg-Brentano configuration, the sample is stationary while the x-ray gun and the detector rotate. The x-ray gun and detector can rotate at the sample rate making it a θ-θ geometry or one may rotate faster than the other making it a θ-xθ geometry where x is the rate at which the detector is moving faster as compared to the

gun. The x-rays which are generated impact the sample and are diffracted by the atoms in the sample. If the beam is not diffracted by the first plane, it travels ahead and gets diffracted by the second plane and the gap between the beams is used to determine the d-spacing.

Every crystal structure has a different d-spacing and by calculating it, the phases are identified. The radiation we require is CuKα_1, hence CuKα_2 is stripped off during final analysis and a nickel filter can be used for stripping out other radiations which may cause background noise in the data. The final data which is obtained is analyzed using PDF cards for identifying the peaks for phases. Only major peaks are identified as minor ones may be due to impurities.

For the current study, the Bragg-Brentano configuration was followed for the purpose of phase identification and determining the lattice parameters of the surface alloyed layer. Due to composition differences, the perfect match for phases and crystal structure was difficult to find on account of the standard format of the PDF cards used for analysis. The primary phases identified included austenite and ferrite in the 2205 DSS along with confirmation of the presence of Cr_2O_3 which acts as the passivation layer to prevent corrosion of the surface. Other phases included Yarlongite, minor quantities of carbides and 304 stainless steel in the case of 316L samples. Though not the same as desired, it was possible to enrich the samples upto a composition close to 304 stainless steel.

The test was performed on a Bruker D8 Discover X-Ray Diffractrometer using an unmounted sample. The Bragg-Brentano θ-θ geometry was used for the analysis with the current was set at 40 Amp and voltage was set at 40 V for a total power of 1600 Watts. The sample stage was stationary and the gun and detector started at an initial θ of 20° and final θ of 100°. This setup was used for the purpose of phase and lattice parameters identification.

The residual stresses are to be measured in the surface alloyed layer which is developed on top of the metal substrate. As the thickness of the layer varies between $100 - 1000$ μm, using XRD was suitable over Neutron Diffraction. This is due to the fact that XRD has a lower penetration depth and thus is suitable for measurement of residual stresses on the surface layer. Neutron diffraction has a higher penetration depth which causes residual stresses present in the bulk material to be included in the results as well, which was undesirable. Other methods to measure residual stresses such as strain gauge method or center hole drilling method were avoided as the layer would be drilled through in the first few seconds of the drill to surface contact and this would lead to drilling cutting into the metal substrate and measuring stresses from the substrate. As XRD is a non-destructive technique, the sample was intact after the

test and thus can be utilized again for other tests. Currently, some companies like Panalytical or Bruker have started making XRD machines which are portable and can be used to perform the tests a regular XRD machine can perform.

The residual stress measurements were conducted at the University of Wisconsin – Madison in their Engineering Research Building using the Panalytical Emperyan X-ray diffraction machine. The machine allows for residuals stress measurements which is not possible with the Bruker D8 at University of Wisconsin – Milwaukee. The ω-angle tilt method was used for this analysis. The samples were cut into 1" X 1" sizes with a thickness of 1 cm. The surface of the sample was left as is to prevent any buildup of residual stresses due to mechanical machining.

The sample surface had previously undergone linear polarization test to quantify corrosion and hence the layer of corrosion which was developed on the surface was removed by brushing the surface and applying mild force. Samples 95 and 96 were analyzed. Some issues were encountered during the experimentation such as fluorescence due to the use of a Cu anode and the metal-containing high quantities of iron. The staff at UW-Madison was informed of sample composition but they were unable to change the anode before analysis. The use of a Chromium anode or a Vanadium filter would have helped reduce the fluorescence.

According to the National Physics Laboratory, the recommended 2θ angle for 316L Stainless Steel to conduct the stress measurements is 147.5°. 316L Stainless Steel was selected as a reference as previous XRD results on the sample surface revealed phases similar to 316L. The selection of the 2θ angle did not produce good results on account of fluorescence produced due to the Cu anode and sample. This gave rise to background noise thus making it difficult to distinguish peaks. As a clear peak was not visible, diffraction was performed to find the most visible peak at the maximum angle. This was seen near the 90° region where the peak was visible with minimum background noise as compared to further peaks. For all the experiments were conducted with the following parameters:

Anode Material	Cu	
Kα_1 Wavelength	1.540598	
Kα_2 Wavelength	1.544426	
Kα_2/Kα_1	0.5	
Divergence Slit	Fixed	0.19 mm
Monochromator Used	No	
Generator Voltage	45	
Tube Current	40	

Table 3.15: Properties of Panalytical Emperyan During Analysis.

The scan axis for both samples was 2θ-ω and the ω offset range was 0° to -30° with steps of -5°. The data which was obtained from the analysis was plotted using Origin. As the peak observed near 90° was selected for calculation of stresses, it was necessary to obtain the 2θ of the peak so as to obtain d-spacing. The plot of d-spacing vs $\sin^2\psi$ is used to calculate the slope 'm' and the residual stress is then calculated by the formula (Prevey et al., 1986),

$$\sigma_r = \frac{E}{(1+\nu)} m \tag{3.1}$$

Where,

σ_r = Residual stress in the material (Tensile or Compressive)

E = Young's modulus of the material

ν = Poisson's ratio of the material

m = Slope of d-spacing vs $\sin^2\psi$

The data points in the range of 89° - 91° were fit using a Gaussian fit to obtain an accurate peak location. For every offset point, the 2θ angle corresponding to the Gaussian fit was used. ψ was calculated using the formulation,

$$\omega = \theta + \psi \tag{3.2}$$

3.3.4 Nano-indentation and Vicker's Microhardness

Surface alloying of the steel was experimented to ensure an increase in the surface properties of mild steel. The objective was to improve the final castings for having properties superior to

WCB steel and comparable to stainless steels such as 316L and 2205 DSS. The hardness of any stainless steel is generally higher than mild steel such as WCB on account of the strengthening agents added in form of alloying elements. This includes the use of Ni, Mn, and Mo as alloying elements. As these elements have been used in the slurry applied on the mold cavity for surface alloying, it is expected that the hardness of the surface alloyed layer will be greater as compared to the base metal. Furthermore, heat treatments also affect the hardness and its effect on the hardness is also important.

Nanoindentation is an advanced characterization technique used for quantification of the hardness and elastic modulus of a material. As opposed to hardness techniques such as Rockwell or Brinell or micro-hardness techniques such as Vicker's Micro-Hardness test, the nanoindentation test helps to indent at a higher degree of magnification. It becomes possible to indent the individual phases, grain boundaries, interfaces, carbides and other aspects of the microstructure. This is not possible with the micro-hardness test and the accuracy of results related to phase hardness is highly accurate. The tests were performed on Agilent Technologies Nanoindenter G200 using mounted samples. Each sample had an array of 4X4 indents on the surface alloyed layer and base metal. The interface between the two was indented through its length. This resulted in an overall hardness of the interface which shows the transition of hardness from the alloyed layer to the base metal. The difference for finding surface in the X and Y axis was set at 50 μm. The allowable drift rate was set at 0.05 nm/s. The maximum thermal drift time was 3 hours. The surface approach distance and surface approach velocity were set to 1000 nm and 10 nm/s respectively with the surface detect stiffness criteria set at 200 N/m. The depth limit for the indent was set at 2000 nm, strain rate target was 0.05 s^{-1}, Harmonic Displacement Target was 2 nm, Frequency Target was 45 Hz, and the Poissons Ratio was set at 0.33. A Berkovich indenter tip was used in this study. Berkovich tip is a three sided pyramid tip which has a half angle of 65.03°. The size of the indents varied according to the differences in composition of the various samples and hence an average size could not be computed.

The second hardness technique used for quantification was Vicker's Microhardness test. A separate sample from the same casting was used for the second hardness test. This is done considering that the previous indentation will lead to formation of stresses and indenting near those locations will lead to irregularities in the final results. The load was set at 500 kgf with a time of 10 seconds. Once the indent was made, the left vertex of the indent is aligned with the vertical line on the eyepiece of the micro-hardness tester. The right line is extended to reach

the opposite vertex of the indent and the distance between the two is used for calculating the hardness of the material. Then the eyepiece is rotated by 180° and the process is followed again to get the second reading. The average of the two is the actual hardness of the sample. 4 of such readings were performed on the surface alloyed layer and the base metal. It was not possible to indent the interface as the scale of the indent was too large to make an accurate indent and provide an accurate value.

3.4 Heat Treatment Techniques

Heat treatment of steels has been performed to improve the mechanical and surface properties. One of the primary reasons for heat treatment of the surface alloyed samples has been to improve their corrosion resistance capability. The other reasons include reducing residual stresses, dissolving carbides, improving the microstructure and strengthening the material. One of the primary reasons for corrosion resistance property of stainless steel is the passive oxide layers. While the as-cast samples showed a presence of the same in XRD plots, the intensity of the peak was low. The same samples showed an increase in the intensity of the Cr_2O_3 post heat treatment cycle.

As the composition of the surface alloyed layer is only comparable to contemporary through section stainless steel alloys, variations in the heat treatment techniques is necessary. The change in composition can lead to differences in the phases formed especially when intermetallics such as α phase in between the grain boundaries which can lead to detrimental effects (Chun, Baba, Terashima, Nishimoto, & Saida, 2013). One of the primary changes in the heat treatment process was to change the time for heat treatment. As the heat treatments are designed based on per section thickness of the alloy, the time was reduced depending on the thickness of the surface alloyed layer. During preliminary tests the samples that were heat treated for the recommended per section thickness time lead to oxidation of the surface leading to chipping of the surface alloyed layer in certain areas.

The first heat treatment cycle was normalizing and tempering of the complete sample. This technique was recommended by Maynard Steel and all the samples cast at Maynard Steel with WCB as base metal underwent the same heat treatment cycle. The first step of the cycle was to normalize the steel at 898 °C for 1 hour per inch thickness followed by air cooling outside the furnace. Then the sample as tempered at 535 °C for 1 hour per inch thickness followed by

quenching in water. The heat treatment cycle is designed for WCB steel but during XRD tests it was observed that the cycle leads to increase in the intensity of oxide layers formed on the surface alloyed layer. The same cycle was performed on the samples cast at the UWM Foundry Lab and at Badger Alloys and the same result as that of Maynard Steel samples was observed. The second heat treatment was solution annealing of the surface alloyed layer. The heat treatment has been extensively described in the literature review with emphasis on the formation of intermetallic phases in the surface alloyed layer. The time for the samples was reduced according to the thickness of the surface alloyed layer. The reduction of time lead to prevention of the chipping of the surface alloyed layer which is an indication of failure. As the temperatures during the operation of the surface alloyed layer in the component would not reach as high as 1100 °C, the failure would not necessarily occur unless an incorrect heat treatment cycle is followed. The samples which were heat treated with reduced time lead to formation of oxides which were observed in XRD plots.

Chapter 4

Mechanism of Surface Alloying

The molten metal flowing through the mold cavity comes in contact with the alloying powders which are applied to the walls of the mold cavity. We consider the effect of convection and diffusion in liquid in the initial region of the melt in contact with the alloying powders as described by Flemings (Flemings, 1974). In case of alloying powders, the molten metal will start the melting and dissolution of the alloying powders present in the slurry. The Fe in the melt dissolves the alloying powders at lower temperatures than the melting point of pure elements. Considering the FeCr and FeNi systems, the melting point of the system would be in the temperature range of the melt. The increase in the temperature of the alloying powders due to the iron melt leads to melting of the alloying powders. The concentration gradient present in the newly forming surface alloyed layer leads to beginning of the substitutional diffusion of Cr and Ni into the Fe bulk. The atomic sizes of Cr and Ni are 166 pm and 149 pm respectively, while that of Fe is 156 pm. As long as there is a difference in the atomic size difference of 15%, substitutional diffusion takes place in the system after melting and during solidification. The Cr and Ni atoms will replace the Fe in the bulk of the melt which will also lead to formation of new interstitial sites in the new alloy system. This system will have a concentration gradient in terms of carbon with the base metal. The carbon will start occupying the interstitial sites in the new system and this will lead to an increase in the carbon weight percentage of the surface alloyed layer. As the alloying elements concentration in the surface alloyed layer stops after a certain depth of saturation, the interface layer between the surface alloyed layer and base metal has high concentration of carbon but no alloying elements thus forming colonies of pearlite. As Ni and Cr are relatively important as compared to the other alloying elements on account of their properties relative to solution strengthening, austenite stabilization, ferrite stabilization

and corrosion resistance, we would be referring to the phase diagrams for Fe-Ni (De Keyzer, Cacciamani, Dupin, & Wollants, 2009) and Fe-Cr (Okamoto, Kacprzak, & Subramanian, 1996) systems shown in figures below.

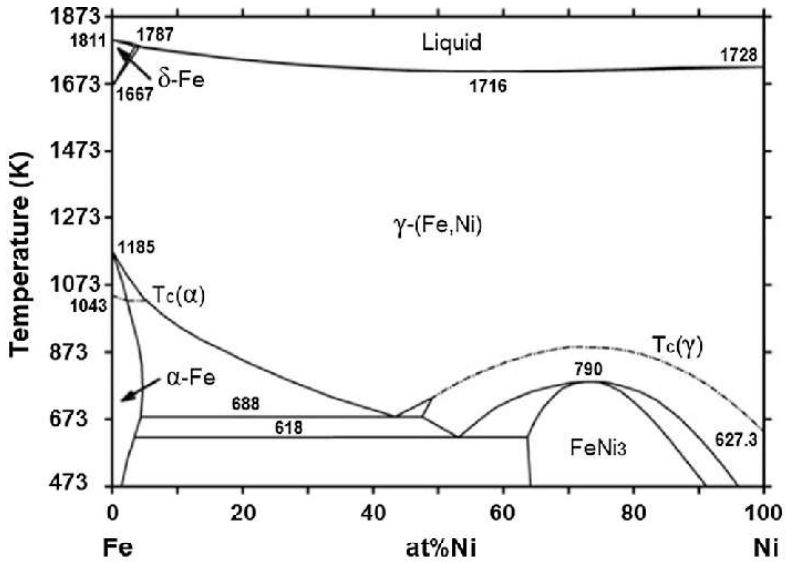

Figure 4.1: Fe-Ni system phase diagram

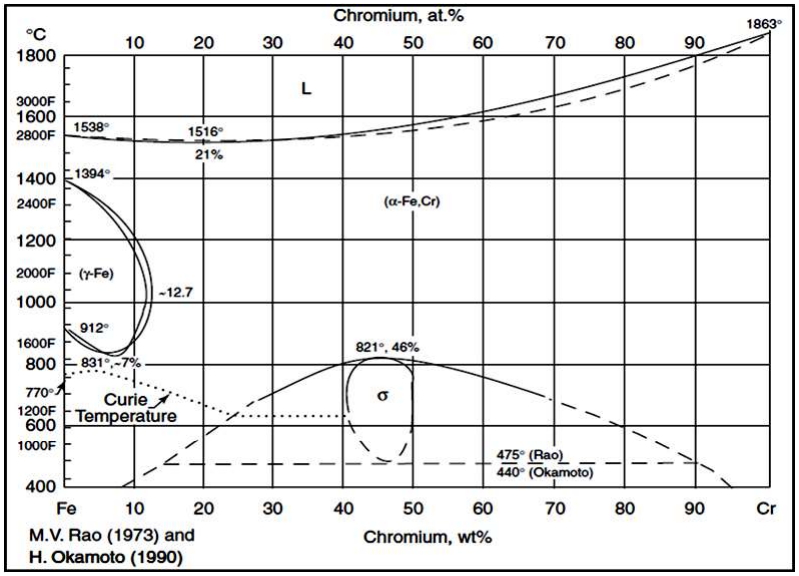

Figure 4.2: Fe-Cr system phase diagram

The melting points of Ni at 1455 °C, Mn at 1246 °C and Si at 1414 °C are lower than that of WCB steel which melts at approximately 1460 °C and a superheat of 300 °C was used. Pouring temperatures were used in the range of 1760 °C to achieve good fluidity and the melt

can flow through the mold cavity as well initiate the alloying and diffusion of the alloying elements. Cr and Mo have higher melting points at 1907 °C and 2623 °C but the alloying of these elements occurs on account of dissolution and then diffusion into the iron melt. There were certain regions of the surface alloyed layer which had higher Cr content than Ni while some regions showed deficiency of either alloying element. This could be attributed to the convection currents set into the melt on account of flow inside the melt cavities which erodes the alloying powder from the mold core surface in the case of REFCOTEC Refcohol 1010 binder.

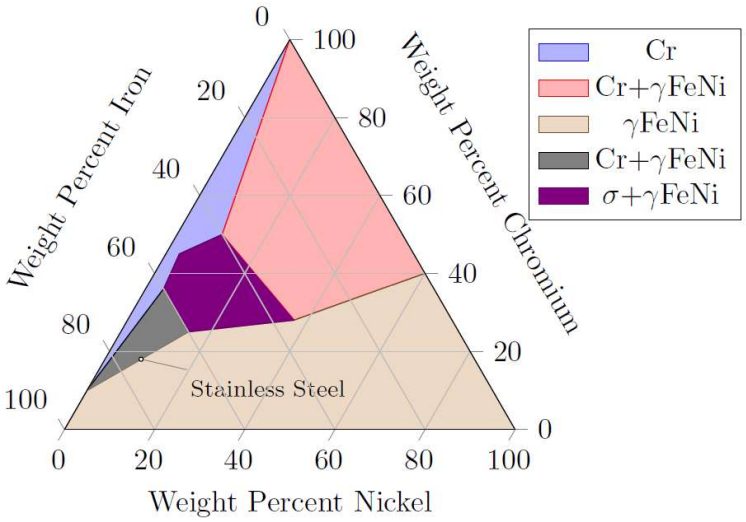

Figure 4.3: 300

It can be seen in a majority of the samples that the base metal has varying microstructures. This is attributed to the concentration of carbon and heat treatment performed on the sample. Additionally, the cooling rate of the melt will affect the microstructures. WCB steel has a ferrite-pearlite microstructure after it has been heat treated. On account of melt conditions being different as compared to industrial pouring environment, the microstructure of the base metal is different. The cooling rate was faster as compared to the industrial conditions on account of the small size of the melt as well as the relative thickness of the mold. One of the other factors was the possibility of excess carbon diffused into the melt. This can come from the graphite crucibles used for melting. Though the crucibles are coated with Zirconia wash, at temperatures approximately 1700 °C, a small crack in the wash can lead to carbon being dissolved and diffused into the melt.

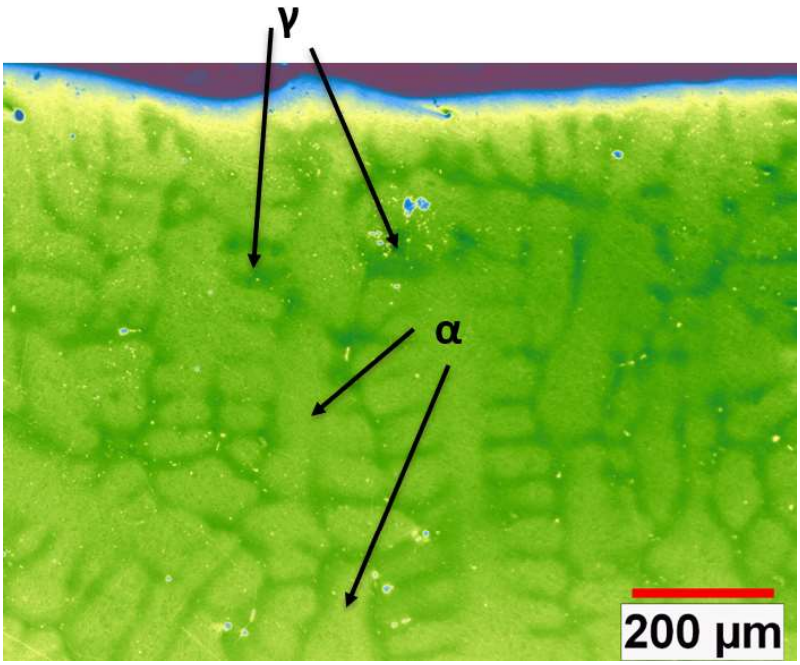

Figure 4.4: R5 optical micrograph showing the presence of a dendritic microstructure which suggests complete melting and solidification of the slurry. The austenite and ferrite phase has been marked in the microstructure.

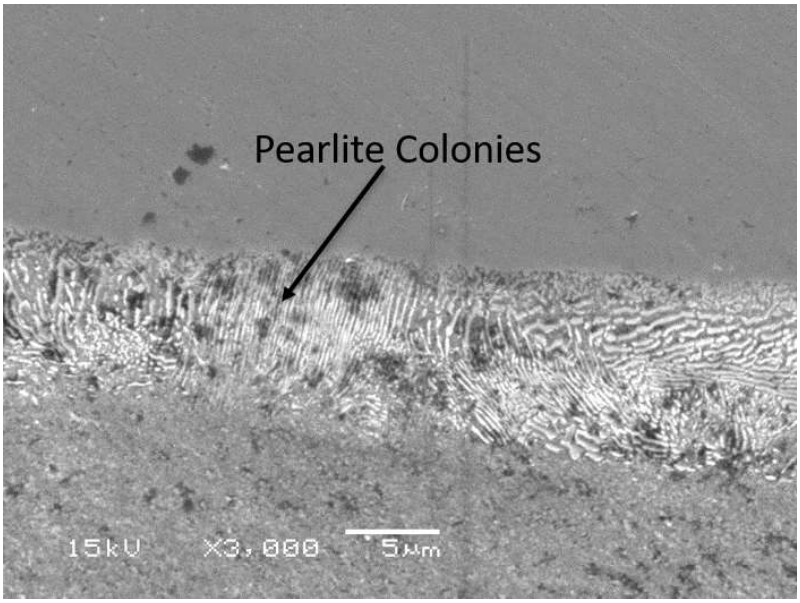

Figure 4.5: Colonies of pearlite formed at the interface layer between the surface alloyed layer and the base metal are shown.

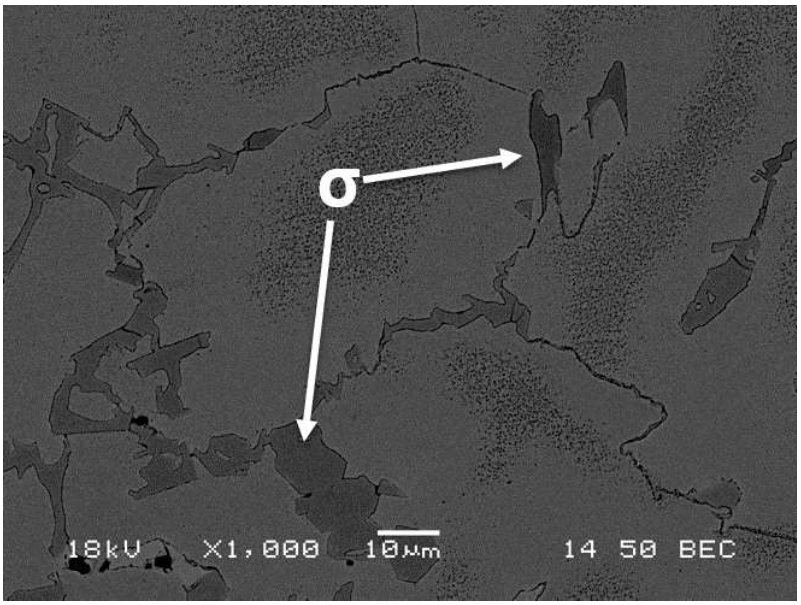

Figure 4.6: The presence of σ phase was confirmed using compositional back scatter electron imaging showing the grain boundaries and the Cr rich σ phase formed at the grain boundaries.

One of the results observed during the EDS analysis is the quantification of carbon weight percentage in the surface alloyed layer and the base metal. The results for both EDS analysis show the weight percentages above 1% and in some cases, as high as 7%. While this can be on account of excess carbon from the water based binder diffusing into the melt or from the graphite crucible diffusing into the melt at the UWM Foundry Lab trials, it does not explain the reason for such high carbon levels in industrially cast samples. As the melt is solidifying and the concentration gradient in the surface alloyed layer aids substitutional diffusion of Cr and Ni into the Fe melt, new interstitial sites would be created as Cr and Ni have similar atomic sizes as that of Fe. This would lead to an increase in the weight percentage of carbon in the surface alloyed layer and base metal assuming no excess carbon diffuses from the sand or the binder. Even in this case, the bulk melt does not have enough carbon to saturate the surface alloyed layer up to 7 weight %. Additionally, the microstructure that is formed, according to practical observations and theoretical phase diagrams as shown in figure 4.7, is austenite, ferrite and M23C6 carbides formed in the surface alloyed layer with Cr carbides being the primary carbides formed. The maximum solubility of carbon in such a system according to figure 4.7 would be limited to 0.6 mass % and thus, the obtained results of weight percentage of carbon higher than 1 would not be theoretically possible. One of the primary reason could be the inability of the EDS software to read the difference between the L lines of Cr and C. As the

weight percentage of Cr is high, the analysis could be inaccurately considering the L line of Cr as C and thus elevating the weight percentage of carbon in the surface alloyed layer.

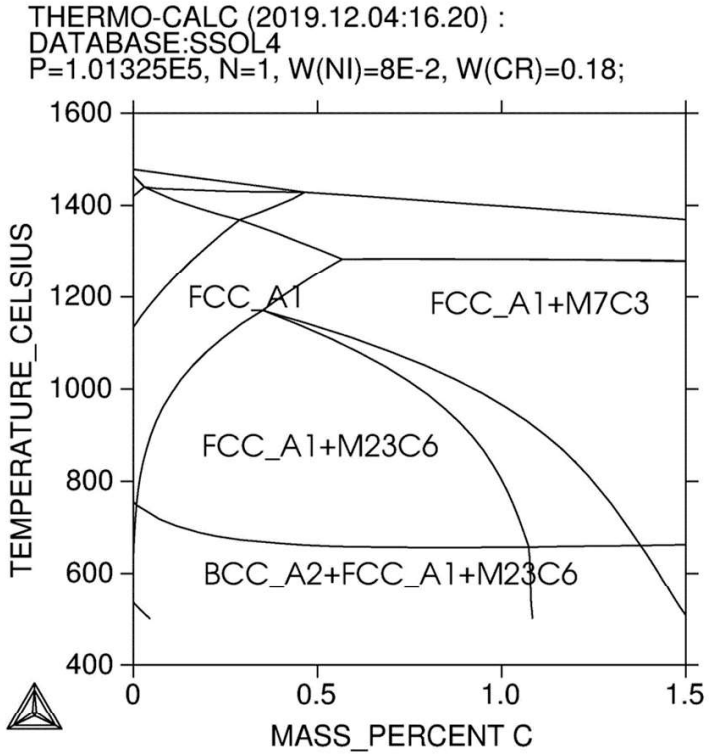

Figure 4.7: Fe-Ni-Cr-C phase diagram with varying levels of carbon showing the expected phases to be formed in a sample with 18 weight % Cr and 8 weight % Ni generated in ThermoCalc using SSOL4 database. Courtesy: Dr. Benjamin Church, University of Wisconsin - Milwaukee.

The base metal shows similar results in terms of carbon weight % which would not be expected as WCB steel has a maximum of 0.3 weight % carbon as a part of its composition. A weight % higher than 2 would lead to formation of grey cast iron with the microstructure showing presence of carbon in form of graphite plates. The presence of elevated carbon weight percentages can be explained in the UWM Foundry Lab samples as the presence of cracks in the refractory wash applied to the graphite crucible used for melting could lead to excess carbon being diffused into the steel melt from the crucible. There was experimental proof of the same on account of pitting observed on the graphite crucible surface. Another reason could be the components present in the water based binder which could lead to the elevation of carbon in the sample. This does not explain the presence of carbon in the samples made at Maynard

Steel and Badger Alloys as the binder used was alcohol based and the powders were not mixed into the binder. The alcohol based binder, REFCOHOL 1010, is used in the foundry industry to coat the mold cavity in order to prevent any reaction between sand and steel. Thus, the samples made in Maynard Steel and Badger Alloys should not show any presence of elevated carbon in the surface alloyed layer or the base metal, but the carbon weight percentage is higher than 1 weight %.

The mounting powder used for the study was phenolformaldehyde compound. The carbon from the compound can possibly cause the carbon weight % reading to rise as the surface alloyed layer that is analyzed is next to the mounting compound. The L line spectrum of EDS shows a high intensity of carbon for every sample that was analyzed during this study. An example of this is seen in figure 4.8.

As there are discrepancies in the EDS data in terms of carbon weight percentage, it is not explained on account of the phases observed via optical microscopy or using XRD analysis. The use of spark spectroscopy also revealed that the base metal has 0.3 or less weight percentage of carbon which was not matching the results obtained using EDS. Spark spectroscopy could not be performed on the surface alloyed layer as the thickness of the surface alloyed layer was not high enough to sustain grinding to even the as-cast surface. Additionally, the use of spark spectroscopy would lead to vaporization of the surface alloyed layer as well as the base metal which can lead to inaccuracy in the carbon weight percentage. Thus, it is recommended to understand that the carbon weight percentage in the samples can be misleading and thus more emphasis is to be put on the XRD patterns, microstructures and the weight percentages of Cr, Ni and Mn in the surface alloyed layer.

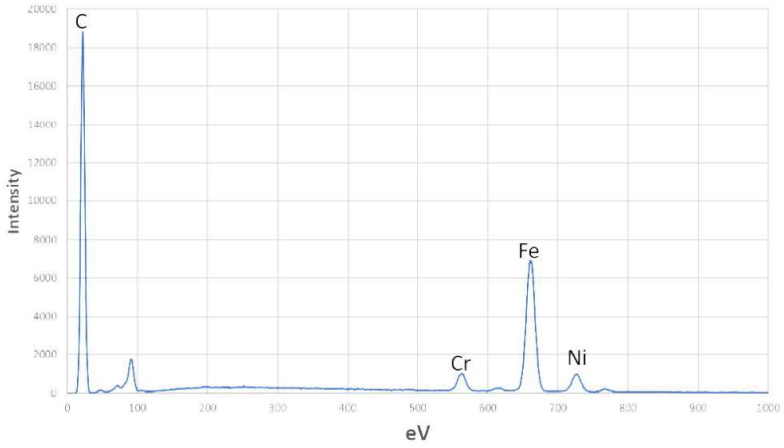

Figure 4.8: Sample 97 cast at Maynard Steel with Ni and Cr as alloying powders. eV vs Intensity obtained using EDS. The intensity of C is shown to be higher than that of Ni, Cr, and Fe which is lower in intensity.

The UWM Foundry samples were made to control the depth of surface alloying. Over the range of the previous samples, the probability of surface alloying of the casting was high but the control of the thickness of the surface alloyed layer was low. This was addressed in the samples made in this set of experiments at the UWM Foundry Lab in small melt sizes. The 12 samples made in this batch included a set to understand the maximum depth up to which surface alloying can be achieved in lab experiments. On account of the small pour sizes, the maximum targeted depth of surface alloyed layer was limited to 4000 μm. The first four samples were surface alloyed with a slurry composition that is comparable to that of 316L stainless steel. The objective was to alloy the powders with the Fe from the base metal to form a surface alloyed layer that is similar to austenitic stainless steel.

Figures 5.54 to 5.73 were from samples made in the UWM Foundry Lab to test the feasibility of REFCOTEC REFCOBAR 1010 gel as a binding agent. The binder lacked any refractory agent such as Zirconia which made it possible to mix the alloying powders into the binder to form a slurry which could be directly applied to the mold surface. As the mold surface is coated with metal powders at a temperature lower than that of the melt, it would act as a heat sink for the melt. The powders present on the sand mold would lead to increased rate of solidification on the mold surface. This is confirmed by multiple characterization techniques as etching reveals a microstructure different as compared to the base metal, EDS shows difference in elemental composition, XRD shows phase change and Spark Spectroscopy confirms the difference in weight

percentages of alloying elements in the base metal and in surface alloyed layer. The crucibles used in the experiments were graphite crucibles which were coated with Zirconia wash to prevent any contact of molten steel with the carbon. While the wash is designed to sustain high temperatures, microcracks formed in the wash surface can lead to significant amounts of carbon being added to the microstructure. This is more visible in the microstructures of samples R1, R5, R6, R7 and R8 with increased concentration of dark phase which is essentially carbon rich. The figures 5.54 to 5.73 show good consistency in the thickness of the surface alloyed layer as well as absence of defects on the surface alloyed layer. The absence of any cracks running from the outer surface to the interface confirms the integrity of the alloyed layer. A crack running from the surface to the bottom would lead to water coming in contact with base metal and initiating corrosion. Though there are minor defects present in the surfaces or the base metal in form of gas porosities, pinholes, and blow holes, these can be eliminated under industrial conditions as working with steel in the UWM Foundry Lab is limited due to the quantity of melt which can be poured. Most of the surface defects can be machined off, which usually takes place in the industry post casting and the remainder of the surface alloyed layer would act as the corrosion and wear resistant layer in the casting.

Energy Dispersive Spectroscopy was used for measuring the elemental composition of the samples. As the surface alloyed layer and the base metal have varying compositions, the confirmation of surface alloying can be made by performing an EDS analysis. The goal was to achieve a composition comparable to that of a contemporary alloy such as 316L or 2205 DSS. From previous results of samples made Maynard Steel and Badger Alloys, it was observed that there is not a straight correlation between the elemental composition of the surface alloyed layer and the corrosion or the hardness of the samples. Thus, the primary goal is to verify the occurrence of surface alloying followed by its closeness to a contemporary stainless steel alloy currently being used in the industry which was targeted in the surface alloyed layer.

Three tests were performed to calculate the elemental composition of the samples. Point and ID has been used for measuring the composition in individual phases of the microstructure, x-ray mapping has been used for finding the distribution of the elements over the area of the surface alloyed layer and line scans to track the drop in concentration of alloying elements through the surface alloyed layer and to identify the interface layer in the sample.

As the process used in the study was designed to achieve a composition in surface alloyed layer which is comparable to contemporary stainless steels, it is important to understand the phases

formed in the surface alloyed layer. This helps to select the correct heat treatment process as well as optimize the composition to obtain desired properties in the surface alloyed layer. An analysis of the base metal without any surface alloying was also performed to observe the differences in the phases formed. The analysis of 316L SS, 2205 DSS and the 316L SS alloying powder was also performed for comparative study.

A critical component of phase identification included the identification of oxide layer in the surface alloyed layer. Chrome oxide is one of the passivation layers which is formed on the surface of stainless steels due to the high content of chromium as an alloying element. This passivation layer provides protection from iron oxide formation on the surface of the components and imparts the stainless properties (Cheng, Feng, Li, Dong, & Li, 2011).

The layers are formed on casting but they are further enhanced by post heat treatment processes and passivation of the samples. The technique for heat treatment varies with the type of alloy used but in this study, two primary heat treatment techniques have been explored. The normalizing and tempering treatments were performed by Maynard Steel for all the samples cast at the Maynard Steel while solution annealing was performed for the UWM and Badger Alloys samples as the samples were received in as-cast condition.

The Maynard Steel samples were made to replicate an elemental composition in the surface alloyed similar to 316L SS. As the technique required sprinkling of the alloying powders over the surface, the retention of the alloying powders was an issue leading to variation in the composition reached and phases formed in the samples. The samples were previously heat treated at Maynard Steel by normalizing at 894 °C for 1 hour per inch followed by air cooling and tempering at 535 °C for 1 hour per inch followed by water quenching.

Chapter 5

Results

5.1 Maynard Steel (Ni and Cr)

5.1.1 Sample 92

Sample 92 was cast at Maynard Steel with the aim of enrichment of the top surface. As the binder was REFCOHOL 1010 and the powder was sprinkled on the binder, there was probability of some powder loss. The sample spectrum shows a peak of ferrite at 44.8° as well as the presence of chromium iron is observed in the spectrum which can also be observed in 4.2. As the samples have been heat treated by Maynard Steel, the formation of oxide layers is dependent on the concentration of alloying elements in the slurry. From the peak present at 35.5°, Chrome oxide has been verified in the surface alloyed layer. This could lead to a higher corrosion resistance in the surface alloyed layer as compared to WCB steel.

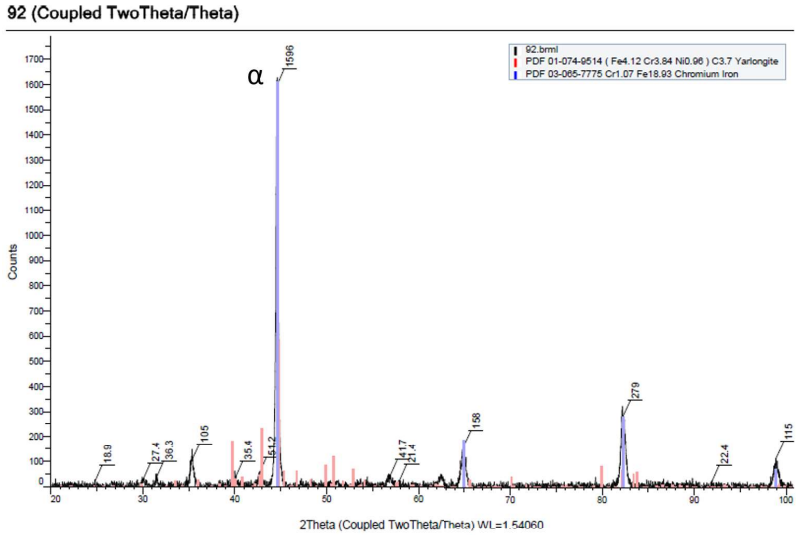

Figure 5.1: XRD plot of sample 92. The alloying powder used for composition is 1.61 grams of stainless steel powder.

5.1.2 Sample 95

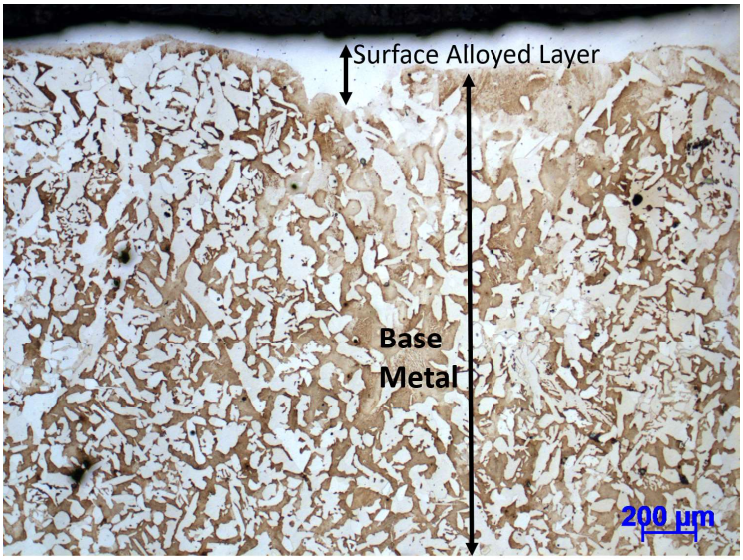

Figure 5.2: Optical micrograph of the surface alloyed layer and base metal of sample 95 cast at Maynard Steel followed by normalizing and tempering. The composition of the slurry for the surface alloyed layer included 2 grams each of Ni and Cr. The light phase is ferrite and the dark phase is pearlite.

The sample was cast at Maynard Steel using lab grade Ni and Cr as the alloying elements for the surface alloyed layer. The base metal was WCB and the casting was normalized and tempered after shake out. The normalization temperature was 898 °C and performed for 1 hour per inch and the tempering was done at 535 °C and performed for 1 hour per inch thickness of WCB. The microstructure of the base metal shows presence of ferrite and pearlite with a well defined interface separating the surface alloyed layer from the base metal. There are pinholes present in the surface alloyed layer which can be on account of dissolved gases present in the melt. The consistency of the depth of surface alloying is low and the surface alloyed layer is absent in a section. This can be on account of the liquid melt pushing powders from the mold core before the diffusion process begins.

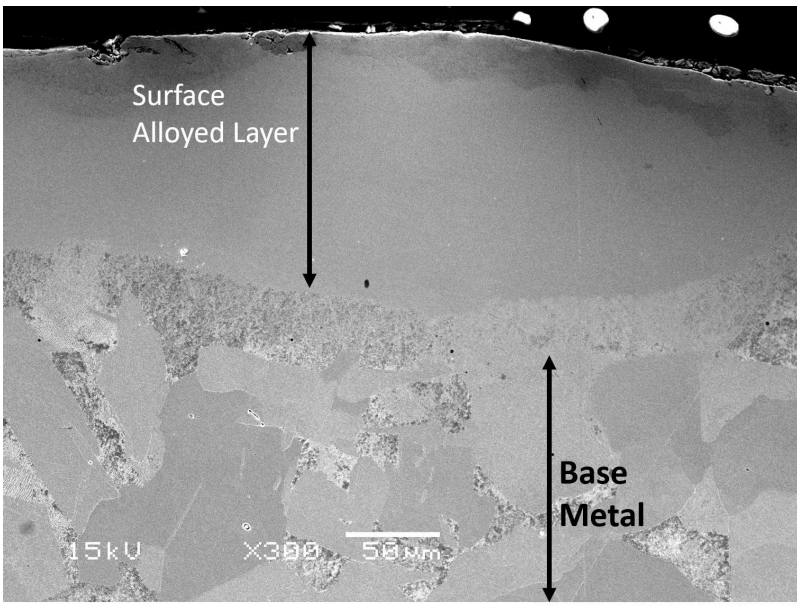

Figure 5.3: SEM image of sample 95 cast at Maynard Steel showing the surface alloyed layer and the base metal along with the interface.

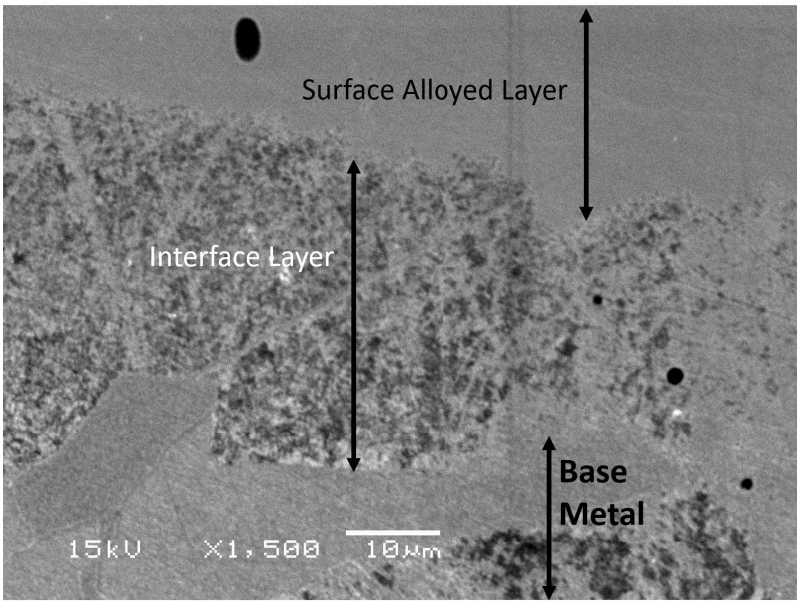

Figure 5.4: SEM image of the interface layer showing colonies of pearlite between the surface alloyed layer and the base metal of sample 95 cast at Maynard Steel.

The magnified view of the interface between the surface alloyed layer and the base metal also shows presence of microporosities. After performing an EDS scan of the interface, it was confirmed that the amount of carbon in the interface is higher than that of the surface alloyed layer. The EDS confirms that the surface alloyed layer is enriched in Ni and Cr with the concentration of the alloying elements decreasing gradually in the interface towards the base metal.

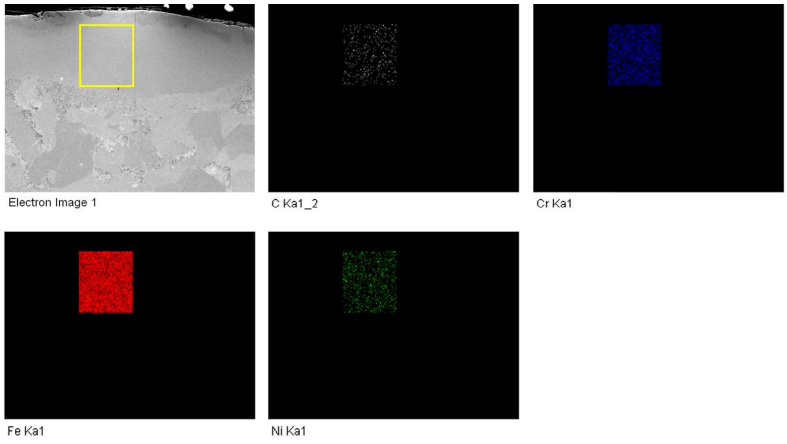

Figure 5.5: EDS X-Ray map of the surface alloyed layer for identifying the alloying elements.

The elemental composition of the alloying elements in the surface alloyed layer as determined

by EDS is given in the table below:

Element	Weight%
Ni	2.04
Cr	4.82
C	1.77
Fe	Balance

Table 5.1: Elemental composition of the surface alloyed layer of the sample 95.

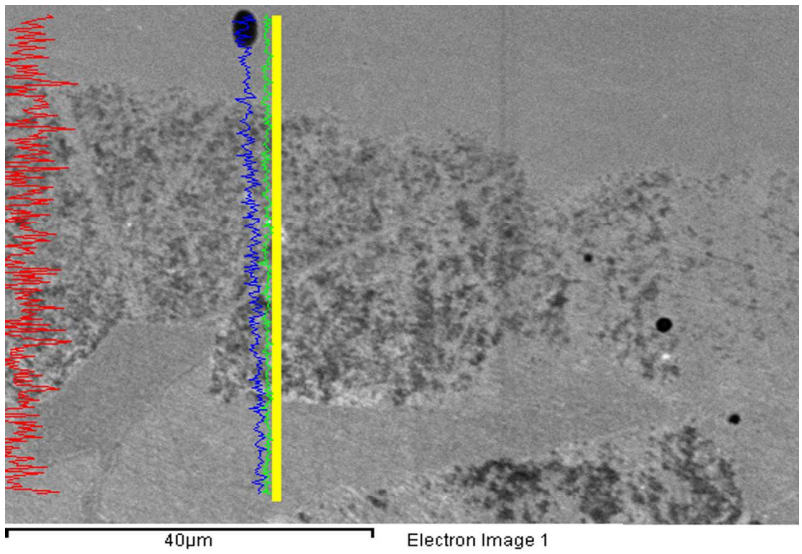

Figure 5.6: EDS line scan of the interface between the surface alloyed layer and the base metal of the sample 95.

The elemental composition of the interface between the surface alloyed layer as determined by EDS and the base metal is given in the table below:

Element	Weight%
Ni	1.08
Cr	2.69
C	2.65
Fe	Balance

Table 5.2: Elemental composition of the interface of the sample 95.

5.1.3 Sample 96

The surface alloyed layer is free from microporosities, blowholes and cracks which are the primary casting defects observed in other samples. The surface alloyed layer has variable depth which can be on account of loss of the alloying powder due to the force exerted by the melt during the pouring process. There is one region where the thickness of the surface alloyed layer is 2 μm and this could lead to erosion of the layer on account of post-processing treatments such as grinding or polishing. This can be avoided by ensuring higher quantities of alloying powders are used for enriching the base metal.

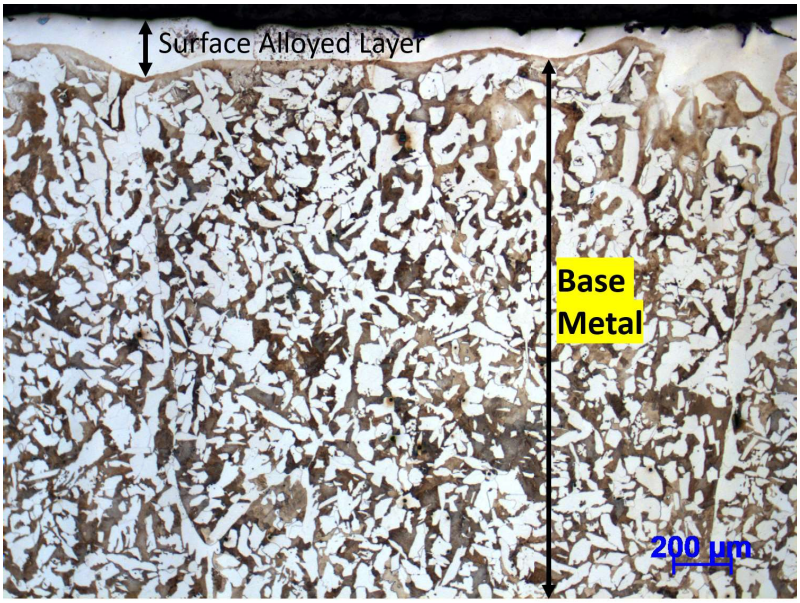

Figure 5.7: Optical micrograph of sample 96 cast at Maynard Steel followed by normalizing and tempering heat treatments. The composition of the slurry for the surface alloyed layer is 2 grams each of Ni and Cr powders.

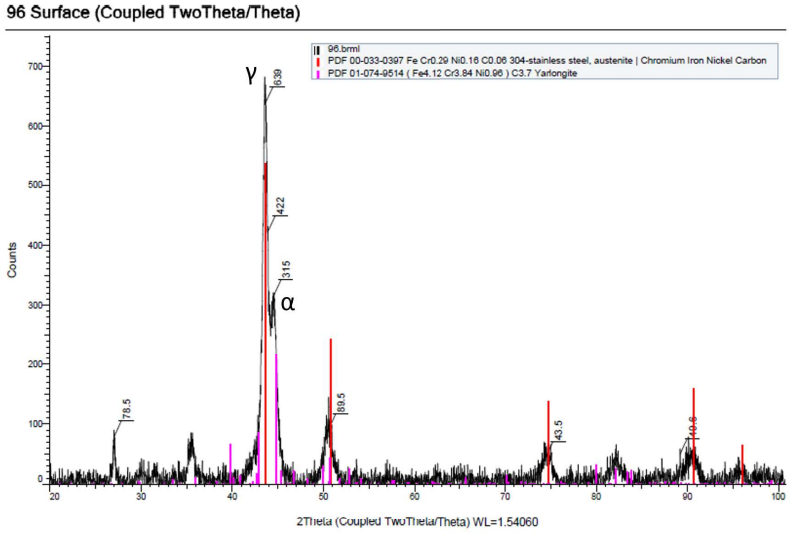

Figure 5.8: XRD plot of sample 96 showing presence of austenite. The surface alloyed layer alloying powder composition is 3.9 grams of Ni and Cr.

Sample 96 was cast at Maynard Steel with Ni and Cr as the alloying elements in the surface alloyed layer. The spectrum shows presence of austenite at 43.5° and ferrite at 45°. As the sample was made at Maynard Steel, it was heat treated after casting by normalizing and tempering. As the chrome oxide layer is already formed, the corrosion resistance would be higher as compared to the base metal. The experiment was targeted to alloy the surface to a composition of 316L SS.

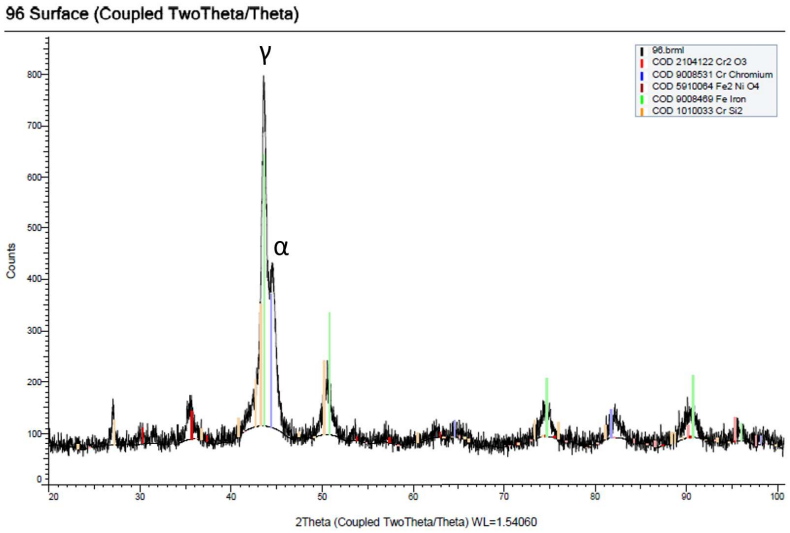

Figure 5.9: XRD plot of sample 96 showing presence of Chromium Oxide. The surface alloyed layer alloying powder composition is 3.9 grams of Ni and Cr.

The SEM of the surface alloyed layer on contrary shows presence of microporosities primarily in the interface layer of the sample. There is cracking of the surface alloyed layer observed on the top section. The interface is continuous through the layer ensures that the alloying process has occurred and the surface layer is not a welded joint formed on top of the WCB steel.

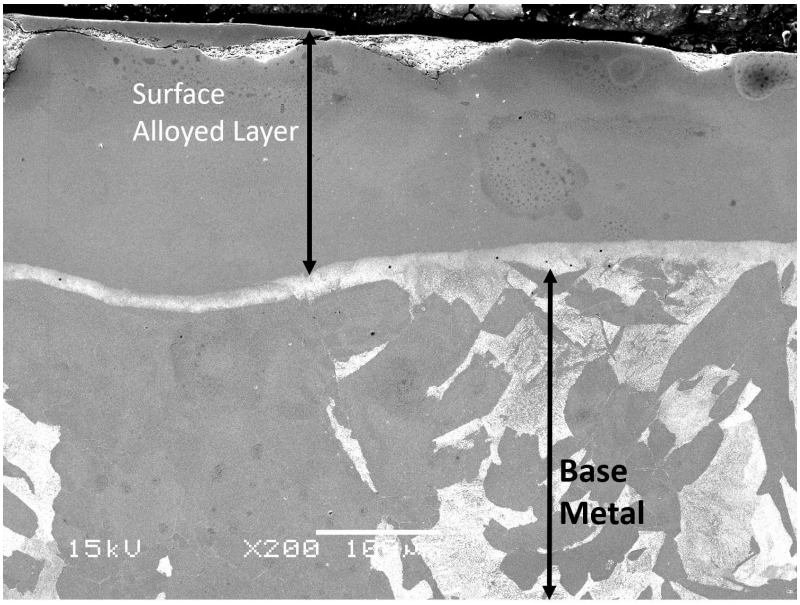

Figure 5.10: SEM image of the surface alloyed layer, interface and the base WCB steel of sample 96 after normalizing and tempering cast at Maynard Steel.

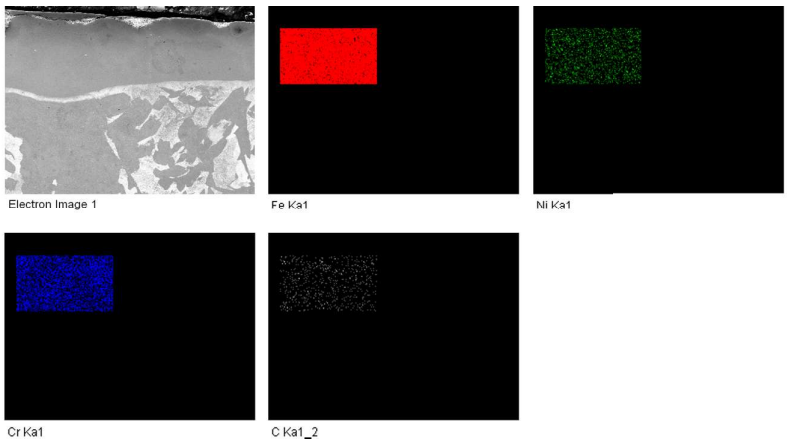

Figure 5.11: Elemental mapping of the surface alloyed layer of sample 96 after normalizing and tempering cast at Maynard Steel.

EDS mapping of the surface alloyed layer confirms the presence of the alloying elements in the surface alloyed layer. The weight percentage of Cr is close to 10 weight% which is the

required quantity for imparting corrosion resistance properties. The weight percentage of Ni is 38% lower than that required for fulfilling the 8 weight% requirement of 316 or 316L stainless steels.

Element	Weight%
Ni	4.89
Cr	9.52
C	2.16
Fe	Balance

Table 5.3: Elemental composition of the surface alloyed layer of the sample 96.

The interface shows a gradual decrease in the alloying elements (Cr-Blue and Ni-Green) and increase in the Fe (Red) as it moves towards the base metal. The weight percentage of carbon increases in this region. This region exhibits the highest rate of M23C6 carbide formation on account of normalizing and tempering heat treatments performed post casting.

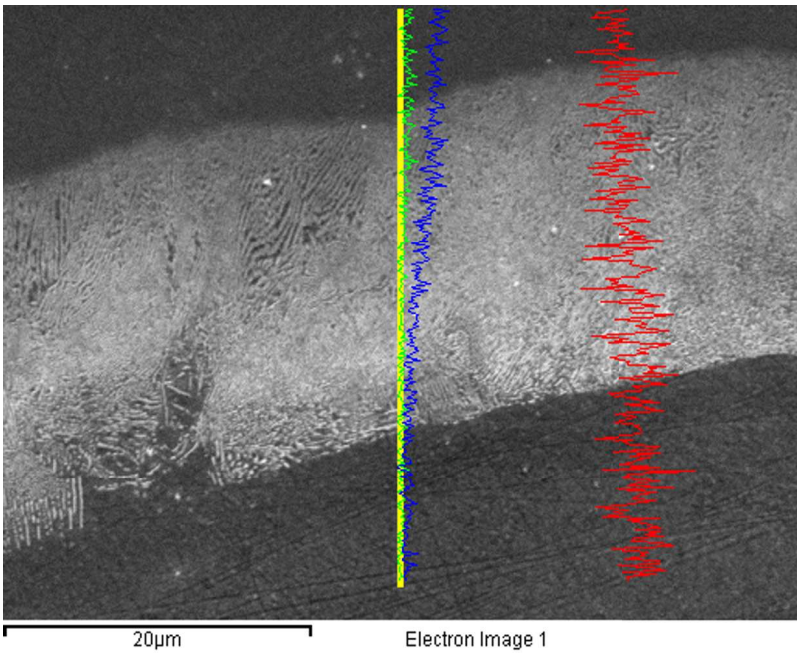

Figure 5.12: Linescan elemental analysis of the interface layer showing colonies of pearlite in sample 96 after normalizing and tempering after casting at Maynard Steel.

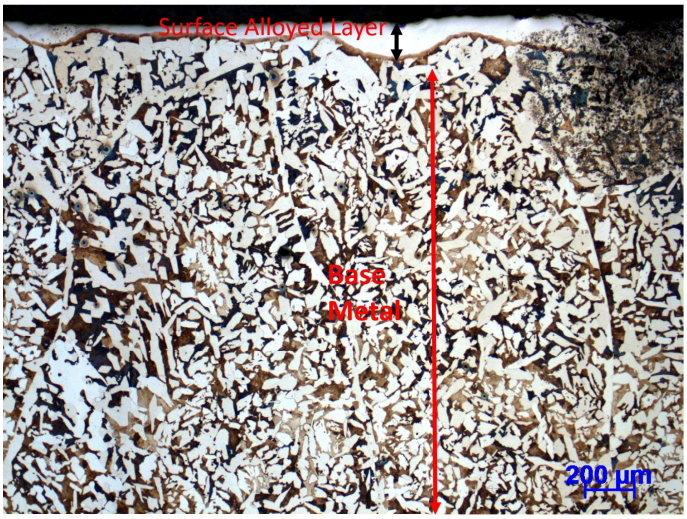

Figure 5.13: Optical micrograph of sample 97 cast at Maynard Steel followed by normalizing and tempering. The composition of the slurry used for surface alloyed layer included 2 grams each of Ni and Cr.

Element	Weight%
Ni	2.17
Cr	3.75
C	2.9
Fe	Balance

Table 5.4: Elemental composition of the interface layer of the sample 96.

5.1.4 Sample 97

The optical micrograph of the sample 97 shows presence of a microstructure of the base metal which is ferrite and pearlite. The surface alloyed layer does not exhibit consistency in the depth of surface alloying but shows absence of any casting defects such as microporosities, blowholes or cracks.

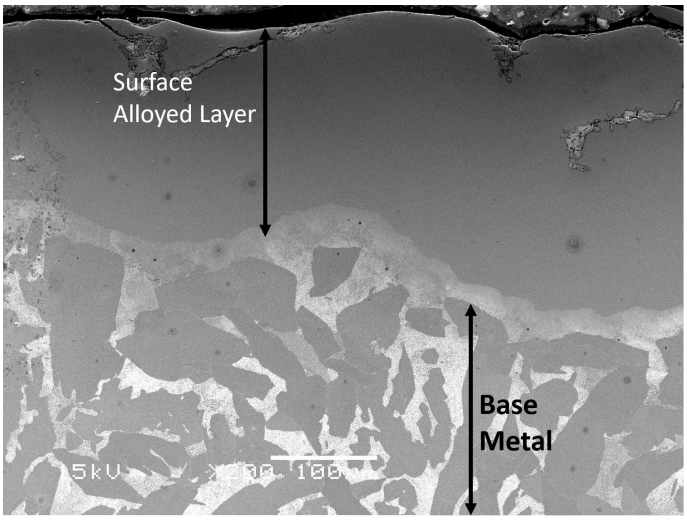

Figure 5.14: SEM image of sample 97 showing the surface alloyed layer, interface and the base metal. The composition of alloying powders used for surface alloying are 2 grams each of Ni and Cr.

The SEM image of sample 97 shows presence of a carbon rich interface between the surface alloyed layer and the base WCB steel which is 10 μm thick on average. The surface alloyed layer shows presence of cracks as well as microporosities. Figure 5.17 focuses on the interface layer of the sample. Though the interface bands of two phases are prominent which do not continue into the base WCB steel or the surface alloyed layer. The darker phases is found to be carbon rich while the lighter phase is rich in iron. The formation of such phases could be due to the heat treatment performed on the samples post casting which has been discussed in the mechanisms of surface alloying chapter.

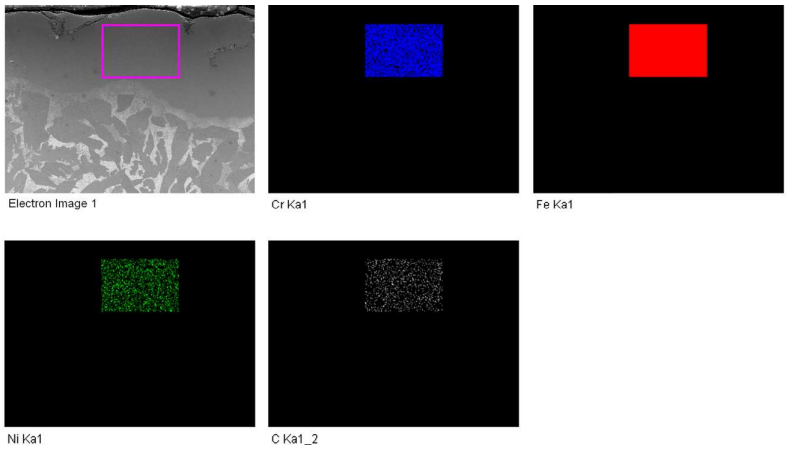

Figure 5.16: Elemental mapping of the alloying elements in the surface alloyed layer of sample 97 after normalizing and tempering cast at Maynard Steel.

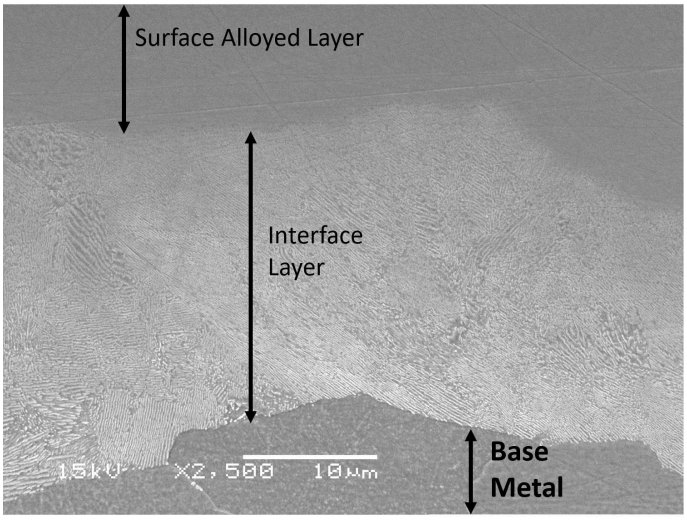

Figure 5.15: SEM image of the interface between the surface alloyed layer and the base metal.

The elemental mapping of the surface alloyed layer confirms the presence of the alloying elements though the quantity of Cr is not high enough to promote the corrosion resistance behavior that is observed in stainless steels. The presence of carbon can be on account of formation of carbides in the surface alloyed layer. This quantity of carbon further increases as the interface is approached. The sample does not exhibit high quantities of alloying elements in the interface as is seen in the case of sample 112.

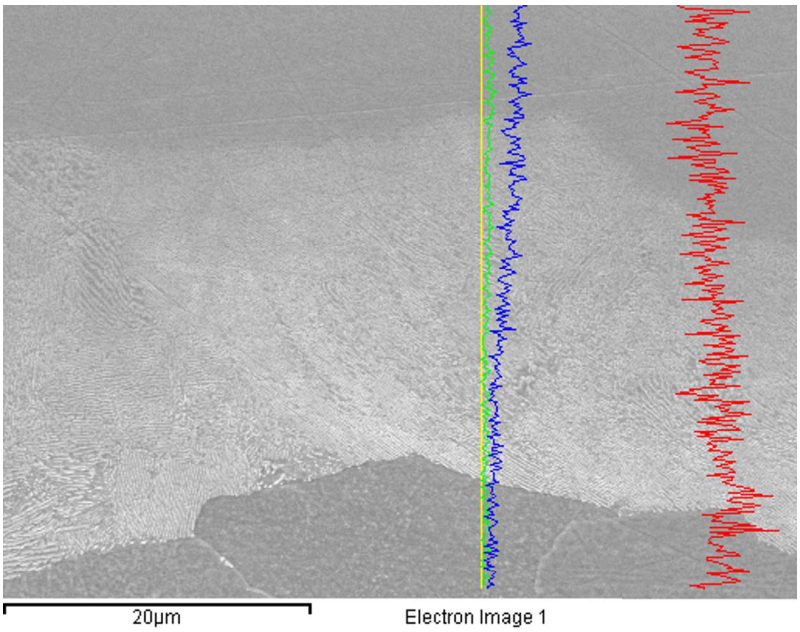

Figure 5.17: Linescan elemental analysis of the interface between surface alloyed layer and the base metal in sample 97 after normalizing and tempering cast at Maynard Steel.

Element	Weight%
Ni	3.38
Cr	7.48
C	2.16
Fe	Balance

Table 5.5: Elemental composition of the surface alloyed layer of the sample 97.

Element	Weight%
Ni	1.76
Cr	3.82
C	3.74
Mn	0.71
Fe	Balance

Table 5.6: Elemental composition of the interface layer of the sample 97.

5.1.5 Sample 112

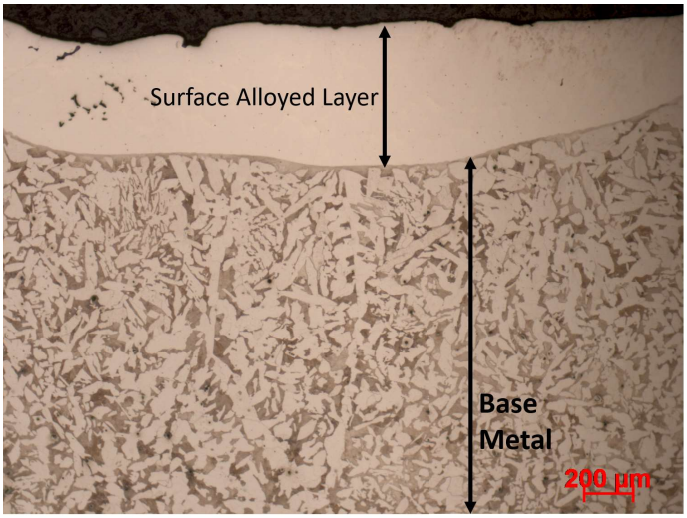

Figure 5.18: Optical micrograph of sample 112 cast at Maynard Steel followed by normalizing and tempering. The composition of the slurry for the surface alloyed layer is 15 grams each of Ni and Cr powders.

There is a well defined interface visible between the base metal and the surface alloyed layer. There are microporosities present in the surface alloyed layer but the thickness of the surface alloyed layer is more uniform as compared to the previous samples. Ferrite and pearlite form the microstructure of the base WCB steel.

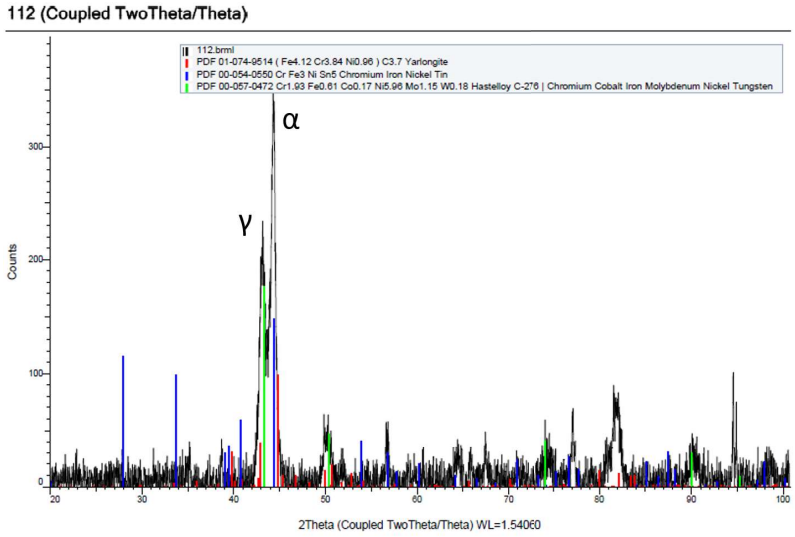

Figure 5.19: XRD plot of sample 112 showing presence of ferrite. The surface alloyed layer alloying powder composition is 15 grams of Ni and Cr.

The elemental composition of sample 112 cast at Maynard Steel consisted of a higher quantity of Ni and Cr. The primary phase in the surface alloyed layer is austenite while a minor peak of chrome oxide is visible around 35°. Though the peak is not intense as compared to the previous samples from the Maynard Steel heat, it would lead to better corrosion resistance as compared to WCB steel.

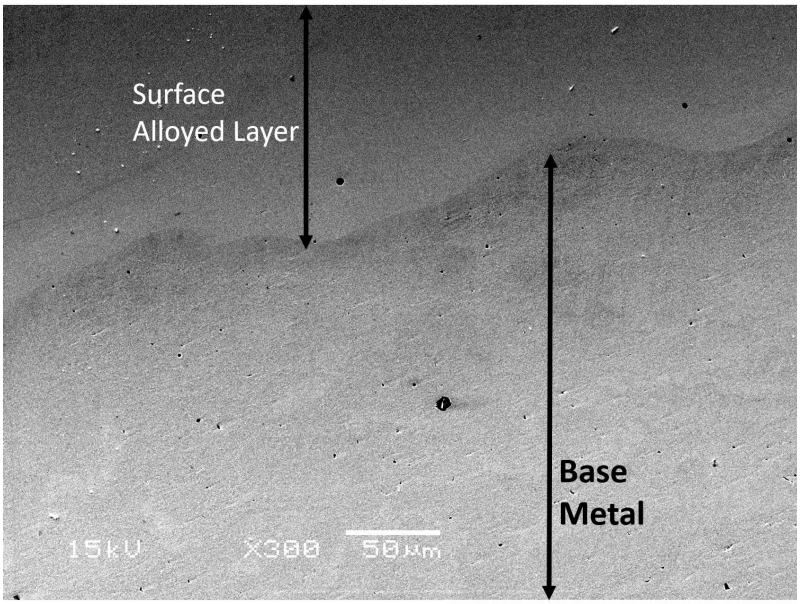

Figure 5.20: SEM image of the surface alloyed layer and the base WCB steel of sample 112 cast at Maynard Steel. The composition of the slurry used for surface alloying included 15 grams each of Ni and Cr.

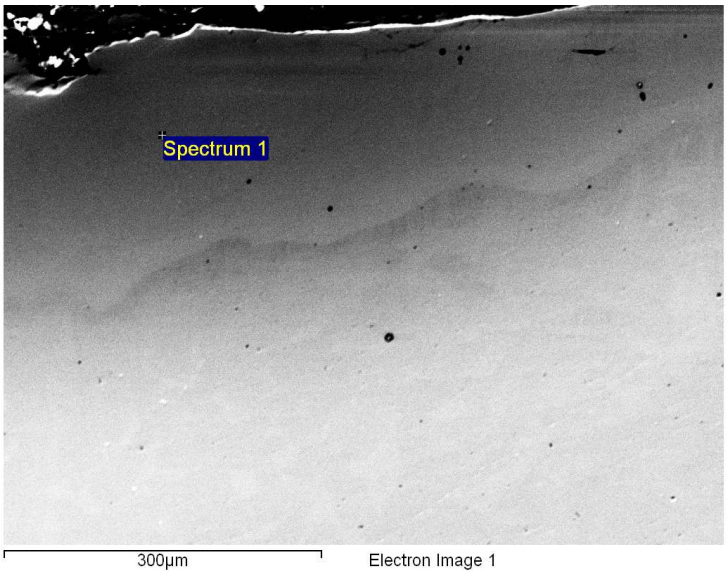

Figure 5.21: Point and ID analysis of the surface alloyed layer of sample 112.

Element	Weight%
Ni	8.48
Cr	10.47
C	1.97
Fe	Balance

Table 5.7: Elemental composition of the surface alloyed layer of the sample 112.

The surface alloyed layer has a high concentration of Ni and Cr in the surface alloyed layer according to the EDS point and ID analysis. Stainless steel alloys have a Cr weight percentage of 10% or higher to promote formation of oxides which aid in corrosion resistance properties of the surface. In 18/8 steels such as 316 or 316L, 8 weight % of Ni leads to solid solution strengthening leading to an increase in the hardness of the sample. The increase in hardness of the surface alloyed layer over the base WCB steel is mentioned in the hardness measurements chapter.

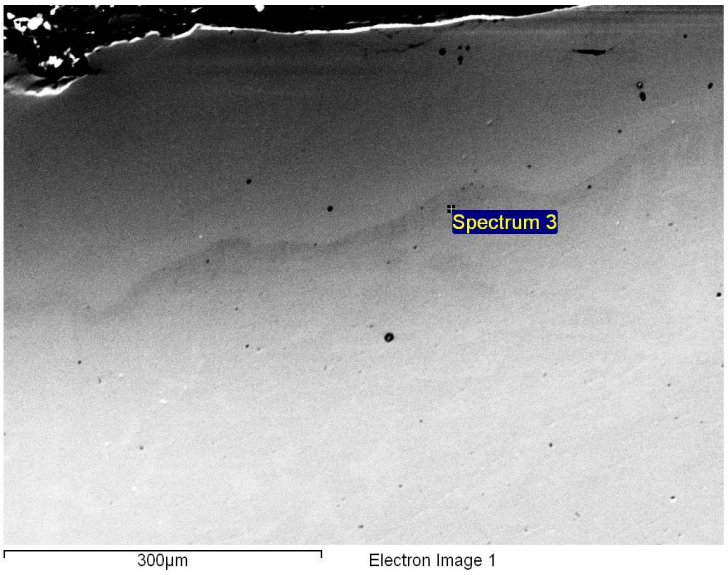

Figure 5.22: Point and ID analysis of the interface between the surface alloyed layer and base metal.

Element	Weight%
Ni	22.17
Cr	15.95
C	25.08
Mn	20.37
Fe	Balance

Table 5.8: Elemental composition of the interface of the sample 112.

As the temperature decreases over the period of solidification and movement of the plane front from the mold surface to the bulk of metal, the melting of alloying powders would decrease and the formation of carbides would initiate.

5.2 Maynard Steel (316L Stainless Steel)

5.2.1 Sample 305

Sample 305 was cast at Maynard Steel using 316L stainless steel powder as the alloying powder for the surface alloyed layer. The base metal was WCB and the particle size of the powder used was 1000 micron and 4 grams of powder was used to coat a mold core of surface area of 0.785 in^2. It was observed that the adherence of 1000 micron particle size of alloying powders is difficult using the REFCOTEC Refcohol 1010 as a binder. The uneven layer of alloying powder led to formation of a uneven surface alloyed layer visible in the optical micrograph.

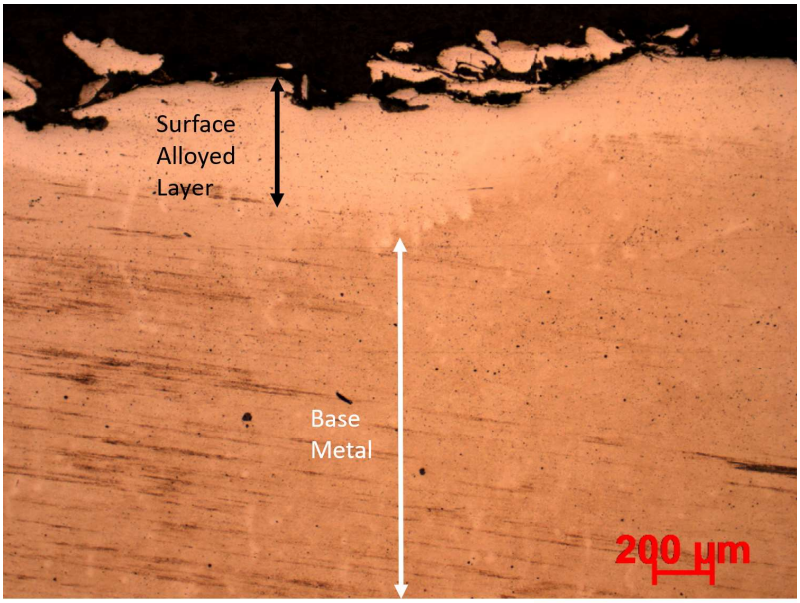

Figure 5.23: Optical micrograph of sample 305 cast at Maynard Steel followed by normalizing and tempering. The composition of the slurry for the surface alloyed layer was 316L stainless steel powder.

The SEM of the surface alloyed layer shows presence of porosity present in the surface alloyed layer. The depth of the surface alloyed layer is inconsistent on account of the higher particle size of the powder. As the powder is not mixed with the binder, there is a possibility of the powder eroding on account of transportation of the push from the molten steel during filling the mold cavity.

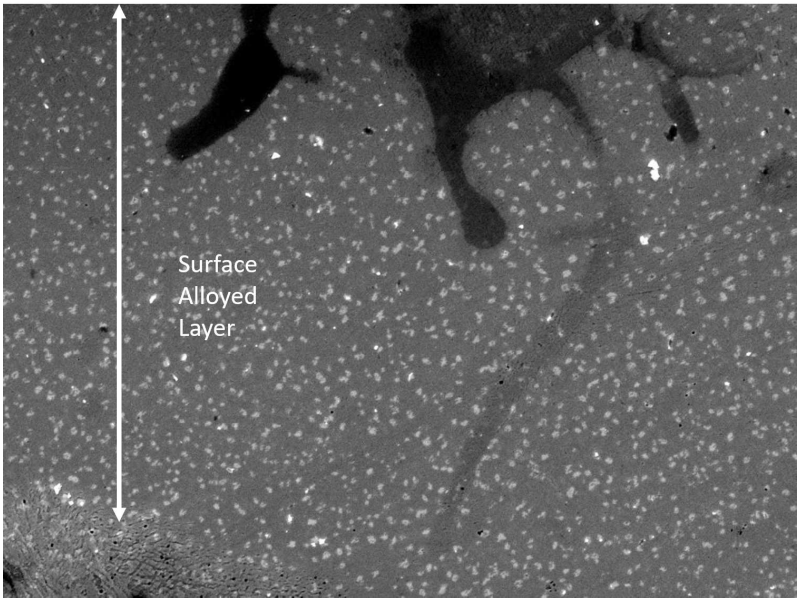

Figure 5.24: SEM image of the surface alloyed layer of sample 305 showing presence of porosities in the surface alloyed layer.

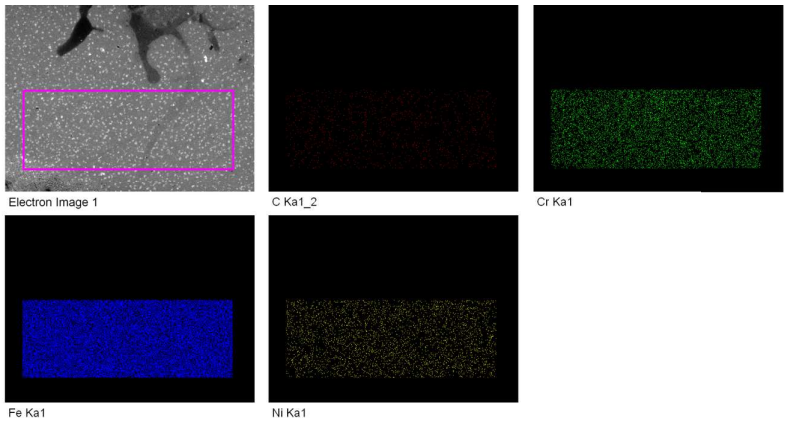

Figure 5.25: Area mapping of the surface alloyed layer of sample 305 to identify the elemental composition of the surface alloyed layer.

EDS analysis confirmed the presence of alloying elements in the surface alloyed layer. As the composition of 316L stainless steel was already achieved in the alloying powders, further addition of WCB steel lead to a higher weight percentage of Fe and lower weight percentages of Ni and Cr in the surface alloyed layer as compared to other trials.

Element	Weight%
Ni	5.58
Cr	5.48
Fe	Balance

Table 5.9: Elemental composition of the surface alloyed layer of the sample 305.

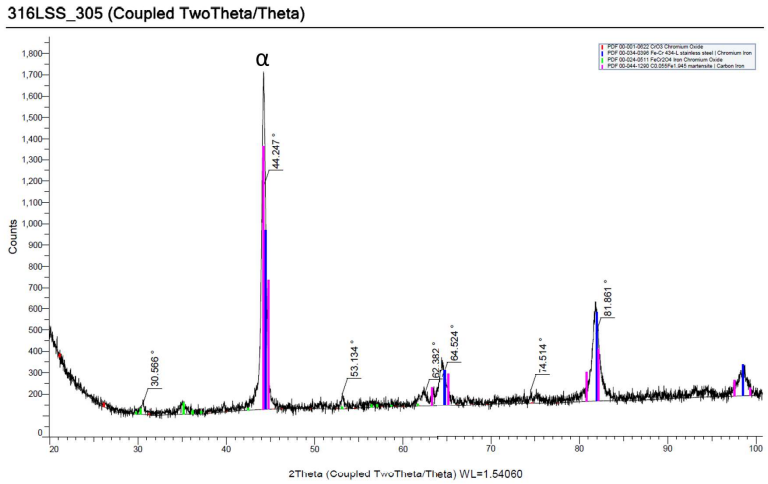

Figure 5.26: XRD plot of sample 305 after heat treatment. The surface alloyed layer alloying powder composition is 4 grams of 1000 μm particle size 316L stainless steel.

The XRD shows presence of ferrite phase in the surface alloyed layer of the sample as the weight percentage of Cr is higher than that of Ni and thus ferrite is stabilized and the weight percentage of Ni is not enough to stabilize austenite as seen in the phase diagram in figure 4.1.

5.2.2 Sample 317

Sample 317 used a particle size of 600 micron and quantity of alloying powder 2 grams of 316L stainless steel alloying powder for the mold surface for the surface alloying process. The smaller particle size allowed for improved adherence of the alloying powder on the mold core surface with REFCOTEC Refochol 1010 as a binder. Thus, the powders did not erode from the mold core surface and created a surface alloyed layer with improved consistency as compared to sample 305.

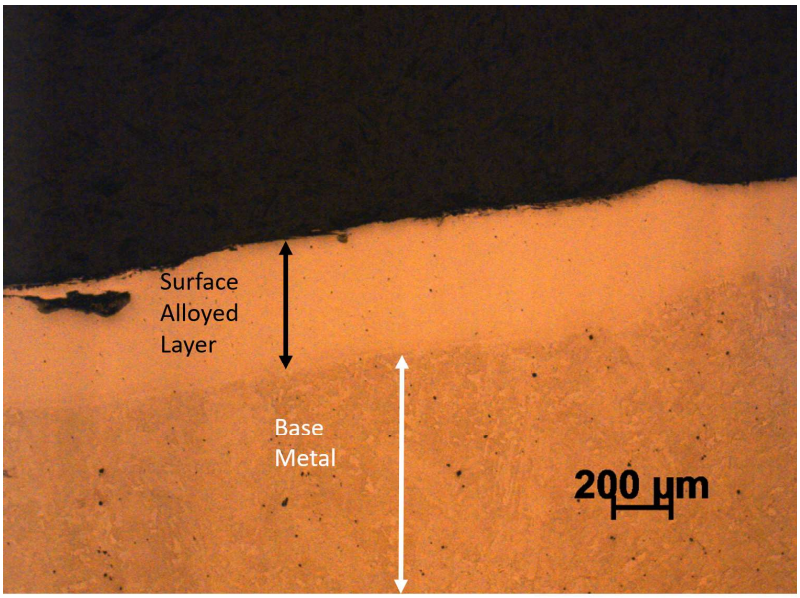

Figure 5.27: Optical micrograph of sample 317 cast at Maynard Steel followed by normalizing and tempering. The composition of the slurry for the surface alloyed layer was 316L stainless steel powder.

The SEM shows absence of microporosities and microcracks in the surface alloyed layer. The interface is not defined in such samples as compared to the other samples cast at Maynard Steel, Badger Alloys, and UWM Foundry Lab. As the carbon is already present in the alloying powder along with iron, the concentration gradient necessary for the carbon from the base metal to diffuse back into the interface of the surface alloyed layer forming pearlite colonies does not take place.

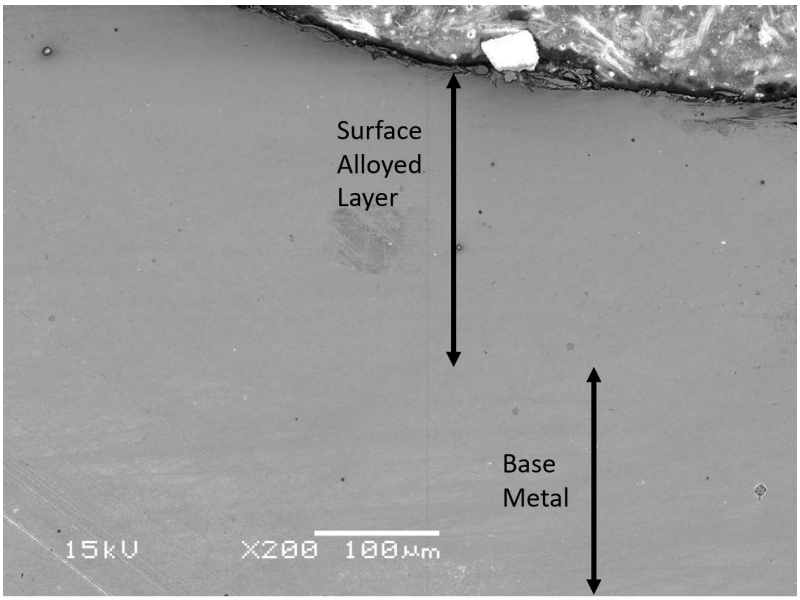

Figure 5.28: SEM image of the surface alloyed layer of sample 317 showing a consistent surface alloyed layer but absence of a clear interface.

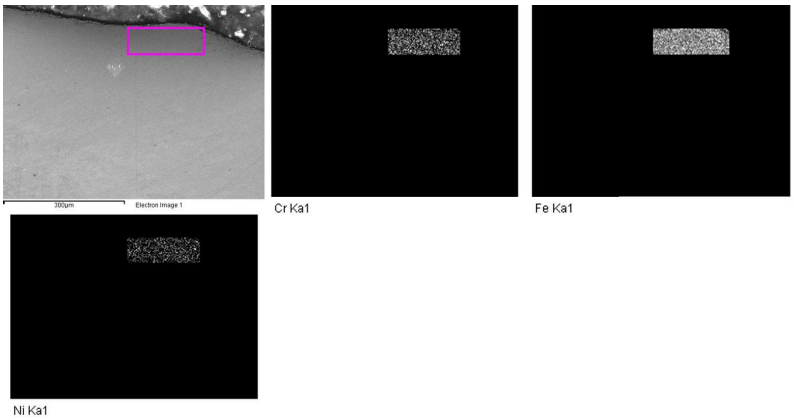

Figure 5.29: EDS mapping of an area of the surface alloyed layer to quantify the alloying elements in the surface alloyed layer.

EDS mapping of the surface alloyed layer confirms the presence of Ni and Cr as alloying elements. The weight percentage of carbon is not calculated using EDS as the hydrocarbons present in the analysis chamber, carbon deposited on the sample surface due to burn from the electron beam or from the mounting powder can lead to incorrect measurements of the carbon weight percentage.

Element	Weight%
Ni	5.14
Cr	5.78
Fe	Balance

Table 5.10: Elemental composition of the surface alloyed layer of the sample 317.

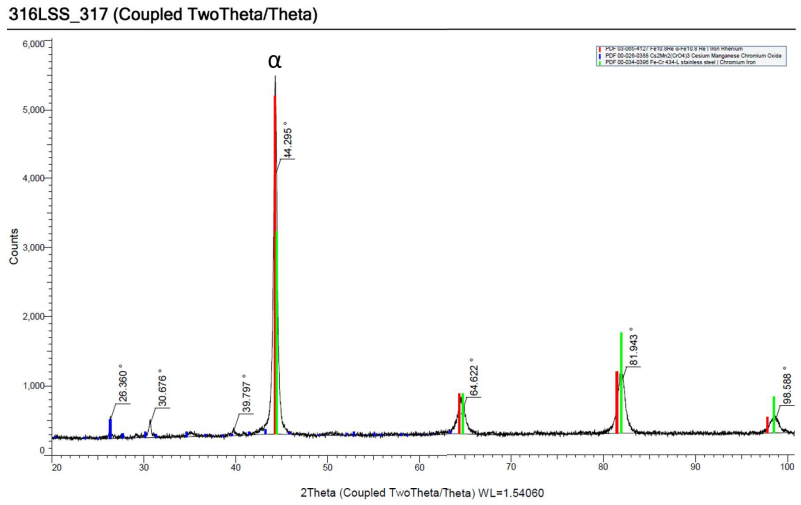

Figure 5.30: XRD plot of sample 317 after heat treatment. The surface alloyed layer alloying powder composition is 2 grams of 600 μm particle size 316L stainless steel.

XRD confirms the presence of ferrite as the primary phases which was also observed in sample 305. Carbides are not observed in the XRD plot of the surface alloyed layer. The low weight percentages of Ni and Cr promote the formation of ferrite phase as compared to the high Cr and Ni weight percentage of 316L stainless steel which promote formation of an austenite phase.

5.2.3 Sample 319

Sample 319 shows another example of the effect of adherence of alloying powders on the mold core surface on the quality of the surface alloyed layer formed on WCB melt. The particle size of the alloying powder used was 600 micron and the quantity of alloying powder was 2 grams. The presence of porosities and cracks can be observed in the surface alloyed layer.

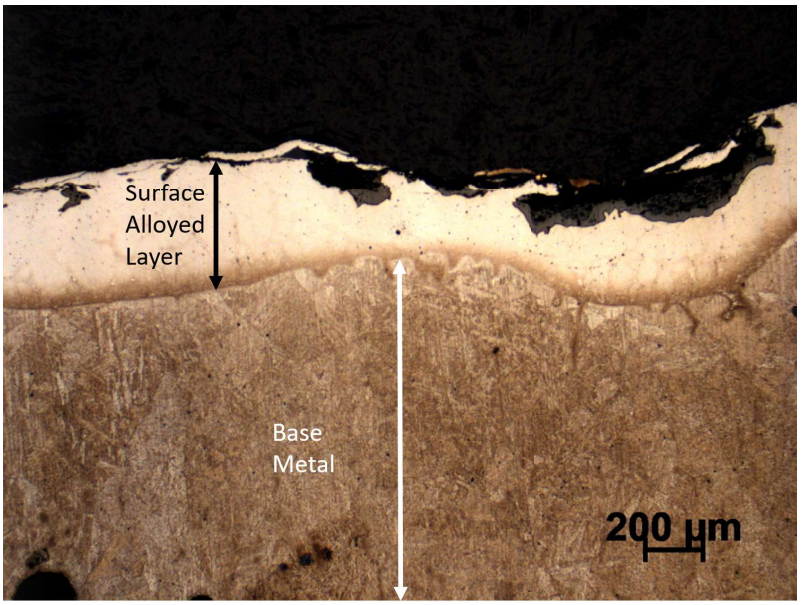

Figure 5.31: Optical micrograph of sample 305 cast at Maynard Steel followed by normalizing and tempering. The composition of the slurry for the surface alloyed layer was 316L stainless steel powder.

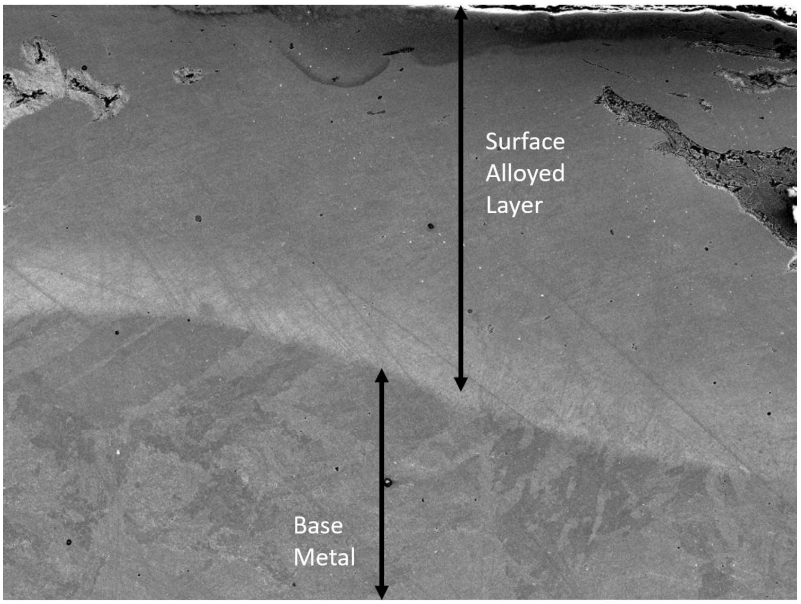

Figure 5.32: 319SEM

SEM shows the presence of a clear interface between the surface alloyed layer and the base metal. Microcracks are also visible in the surface alloyed layer. The interface does not have

colonies of pearlite indicating that the weight percentage of carbon in the interface is lower than 0.6 weight % at which pearlite is observed.

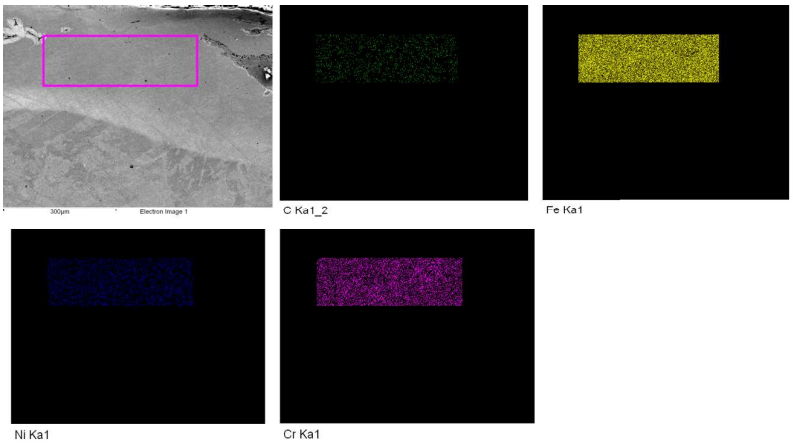

Figure 5.33: 319EDS

EDS mapping of the surface alloyed layer confirms the presence of Ni and Cr as the alloying elements. The weight percentage of Cr is lower than samples 305 and 317 which were cast in the same heat. One of the reason for such low weight percentage can be on account of the melt not reaching a high temperature to promote the complete diffusion of Cr into the steel melt.

Element	Weight%
Ni	4.98
Cr	1.65
Fe	Balance

Table 5.11: Elemental composition of the surface alloyed layer of the sample 319.

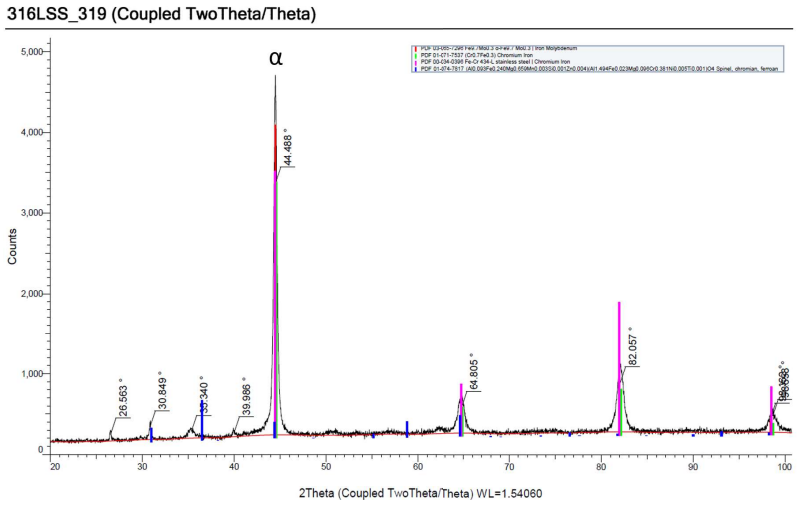

Figure 5.34: XRD plot of sample 319 after heat treatment. The surface alloyed layer alloying powder composition is 2 grams of 600 μm particle size 316L stainless steel.

Ferrite is the primary phase observed in the surface alloyed layer.

5.2.4 Sample 321

The SEM image shows absence of any castings defects such as porosities, cracks or gas entrapment. The interface between the surface alloyed layer and the base metal is visible as compared to the other samples from the same trial.

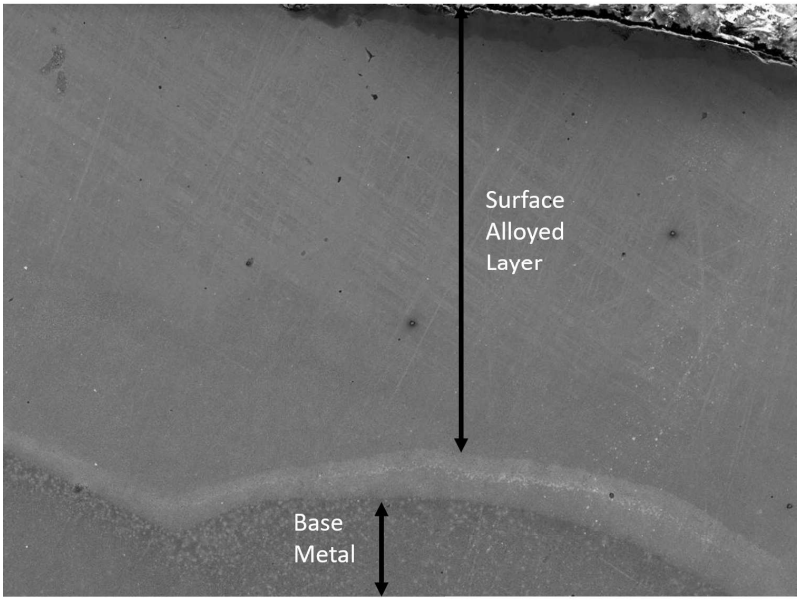

Figure 5.35: 321 SEM

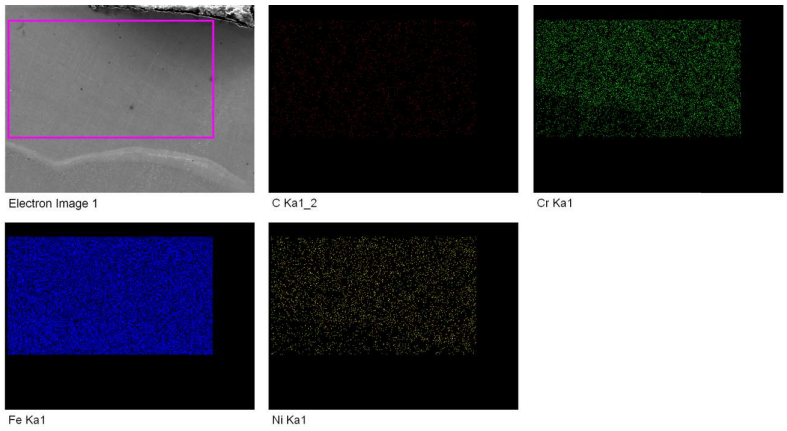

Figure 5.36: 321EDS

EDS mapping confirms the presence of alloying elements in the surface alloyed layer. As the weight percentage of Ni and Cr in the surface alloyed layer is higher, this would lead to more interstitial sites during the diffusion process. The carbon is attracted towards these sites and leads to formation of pearlite colonies at the surface alloyed layer. This phenomenon is also observed in samples from other trials which have a higher weight percentage of Ni and Cr.

Element	Weight%
Ni	5.55
Cr	6.32
Fe	Balance

Table 5.12: Elemental composition of the surface alloyed layer of the sample 321.

The primary phase observed in the surface alloyed layer after normalizing and tempering is ferrite.

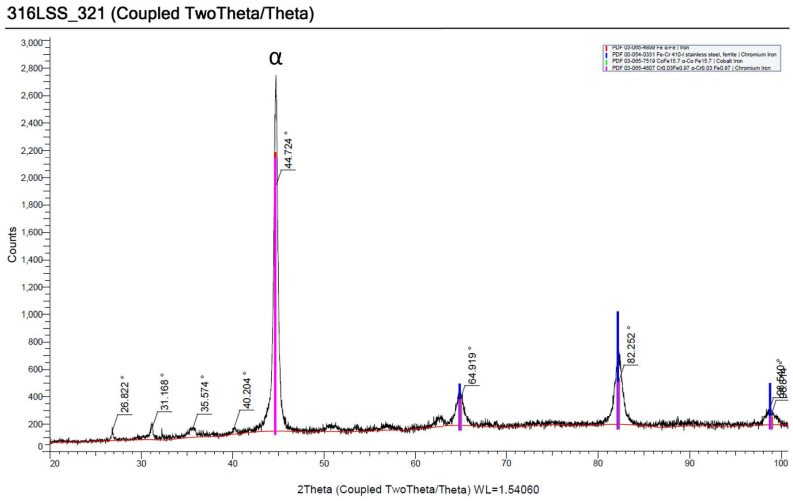

Figure 5.37: XRD plot of sample 321 after heat treatment. The surface alloyed layer alloying powder composition is 4 grams of 600 μm particle size 316L stainless steel.

5.3 Badger Alloys Trials

Badger Alloys trials were the first attempt to cast an industrial prototype with a surface alloyed layer present. The base metal was WCB steel as used with other trials at Maynard Steel and UWM Foundry Lab. Butterfly valve was the component selected for the trials with the molds provided by Badger Alloys. Apart from the riser section, the sample was surface alloyed with Ni and Cr powders. The powders were 95% pure and this helped to study the effect of impurities present in the alloying powders on the chemistry and the properties of the surface alloyed layer.

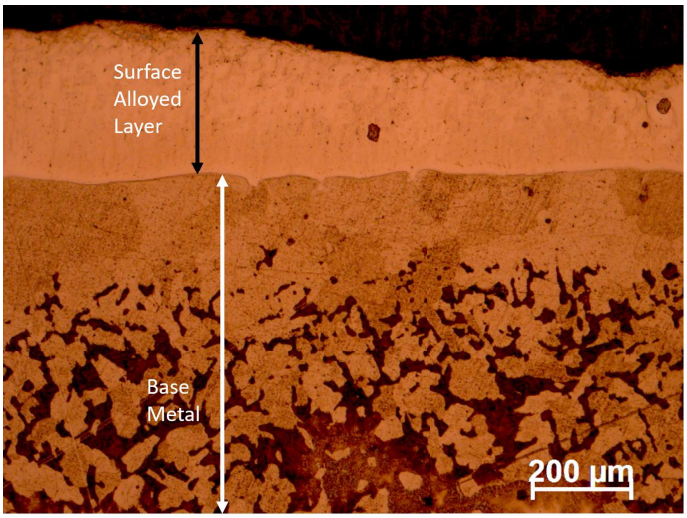

Figure 5.38: Optical image of the surface alloyed butterfly valve in as-cast condition cast at Badger Alloys. The surface alloyed layer and the base metal are visible. The sample was made using 40 micron particle size of Ni and Cr powders. Ni was 0.8 grams and Cr was 1.84 grams per 16 cm^2

A consistent surface alloyed layer is observed in the butterfly valve samples. There is relatively low variation in the depth of surface alloyed layer as compared with the samples cast at Maynard steel. One of the reasons for this could be the larger area of surface alloying as the mold cavity had an area of approximately 720 cm^2 as compared to the slurry coated surface area of mold core at Maynard Steel which had a surface area of approximately 80 cm^2. The melt poured at Maynard Steel was 10,000 lb compared to the 500 lb melt poured at Badger Alloys. This lead to lower redistribution of the alloying powders during the diffusion process and the faster cooling rates led to higher alloying powder diffusion.

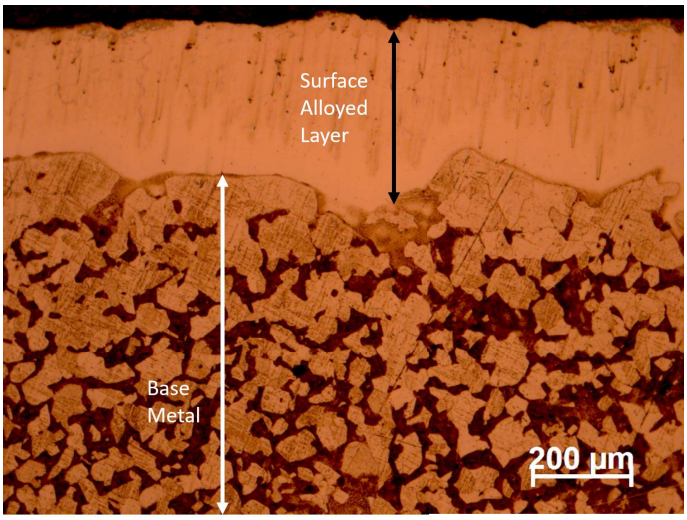

Figure 5.39: Optical image of the as-cast surface alloyed butterfly valve cast at Badger Alloys. Pinholes on account of trapped gases are visible in the surface alloyed layer. The sample was made using 80 micron particle size of Ni and Cr powders. Ni was 0.51 grams and Cr was 1.19 grams per 16 cm^2

There is presence of microporosities in the surface alloyed layer as well as the interface layer through the sample. There are larger porosities present in the surface alloyed layer which could be on account of the gases release from the binder slurry.

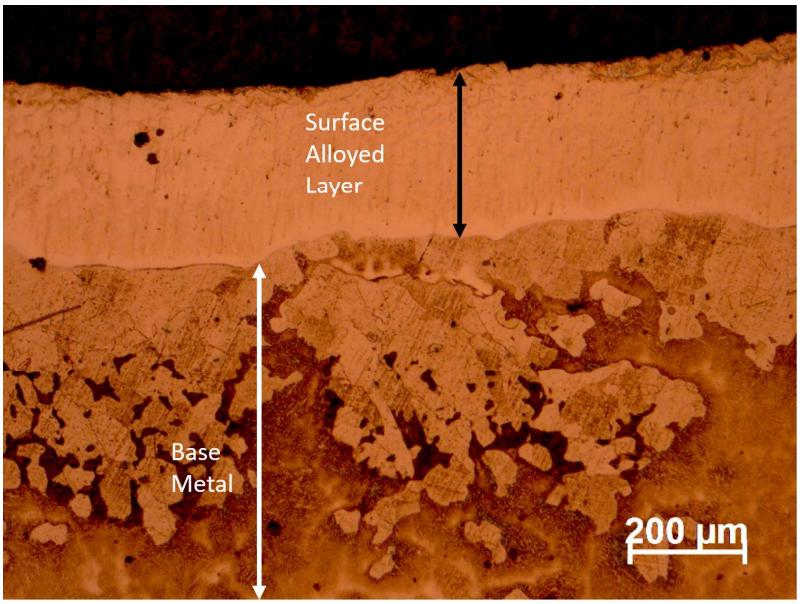

Figure 5.40: Optical image of the as-cast surface alloyed butterfly valve cast at Badger Alloys. Porosities are visible in the surface alloyed layer. The sample was made using 2000 micron particle size of 316L stainless steel powder. 2.192 grams of powder per 16 cm^2

The electro-etching of the surface alloyed layer was performed using an etchant made with 15% HCL and 85% Ethanol and passing a 2 Amp current using an electrode placed on the surface alloyed layer. The microstructure revealed is similar to the observed in 2205 DSS in its as-cast condition where the light phase is austenite and dark phase is ferrite, confirmed by composition analysis, that is typical of 2205 DSS and is seen in the reference figure 5.42 (Luo, Li, Dong, & Xiao, 2017). The A stands for austenite phase while F stands for the ferrite phase.

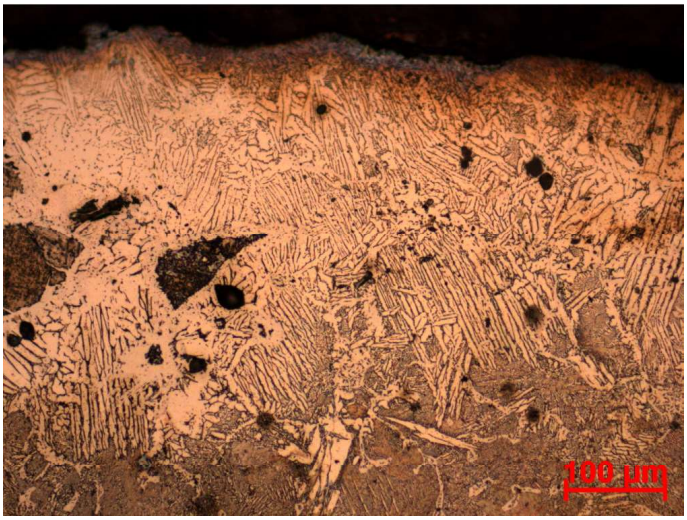

Figure 5.41: Optical image of the surface alloyed as-cast butterfly valve cast at Badger Alloys post electro-etching the surface alloyed layer showing presence of ferrite and austenite in the surface alloyed layer.

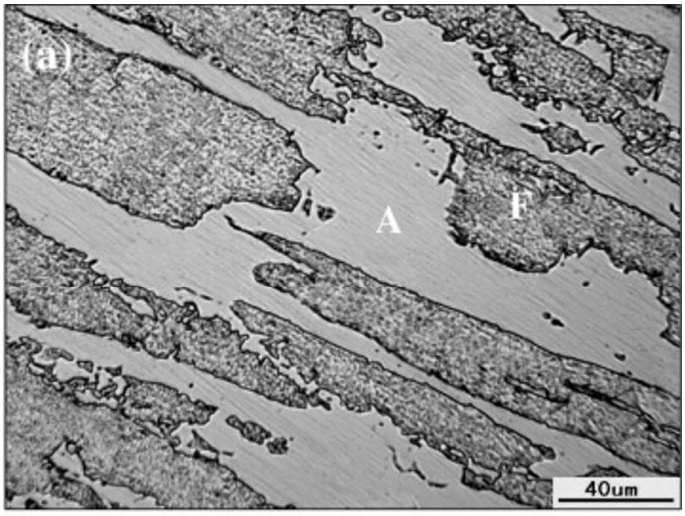

Figure 5.42: Microstructure of as-cast 2205 DSS. A stands for austenite phase and F stands for ferrite phase.

The samples were not heat treated by Badger Alloys as opposed to Maynard Steel and thus were analyzed initially in as-cast condition. The base metal shows a ferrite and pearlite structure which was also observed in Maynard Steel samples and is typical fo WCB steel. The interface does not show any presence of cracks or delamination which may lead to failure during operation.

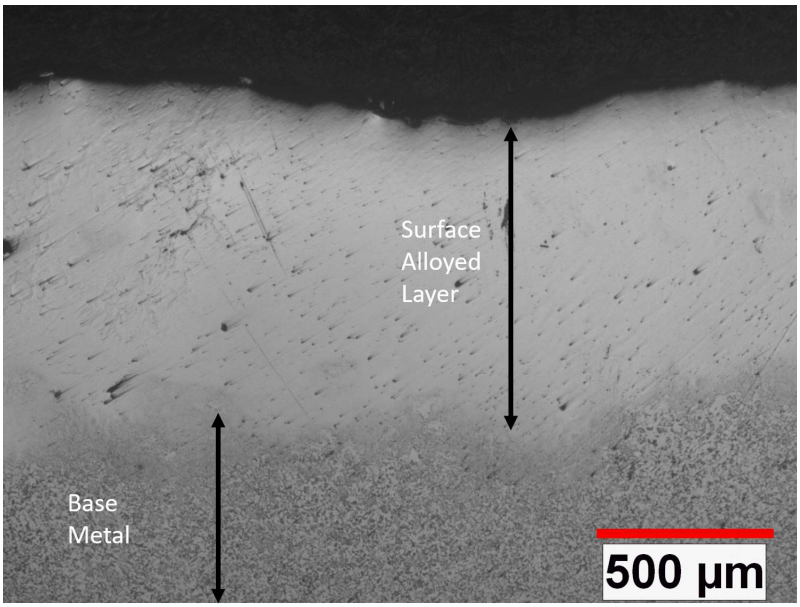

Figure 5.43: Optical image of the surface alloyed butterfly valve after normalizing and tempering heat treatments cast at Badger Alloys showing the dissolution of the elements in the interface layer into the surface alloyed layer and base metal.

Solution annealing is the preferred heat treatment for 2205 DSS as it leads to the dissolving of carbides and the σ and χ phases which are detrimental to the corrosion resistance behavior and mechanical properties. The sample was solution annealed at 1000 °C for a period of 10 minutes. The time of annealing was lowered as the previous tests for periods of 1 or 2 hours which is the recommended time for through section 2205 DSS lead to formation of oxide layers on the samples surface leading to detrimental effects in form of chipping of the surface alloyed layer. As seen from the optical micrograph, it can be seen that the interface is diffused into the surface alloyed layer to a higher degree as compared to the sample before heat treatment.

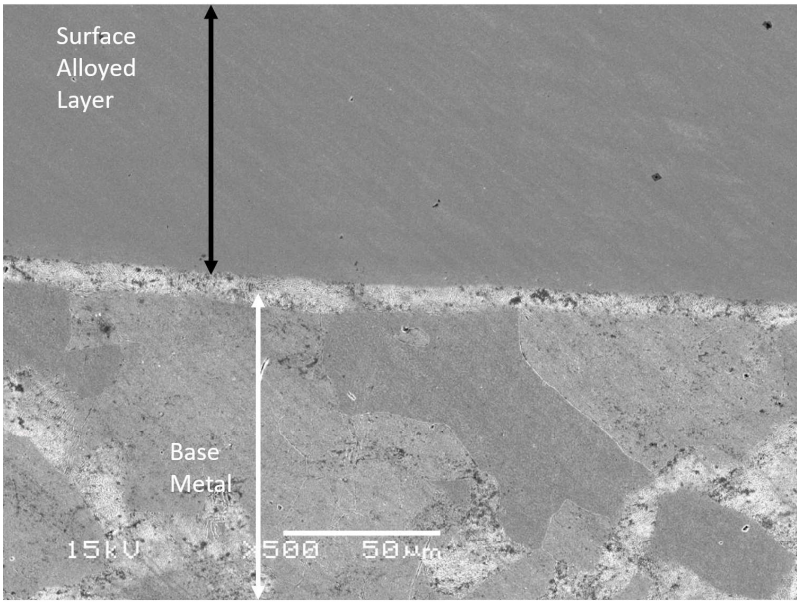

Figure 5.44: SEM image of the surface alloyed butterfly valve cast at Badger Alloys in as-cast condition. The surface alloyed layer and the base metal along with the interface in between. The composition of the slurry used for surface alloying includes 4 grams of Ni and Cr each.

The SEM image of the surface alloyed layer shows a well defined interface layer between the surface alloyed layer and the base WCB steel. Microporosities are visible in the surface alloyed layer and in the interface layer as well. As compared to the samples made at UWM Foundry Lab, the interface does not exhibit presence of dendrite arms which are formed during the solidification process.

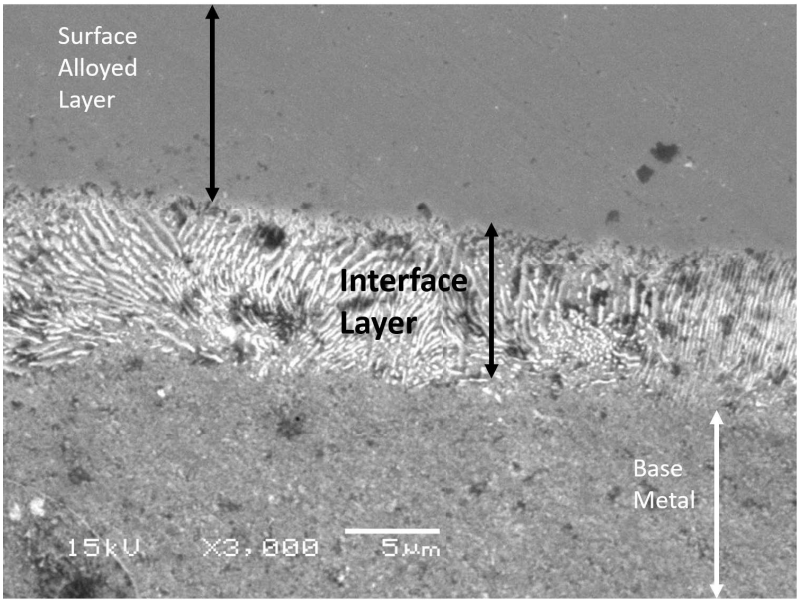

Figure 5.45: SEM image of the as-cast interface between the surface alloyed layer and the base metal of the butterfly valve sample cast at Badger Alloys.

The magnified view of the interface layer is similar to that of samples in the Maynard Steel trials. As the interface is a zone which is alloyed as compared to the surface alloyed layer and has a higher concentration of carbon, there is a higher degree of pearlite formation in this region. All the particles pushed by the growth front which do not undergo diffusion into the surface alloyed layer form carbides in this region. Chromium has the tendency to form $M_{23}C_6$ carbides at temperatures in the range of 760 °C (Krauss, 2015).

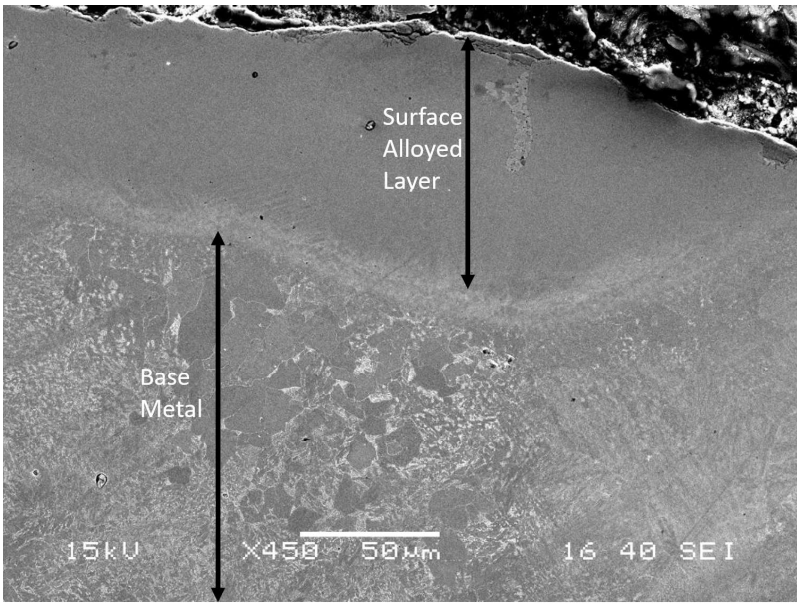

Figure 5.46: SEM image of the surface alloyed butterfly valve cast at Badger Alloys after solution annealing at 1000 °C for 10 minutes.

The sample post heat treatment shows an interface layer which has diffused into the surface alloyed layer with a change in the microstructure of the base WCB steel. The table below shows the elemental composition of the surface alloyed layer

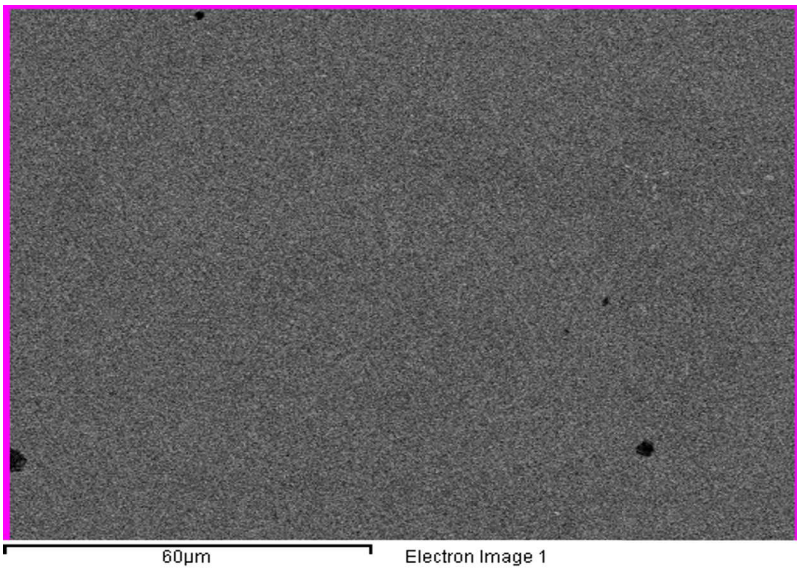

Figure 5.47: Elemental mapping of the surface alloyed layer of butterfly valve sample cast at Badger Alloys in as-cast condition.

Element	Weight%
Ni	4.51
Cr	19.71
C	1.97
Mn	1.58
Si	1.43
Fe	Balance

Table 5.13: Elemental composition of the surface alloyed layer of the butterfly valve sample in as-cast condition.

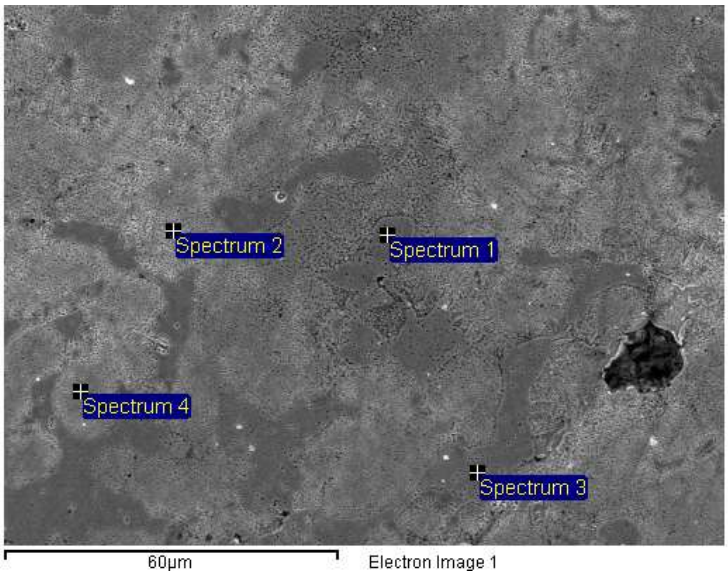

Figure 5.48: Point and ID elemental analysis of the surface alloyed layer of the butterfly valve sample cast at Badger Alloys after solution annealing at 1000 °C for 10 minutes.

The point and ID elemental analysis of the surface alloyed layer confirms the presence of alloying elements. The composition of the surface alloyed layer is similar to that of the targeted compositon of 2205 DSS in terms of weight percentages of Cr, Ni, Mn, Si, and Mo. The sample exhibits increase in the hardness of the surface alloyed layer due to solid solution strengthening effect of Ni and Mo. The quantity of carbon is higher in the surface alloyed layer as compared to the normal composition of 2205 DSS.

Spectrum	C Weight%	Si Weight%	Cr Weight%	Mn Weight%	Ni Weight%	Mo Weight%	Fe Weig
1	3.27	1.77	19.72	2.13	4.88	4.71	Balar
2	3.03	1.62	19.73	3.05	7.23	-	Balar
3	3.6	1.86	20.64	3.26	5.17	-	Balar
4	3.53	1.13	20.33	2.72	7.21	3.42	Balar

Table 5.14: Elemental composition of the surface alloyed layer of the butterfly valve sample cast at Badger Alloys after solution annealing at 1000 °C for 10 minutes.

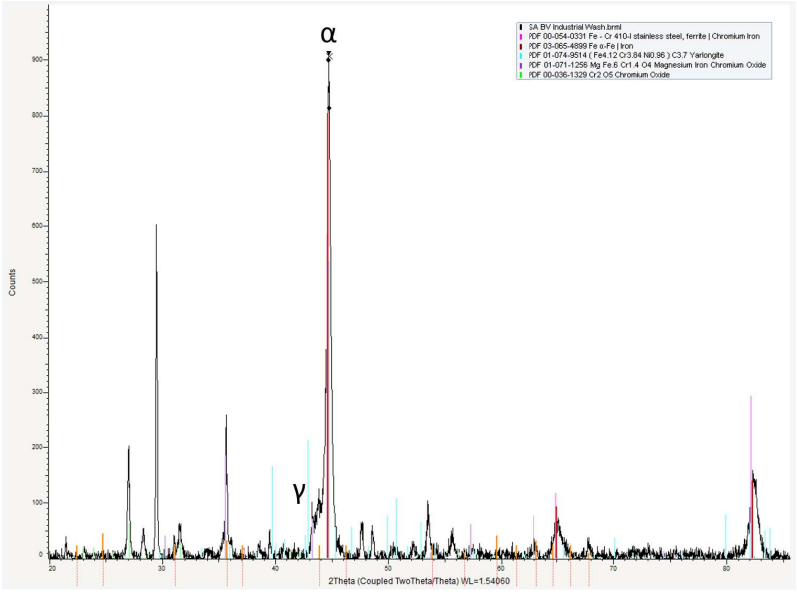

Figure 5.49: XRD plot of industrial wash slurry butterfly valve sample 1. Ni and Cr powders of particle size 40μm were used for alloying the base metal.

The spectrum shows presence of ferrite as the primary phase at 44.5°. As the sample was made at Badger Alloys, it was not heat treated before analysis. The chrome oxide layer can be observed at 27° and at 32.5°. This initial layer of Cr_2O_5 would lead to corrosion resistance behavior which is also considered on account of high weight percentage of Cr in the surface alloyed layer. The experiment was targeted to alloy the surface to a composition of 2205 DSS; the results indicates the process lead to adequate dissolution and alloying of the elements.

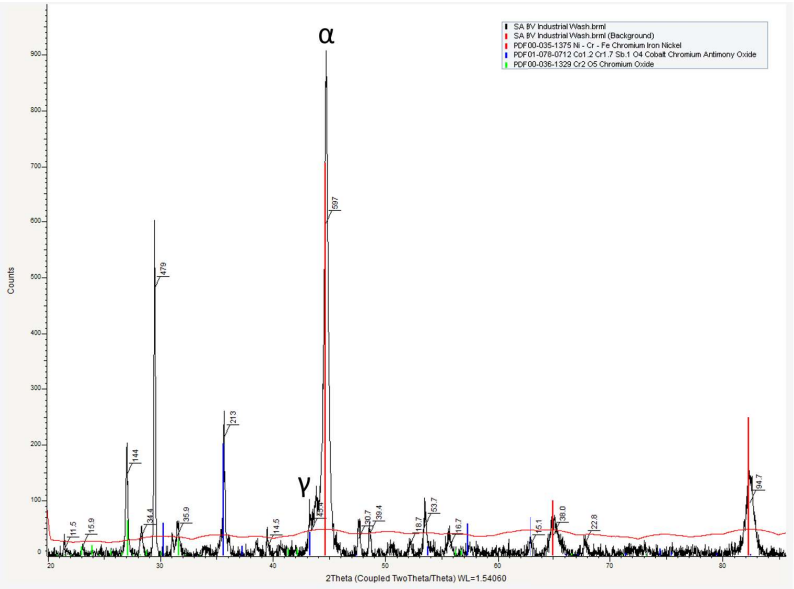

Figure 5.50: XRD plot of industrial wash slurry butterfly valve sample 2 showing presence of ferrite as the primary phase. Ni and Cr powders were used for alloying the base metal.

5.4 UWM Foundry Lab

5.4.1 R1

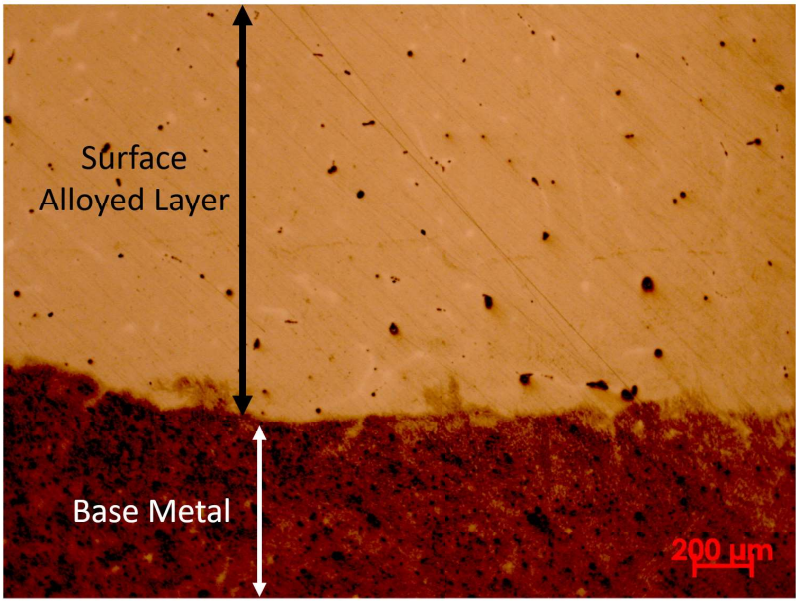

Figure 5.51: Sample R1 cast in UWM Foundry Lab as quartz tube experiment. Ni, Cr, Fe-Mn and Fe-Si used as alloying elements. Targeted thickness of 1000 μm.

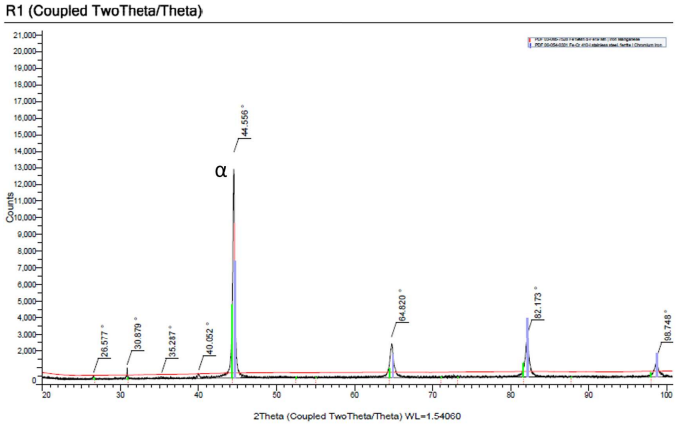

Figure 5.52: XRD plot of sample R1 before heat treatment. Austenite is the primary phase present in the surface alloyed layer.

Sample R1 was cast at the UWM Foundry Lab in a quartz tube experiment with the melt being poured into the mold under vacuum conditions. The XRD shows a peak of ferrite formed at 44.556° and absence of any peaks of carbides or oxides. The targeted composition of the slurry applied on the mold cavity was 316L stainless steel.

5.4.2 R2

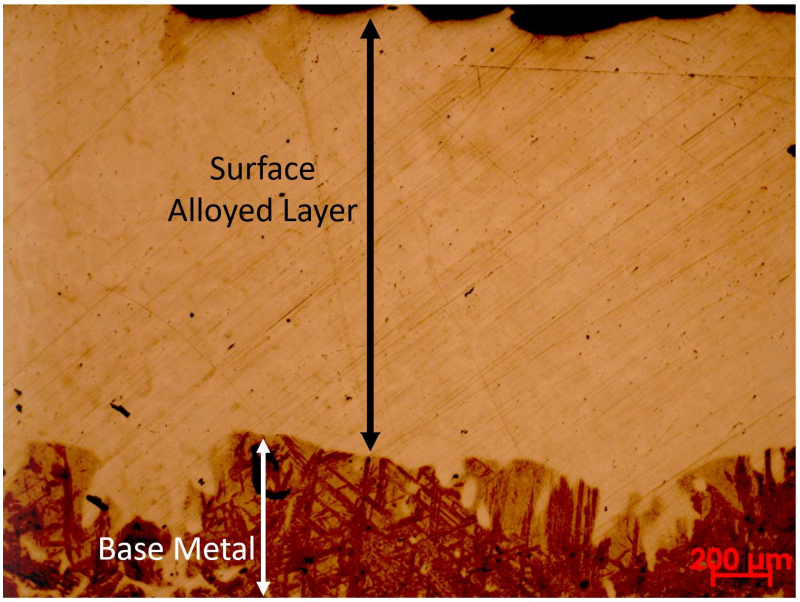

Figure 5.53: Sample R2 cast in UWM Foundry Lab as quartz tube experiment. Ni, Cr, Fe-Mn, and Fe-Si used as alloying elements. Targeted thickness of 2000 μm.

5.4.3 R3

Sample R3 was made in the UWM Foundry Lab with a targeted composition comparable to that of 316L stainless steel. 316L stainless steel is used in the water industry for making components that require corrosion resistance. The composition of the alloying powders used in the slurry for coating the mold cavity included 1.45 grams of Ni and 2.62 grams of Cr. The sample was made as a part of the quartz tube experiments with WCB steel as the base metal.

Figure 5.54 shows a sample with a surface alloyed layer having a targeted depth of 3000 μm. The targeted composition of the surface alloyed layer is 316L. As mentioned in the experimental section, the experiments were designed to control the depth of surface alloying. The sample had been etched with 3% Nital for a period of 5 seconds. Since Nital is only effective for mild steel, the surface alloyed layer is unetched. Though it is possible to observe minor grain boundaries, this can be attributed to the fact that the alloyed layer is comparable in composition and does contain a higher quantity of carbon as compared to contemporary stainless steel.

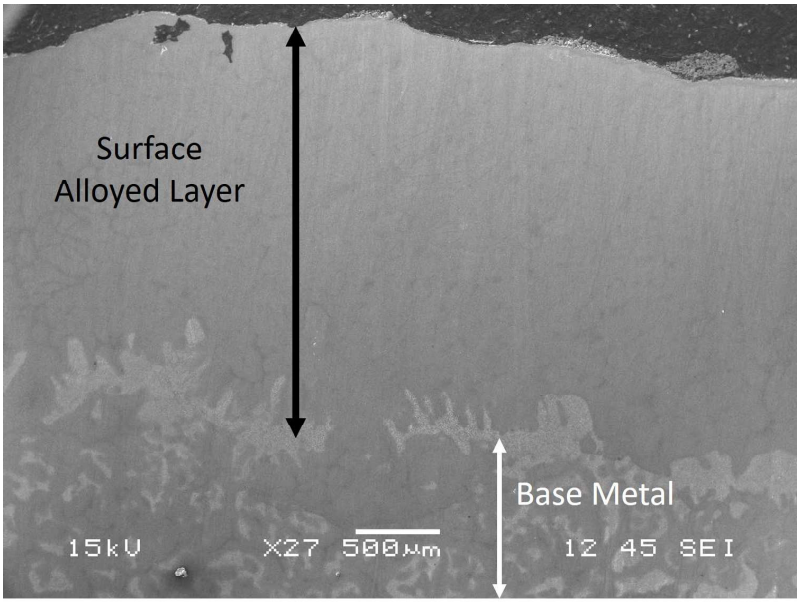

Figure 5.54: SEM image of sample R3. Ni, Cr, Fe-Mn, and Fe-Si were used as alloying elements. Depth of surface alloying is 3000 μm. REFCOBAR 1010 Gel was used as binder.

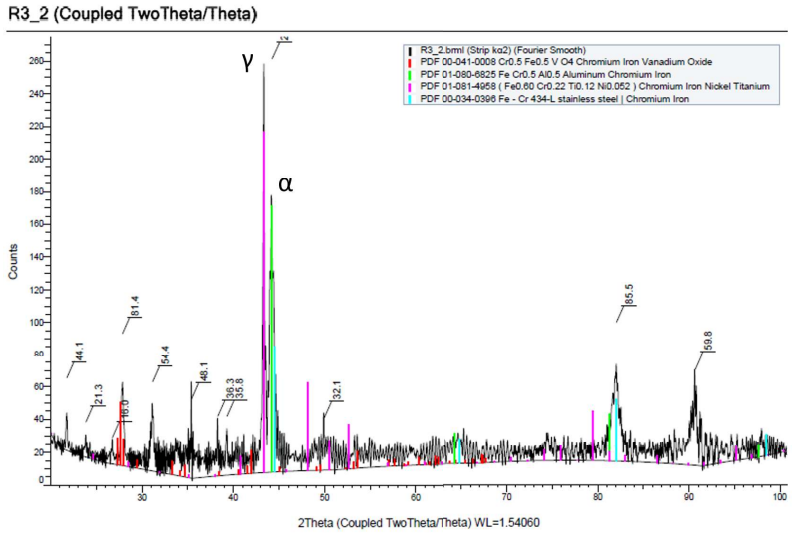

Figure 5.55: XRD plot of sample R3 before heat treatment. Austenite, oxides, and carbides are observed in the surface alloyed layer.

Sample R3 was an open pour experiment cast at the UWM Foundry Lab with the slurry composition targeted to 316L stainless steel. The sample had a depth of 3000 μm and the surface did not exhibit presence of residual oxidized alloying powders. Austenite is primary phases formed in the surface alloyed layer and observed at 43.5°.

Sample	Average Hardness of Base Metal (GPa)	Average Hardness of Surface Alloyed Layer (GPa)
R3	7.69	8.22

Table 5.15: Average hardness comparison of base metal and surface alloyed layer after nanoindentation tests for UWM R3 sample.

The EDS point and ID analysis was used for identifying the chemical composition of the surface alloyed layer and for confirming the diffusion of alloying elements with the WCB steel base metal. The presence of Cr and Ni has been confirmed in the surface alloyed layer with and the results are shown in figure 5.56 and in table 5.16.

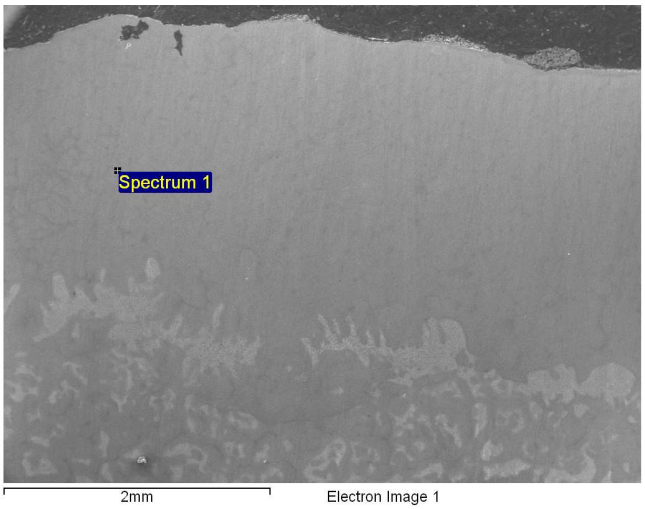

Figure 5.56: Point and ID elemental analysis of surface alloyed layer fo sample R3.

Element	Weight Percentage
Ni	11.47
Cr	3.69
Fe	Balance

Table 5.16: Weight percentages of Ni and Cr in the surface alloyed layer of sample R3 using Point and ID.

The low weight percentage of diffusion of Cr can be attributed du to the low temperature of WCB steel when coming in contact with the alloying powder slurry. As Ni has a lower melting point as compared to Cr, the melting and diffusion of Ni into the WCB melt was completed. On account of a higher melting point of Cr, the complete melting would take longer which means the melt has to be held at temperature above 1600 °C which is difficult in a quartz tube experiment. The excess Cr is left behind in the mold cavity.

5.4.4 R4

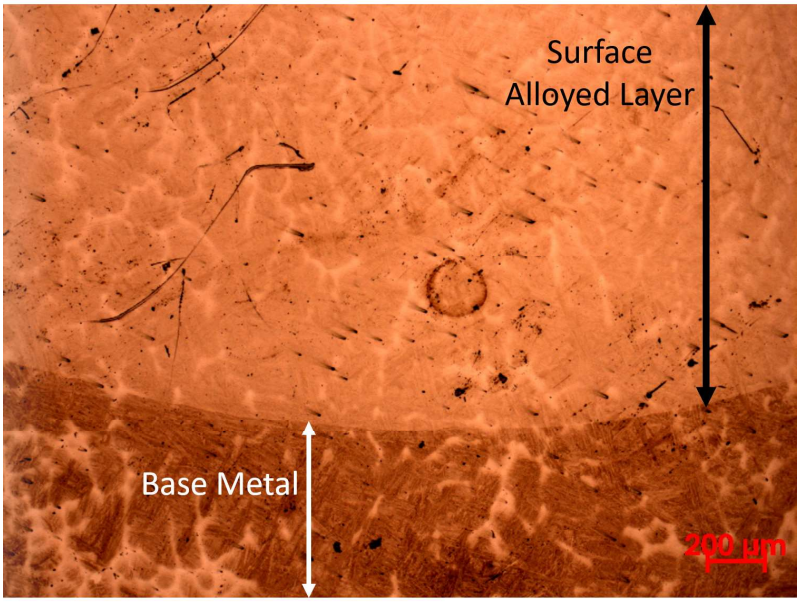

Figure 5.57: Sample R4 cast in UWM Foundry Lab as quartz tube experiment. Ni, Cr, Fe-Mn, and Fe-Si used as alloying elements. Targeted thickness of 4000 μm.

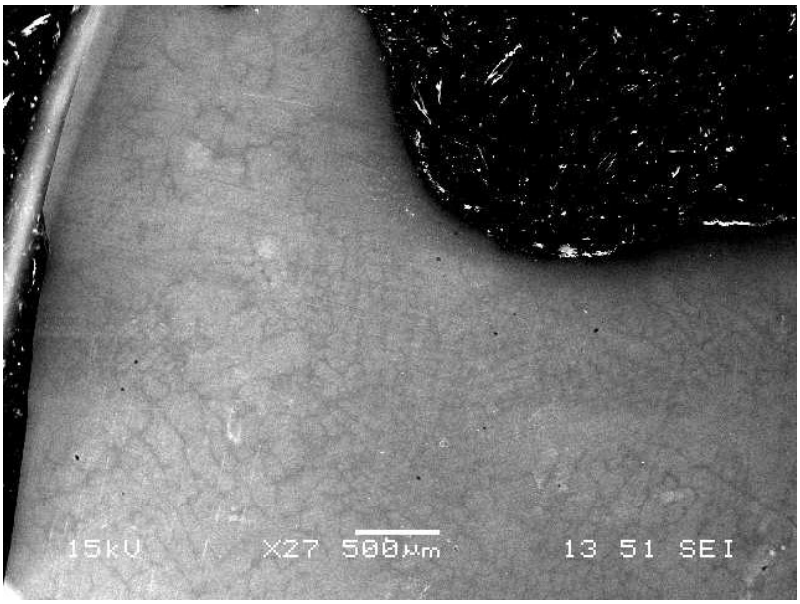

Figure 5.58: SEM image of sample R4 showing only the surface alloyed layer. Ni, Cr, Fe-Mn, and Fe-Si were used as alloying elements. Targeted depth of surface alloying is 4000 μm. REFCOBAR 1010 Gel was used as binder.

Sample R4 was made in the UWM Foundry Lab in a quartz tube experiment with 316L as the targeted composition and 4000 μm as the targeted depth of surface alloying. While the alloying depth was in the range of 3950 - 4100 μm range, the confirmation of surface alloying was done by the point and ID test, which has been expanded in section 3.3.2. The location of the point has been shown in the image below:

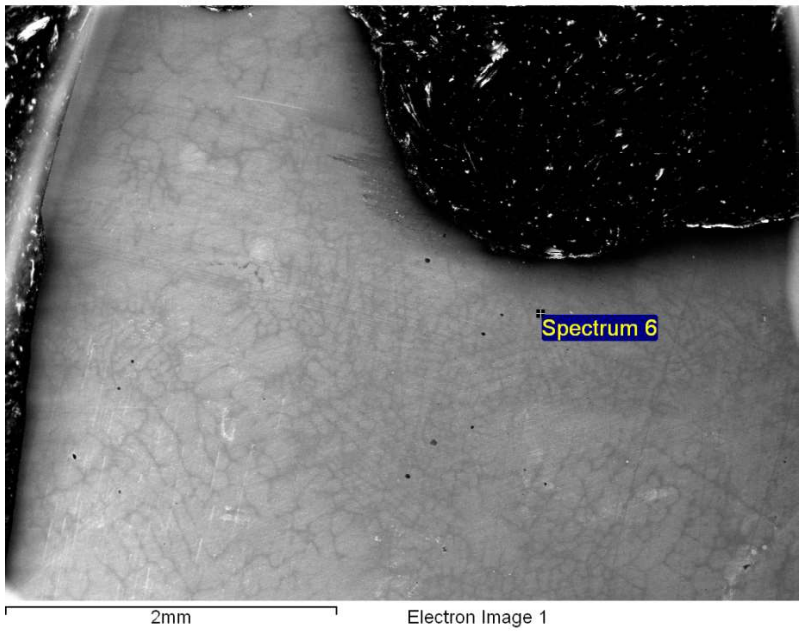

Figure 5.59: Point and ID location in sample R4. The location is on the surface alloyed layer of the sample. Ni, Cr, Fe-Mn, and Fe-Si are the alloying elements in the surface alloyed layer. REFCOBAR 1010 was used at the binder gel.

The location was confirmed after etching the sample with 3% Nital as the surface alloyed layer does not react with Nital and remains unetched. The point and ID confirmed the presence of alloying in the surface alloyed layer but the quantities of alloying elements are lower as compared to that of the targeted composition of 316L stainless steel. As mentioned above, the weight percentages of alloying elements in the surface alloyed layer does not have a correlation to the corrosion resistance of the layer as chrome oxide is a critical factor which acts as the passivation agent for preventing corrosion buildup. The elemental composition of the surface alloyed layer of sample R4 is given below:

Element	Weight%
Ni	2.12
Cr	5.38
Si	0.91
Mn	0.98
Fe	Balance

Table 5.17: Elemental composition of the surface alloyed layer of the sample R4.

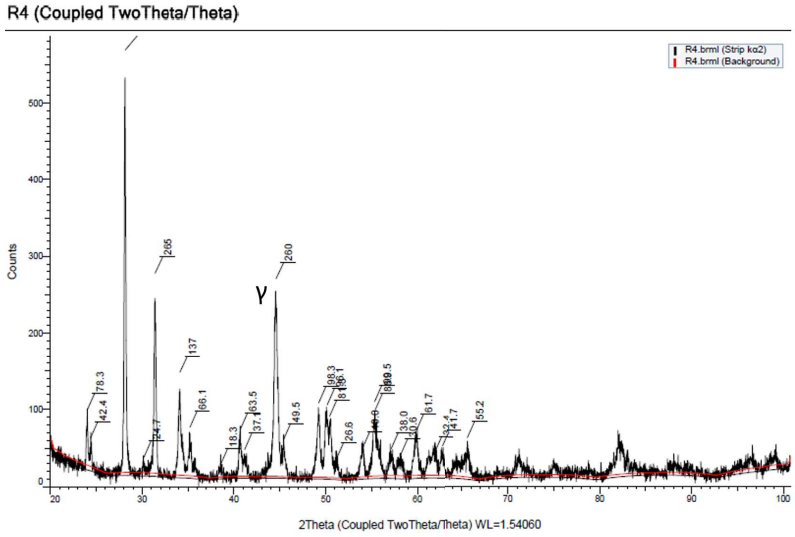

Figure 5.60: XRD plot of sample R4 before heat treatment. Low austenite intensity and high oxide and carbide intensity.

Sample R4 was the last quartz tube pour cast in the UWM Foundry Lab. The chemical composition of the slurry was comparable to that of 316L SS as in the case of sample R1. The sample had issues during the experimental stage of melting on account of the induction coil malfunctioning. The sample after solidification showed presence of high degree of unalloyed oxidized powder on the surface which is characteristic of incomplete melting and solidification of the alloying powders, especially Cr with a high melting point of 1907 °C. The austentie and ferrite peaks have a low intensity as compared to the other samples from the same trial. There was surface alloying of the base metal but it did not lead to formation of an alloy similar in composition to the expected composition.

5.4.5 R5

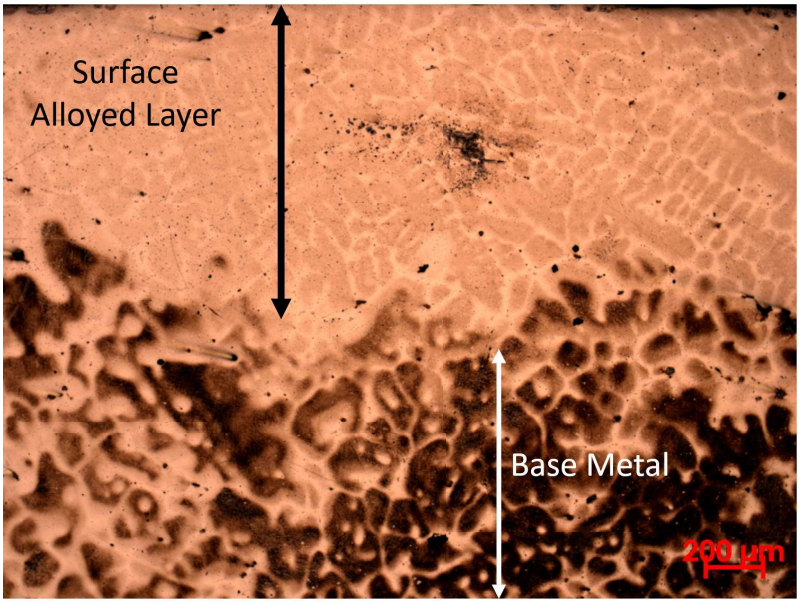

Figure 5.61: Sample R5 cast in UWM Foundry Lab as quartz tube experiment. Ni, Cr, Fe-Mn, and Fe-Si used as alloying elements. Targeted thickness of 1000 μm.

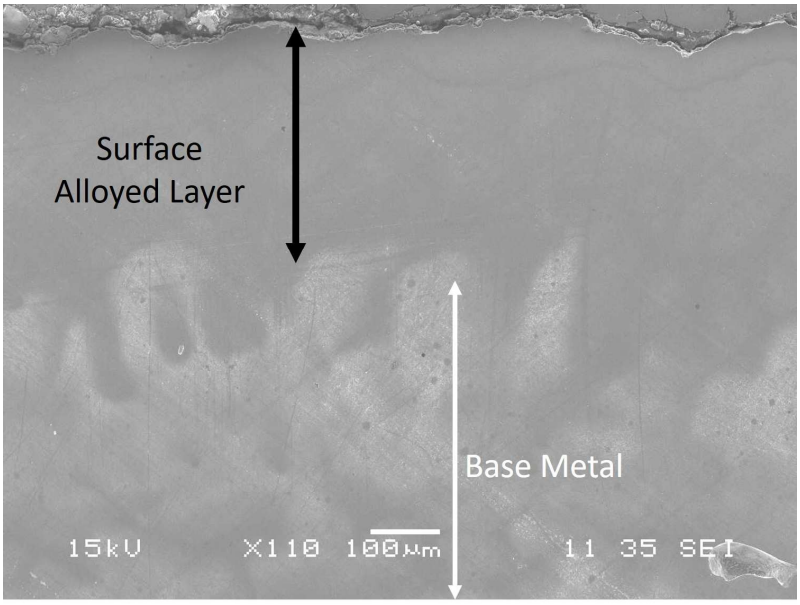

Figure 5.62: SEM image of sample R5. Ni, Cr, Fe-Mn, and Fe-Si were used as alloying elements. Depth of surface alloying is 1000 μm. REFCOBAR 1010 Gel was used as binder.

Sample R5 as seen in the SEM section does not show a clear interface between the surface alloyed layer and base metal. Sample R5 was cast with the alloying elements selected to a composition targeted to that of 2205 DSS and for 1000 μm depth of surface alloying. Figure 5.63 is of point and ID elemental composition test performed on an unetched section of the surface alloyed layer. The concentration of Cr and Ni is lower than expected and this can be on account of faster cooling rate thus inhibiting the time required for dissolution of the alloying elements. This can be further explained as the dendritic solidification occurring in the melt starting at the slurry of the alloyed elements would lead to solute trapping, in this case the solute is alloying powder in the slurry. As the concentration of solute decreases along with the increase in the length of dendrite from the mold walls coated with alloying slurry, this is visible in the EDS results.

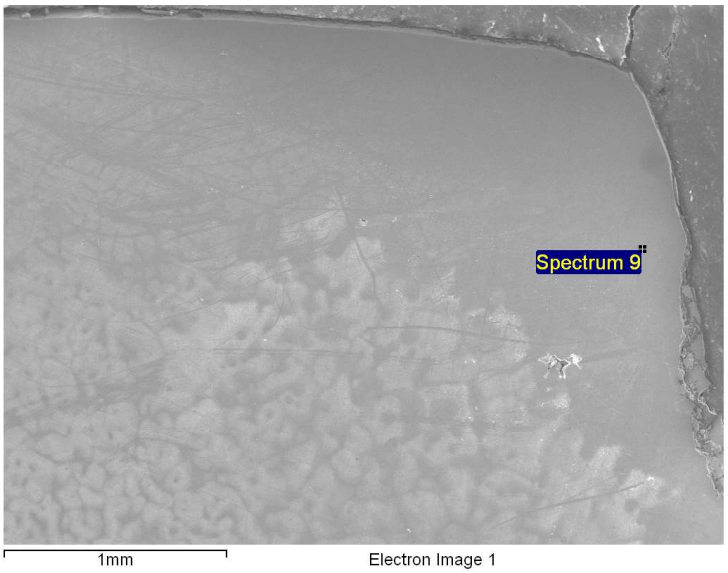

Figure 5.63: Point and ID of surface alloyed layer in sample R5.

The elemental composition of the surface alloyed layer at that point has been calculated to be:

Element	Weight%
Ni	2.99
Cr	5.42
Fe	Balance

Table 5.18: Elemental composition of the surface alloyed layer of the sample R5.

A second point and ID has been performed on the area closer to the interface between the surface alloyed layer and the base metal. The selection of the darker phase in the interface revealed a higher concentration of Cr and Ni as compared to that of table 5.18. One of the reasons could be convection currents set up in the melt inside the mold which pick up agglomerated alloying elements and which get trapped in between dendrites causing alloying elements enriched pockets.

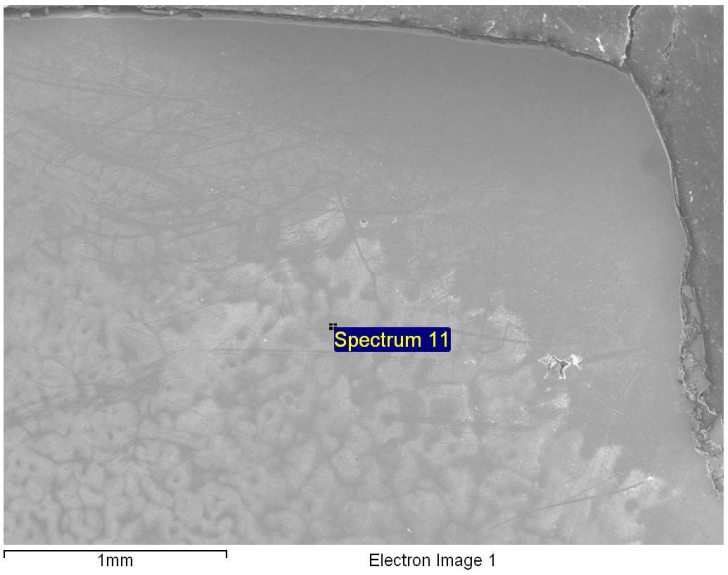

Figure 5.64: Point and ID scan in interface of sample R5.

Element	Weight%
Ni	5.22
Cr	8.45
Fe	Balance

Table 5.19: Elemental composition of the surface alloyed layer of the sample R5 at one location shown in the figure.

The x-ray mapping of the surface alloyed layer reveals the distribution of the alloying elements over a larger surface area. As the interface is hard to distinguish from the surface alloyed layer, the use of x-ray mapping helps for understanding the concentration of the elements scattered through the alloyed layer. For sample R5, Fe, Ni, and Cr were mapped on the surface alloyed layer as these were the primary elements observed during point and ID scans.

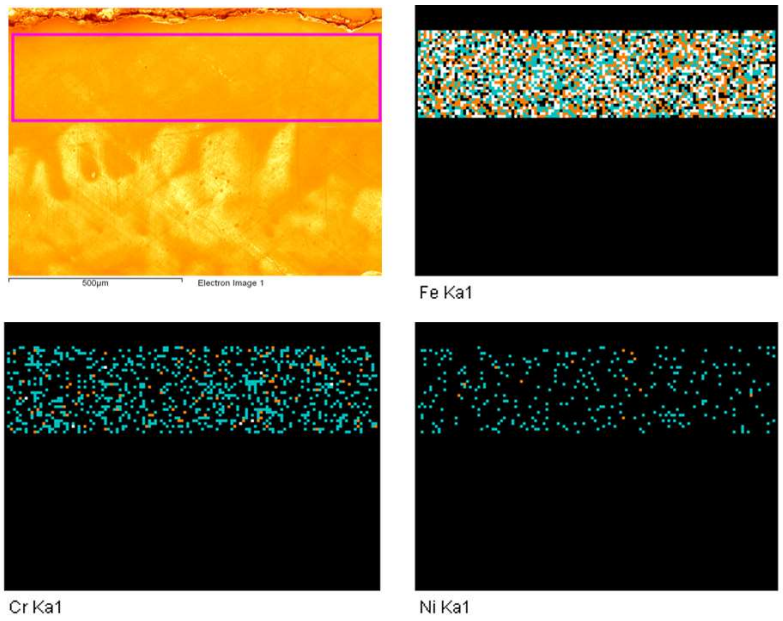

Figure 5.65: X-Ray maps of a section of surface alloyed layer of the sample R5 showing presence of Ni, Cr, and Fe in the surface alloyed layer.

Element	Weight%
Ni	3.68
Cr	5.55
Fe	Balance

Table 5.20: Elemental composition of the surface alloyed layer of the sample R5 by x-ray mapping.

5.4.6 R6

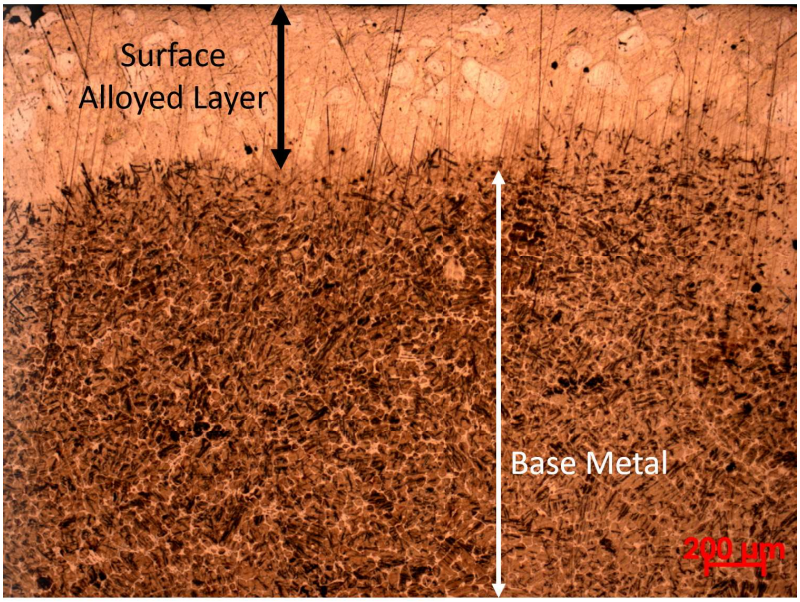

Figure 5.66: Sample R6 cast in UWM Foundry Lab as open pour experiment. Ni, Cr, Fe-Mn, and Fe-Si used as alloying elements. Targeted thickness of 1000 μm.

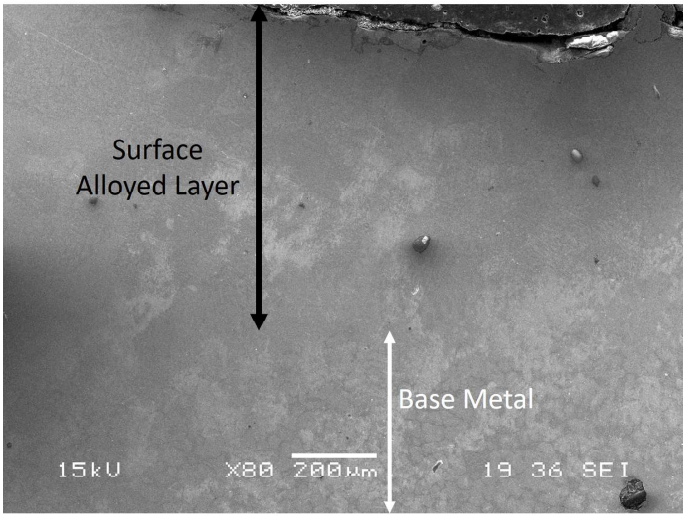

Figure 5.67: SEM image of sample R6. Ni, Cr, Mo, Fe-Mn, and Fe-Si were used as alloying elements. Targeted depth of surface alloying is 1000 μm. REFCOBAR 1010 Gel was used as binder.

Sample R6 as shown in figure 5.67 shows an absence of a well defined interface between the surface alloyed layer and the base metal. A gradual decrease in the concentration of the alloying elements can cause the interface to get integrated in the surface alloyed layer and the base metal. The indication of change in the composition is provided by the change in microstructure below the surface alloyed layer. Minor defects can be observed in the alloyed layer but these can be eliminated if the casting occurs under industrial scale conditions as temperature of the melt is maintained above its melting point with added superheat as well as degassing of the melt is possible to remove any entrapped gasses.

Sample R6 was made with a targeted composition of 2205 DSS using REFCOBAR 1010 gel as the binder for the slurry. This sample showed increased enrichment of the alloyed layer as compared to the samples made at Maynard Steel. This can be on account of absence of fissures in the dried slurry. The previous samples were heated in a low temperature furnace for removing excess water but the development of water vapor lead to formation of cracks in the slurry. This may have caused fragments of slurry to break and enrich elsewhere.

From the EDS analysis of sample R6 it is visible that the composition can be closely compared to that of 2205 DSS. X-ray mapping of the surface alloyed layer shows a good distribution of the alloying elements over the area of the alloyed layer. This is visible in figure 5.68

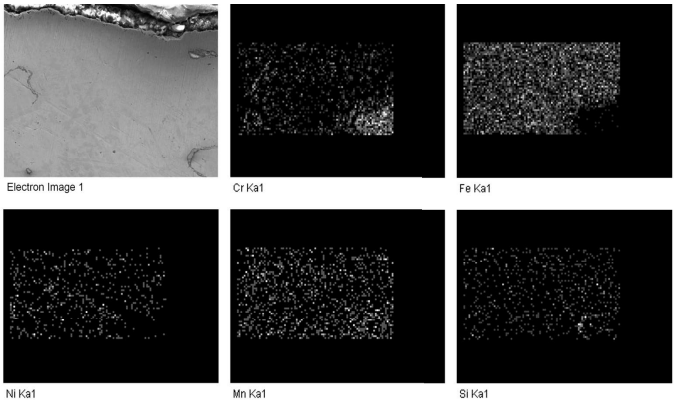

Figure 5.68: X-ray mapping of the surface alloyed layer of the sample R6 showing distribution of Fe, Ni, Cr, Mn, and Si in the surface alloyed layer.

The chemical composition of the alloyed layer is given in table 5.21.

Element	Weight%
Ni	6.23
Cr	26.66
Mn	3.58
Fe	Balance

Table 5.21: Elemental composition of the surface alloyed layer of the sample R6 estimated by x-ray mapping.

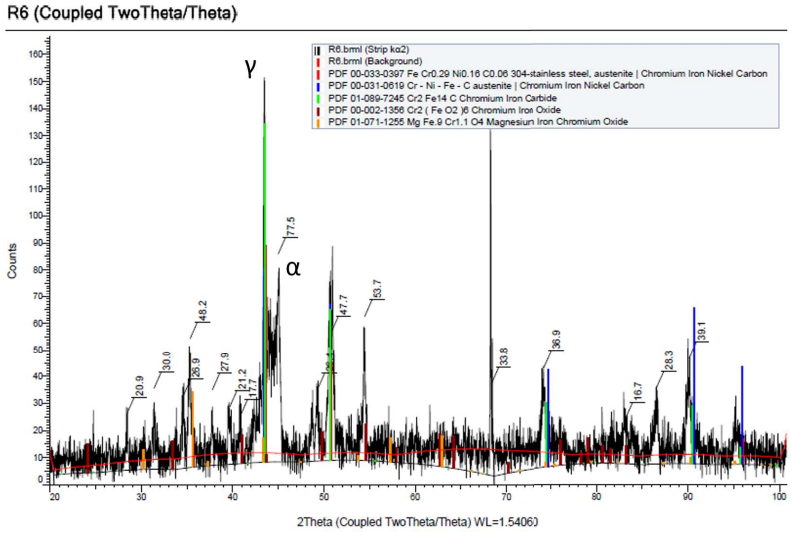

Figure 5.69: XRD plot of sample R6 before heat treatment. Surface alloyed layer shows high concentration of oxides, carbides and hydrates.

Sample R6 was the first open pour experiment performed in the UWM Foundry Lab. The sample slurry composition was 2205 DSS with an expected alloying depth of 1000 μm. The sample mold cavity did not exhibit any residues of the oxidized Cr powder which was observed in sample R4. The sample shows presence of the austenite peak at 43.5° and ferrite at 45°. As 2205 DSS is a duplex stainless steel with ferrite and austenite, the phases obtained in the scan are a good indication of the completion of the melting and solidification of the alloying powders and mild steel. Peaks of chrome iron carbide at 41° and chrome iron oxide at 35°. The sample has carbon inclusion from the graphite crucible on account of cracks in the refractory wash layer of the crucible which led to the melt coming in contact with the crucible. This is visible in the carbide formations in the surface alloyed layer which are not observed in samples which did not undergo the same issue.

5.4.7 R7

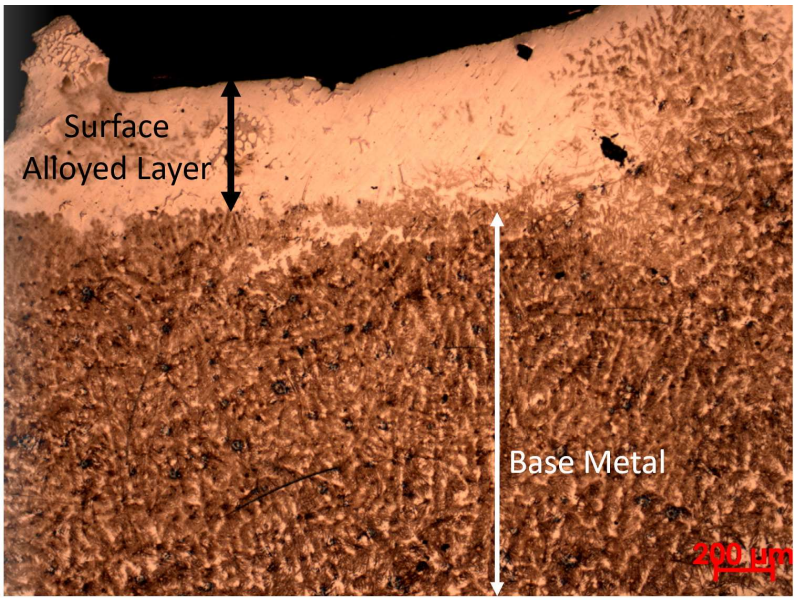

Figure 5.70: Sample R7 cast in UWM Foundry Lab as quartz tube experiment. Ni, Cr, Fe-Mn, and Fe-Si used as alloying elements. Targeted thickness of 2000 μm.

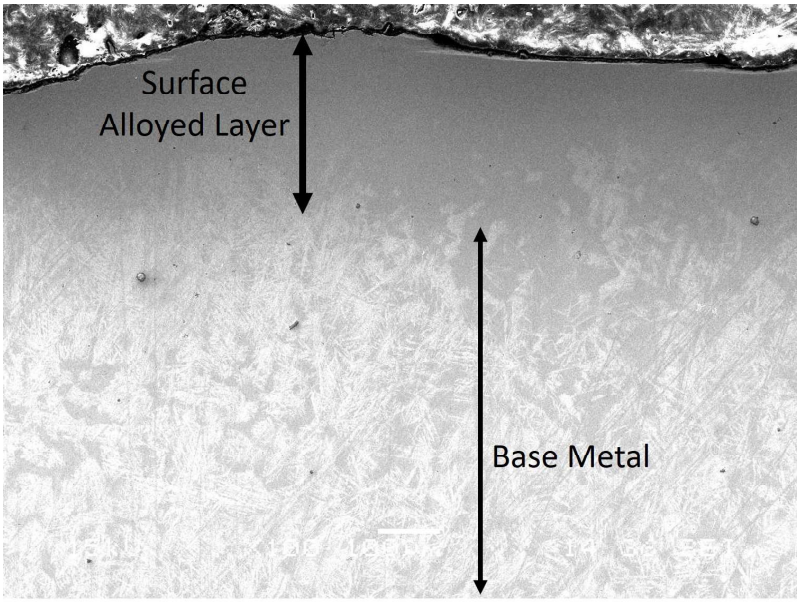

Figure 5.71: SEM image of sample R7. Ni, Cr, Mo, Fe-Mn, and Fe-Si were used as alloying elements. Targeted depth of surface alloying is 2000 μm. REFCOBAR 1010 Gel was used as binder.

Sample R7 has a similar trend as in the case of sample R6. The absence of a well defined interface is observed with the surface alloyed layer transitioning into the base metal over a range. The microstructure is dendritic with primary dendrites and secondary arm dendrites.

5.4.8 R8

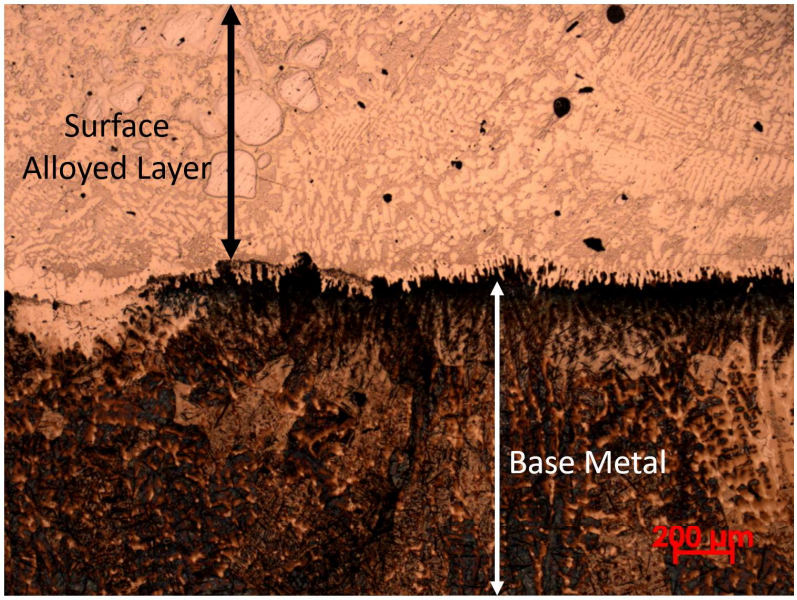

Figure 5.72: Sample R8 cast in UWM Foundry Lab as quartz tube experiment. Ni, Cr, Fe-Mn, and Fe-Si used as alloying elements. Targeted thickness of 2000 μm.

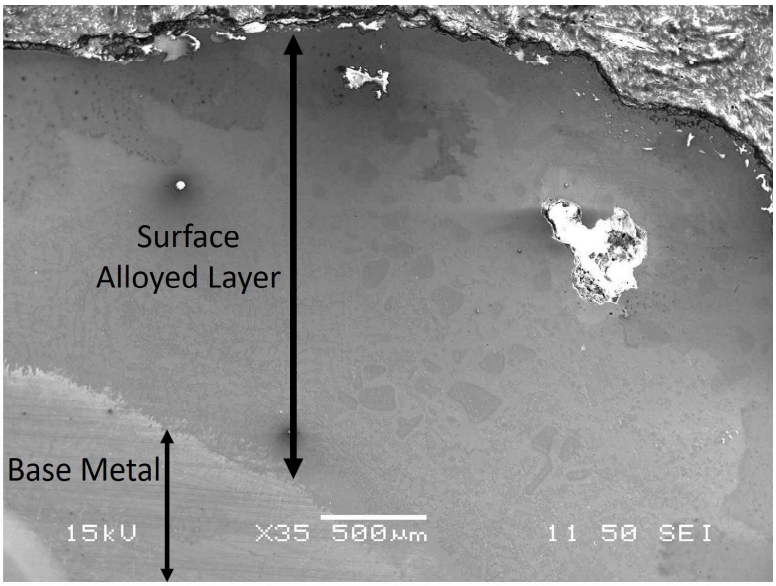

Figure 5.73: SEM image of sample R8. Ni, Cr, Mo, Fe-Mn and Fe-Si were used as alloying elements. Targeted depth of surface alloying is 1000 μm. REFCOBAR 1010 Gel was used as binder.

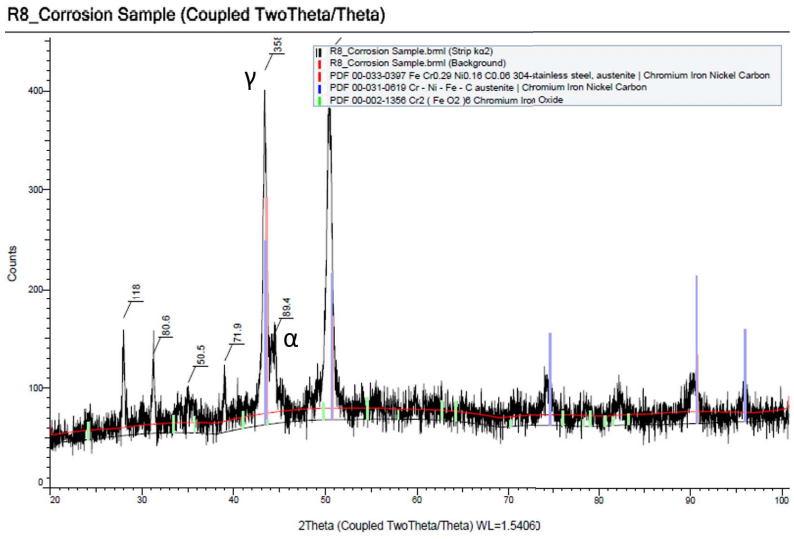

Figure 5.74: XRD plot of sample R8 before heat treatment. Austenite and ferrite are the primary phases formed in the surface alloyed layer.

Sample R8 was an open pour experiment with the aim to alloy the surface with a slurry of composition comparable to 2205 DSS. The sample was made in the UWM Foundry Lab and the pouring temperature for the sample was approximately 1850 °C which is lower than the melting point of Cr. This lead to a minor quantity of Cr powder being oxidized and stuck to

the surface alloyed layer. This initially came off in form of chips but up on sand blasting the sample, the XRD scan revealed a peak of austenite and ferrite at approximately 43.5° and 45° respectively. This is similar to that of sample R6 and further the similarity can also be seen in the formation of the 304 SS in the surface alloyed layer. Chromium Iron Nickel Carbon and Chromium Iron Oxide is observed in form of multiple peaks through the scan.

5.4.9 R9

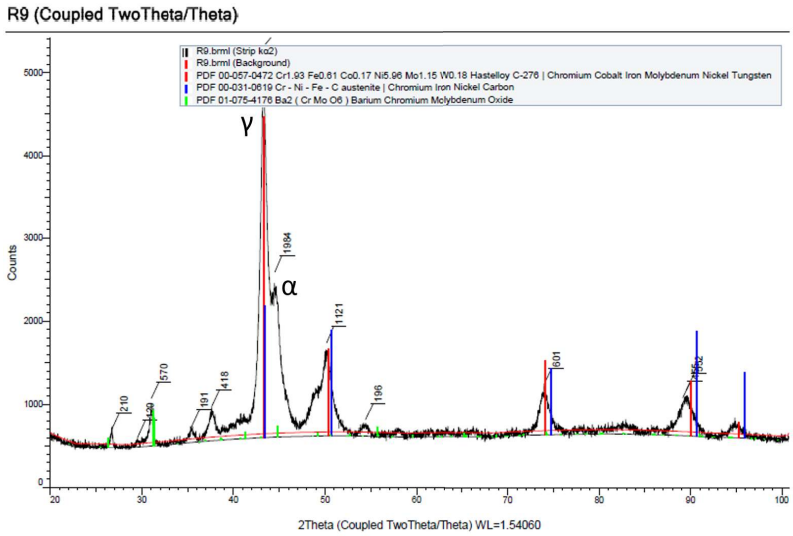

Figure 5.75: XRD plot of sample R9 before heat treatment. Austenite and ferrite are the primary phases along with presence of oxides and carbides.

The slurry for sample R9 had a chemical composition similar to 2205 DSS with a depth of surface alloying up to 1000 μm. The sample was cleaned using a sand blaster to remove any mold sand or other residues. An austentie peak is visible at approximately 44° and the ferrite peak is visible at approximately 45°. The difference in this sample with the rest is the formation of C-276 Hastelloy in the surface alloyed layer which is identified using XRD. This is observed with the PDF card for the alloy which was identified during analysis at 50°, 74.5°, 90°, and 95°. C-276 Hastelloy is a high Ni superalloy which has good corrosion resistance properties. As this alloy is solid solution strengthened, it can be considered a possibility that the alloy was formed on the highest surface of the alloyed layer on account of higher Ni concentration (*ALLOY C-276 (UNS N10276 / W.Nr. 2.4819)*, n.d.). As we have seen in EDS analysis, the concentration of alloying elements decreases through the section of the surface alloyed layer. This alloy is not identified in any other samples apart from R9.

5.5 Residual Stress Analysis

Residual Stress Analysis was carried out at the Nanoscale Imaging and Analysis Center at the University of Wisconsin - Madison. The machine used was Malvern Panalytical Empyrean X-RAY Diffractometer as Bruker D8 at the University of Wisconsin - Milwaukee is not suitable for residual stress measurements. The measurement of residual stresses in 316L stainless steel alloy is usually performed at 2θ of 146.5°. The plane stress elastic model was used for the sample in which σ_1 and σ_2 exists but $\sigma_3 = 0$ as it is assumed to be perpendicular to the surface (Prevey et al., 1986). Using the $\sin^2$ vs ψ technique, multiple tilts were selected for the samples over which intensity, d and ψ was measured.

Comparing the x-ray diffraction residual stress measurement to the drilling method, diffraction is a non-destructive technique. As the samples tested in this study are surface alloyed, the stresses are to be measured only in the surface alloyed layer. The hole drilling technique can lead to damage to the sample. The surface alloyed layer ranges from 100 μm to 4000 μm and drilling will cut through the alloyed layer and come in contact with the base metal. The measurements from this technique would be inaccurate on account of stresses from base metal released due to drilling. Additionally, the samples cannot be reused for repeated tests after heat treatment cycles. The sample was sectioned into 1 inch X 1 inch X 0.5 inch for the analysis. The sides of the sample were WCB and hence it is possible that the background noise in the data could be on account of diffraction due to the WCB lattice.

The measurements for sample 95 are as follows:

Scan Range	69.4089°	94.90790869°
Scan Type	Continuous	
ϕ	180	
ψ	0	
Z	1.916	
Time per step	207.315	

Table 5.22: Scan properties for sample 95. The targeted composition of slurry for alloying of the surface alloyed layer sample 95 was 2 grams each of Ni and Cr.

We can refer to table 3.15 for the additional properties required for the system operation. The scan range was obtained after conducting a scan over the entire range to identify suitable

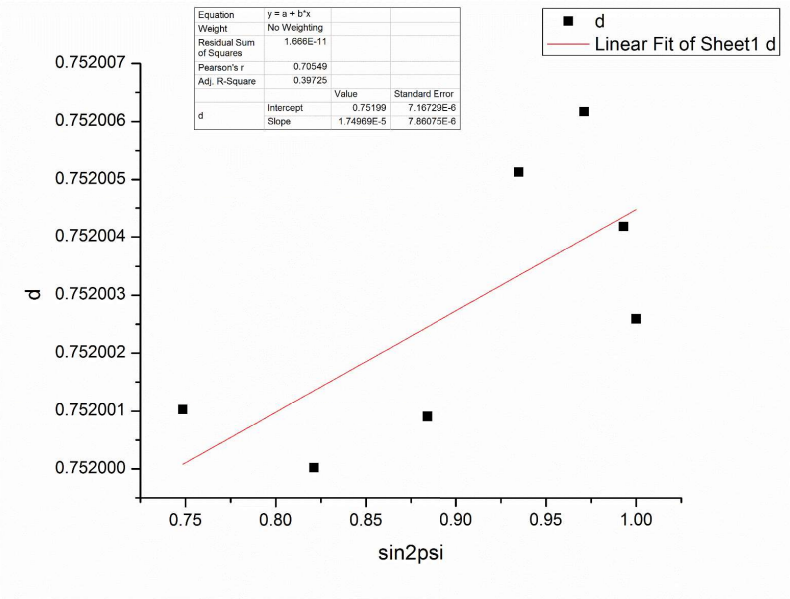

Figure 5.76: d-spacing vs $\sin^2\psi$ plot for sample 95

peaks. After completing the fitting using Gaussian fit and plotting the d-spacing vs $\sin^2\psi$, a linear fit was applied to the plot.

Negative Offset	2θ	Intensity	d	ψ	$\sin^2\psi$
0	90.15037	873.88586	0.75200259	-90.15	0.999993112
5	90.1922	904.00589	0.752004188	-85.19	0.992597244
10	90.23207	954.16498	0.752006169	-80.23	0.971216193
15	90.21164	1015.61324	0.75200513	-75.21	0.934847776
20	90.0891	1014.44248	0.752000909	-70.09	0.884019959
25	89.98697	1104.49971	0.752000019	-64.99	0.821219561
30	89.90527	1167.94028	0.752001028	-59.91	0.748566792

Table 5.23: d vs $\sin^2\psi$ plot points

From the table it is seen that as the offset angle changes, there is an increase in the d-spacing of the sample. The change in d-spacing is corresponds to the change in diffraction angle. A crystal would undergo a change in d-spacing depending on the stresses present (Prevey et al., 1986). The sample above shows a decrease in its d-spacing which is correlated to presence of compressive stress.

The final residual stress measurements are given as follows:

Residual Stress (Pa)	E (Pa)	ν	Slope
3.65E+06	2.77E+11	0.33	1.75E-05

Table 5.24: Residual Stress Measurements for Sample 95

For sample 96, the initial data can be derived from table 3.15 for system operation. The scan range was obtained after conducting a scan over the entire range to identify suitable peaks. After completing the fitting using Gaussian fit and plotting the d-spacing vs $\sin^2\psi$, a linear fit was applied to the plot.

Scan Range	72.0469°	92.08371136°
Scan Type	Continuous	
ϕ	180	
ψ	0	
Z	2.6	
Time per step	236.64	

Table 5.25: Scan properties for surface alloyed layer of sample 96. The targeted composition of slurry for alloying of the surface alloyed layer sample 96 was 2 grams each of Ni and Cr.

Negative Offset	2θ	Intensity	d	ψ	$\sin^2\psi$
0	90.30529	957	0.752010675	-90.30529	0.999971609
5	90.28486	1025	0.752009294	-85.28486	0.993242854
10	90.26444	1119.5	0.752008009	-80.26444	0.971404814
15	90.26444	1195.25	0.752008009	-75.26444	0.935301896
20	90.24401	1274.64147	0.75200682	-70.24401	0.885745784
25	90.22359	1367.74578	0.752005726	-65.22359	0.824373384
30	90.18274	1437.17718	0.752003825	-60.18274	0.752757009

Table 5.26: d vs $\sin^2\psi$ plot points

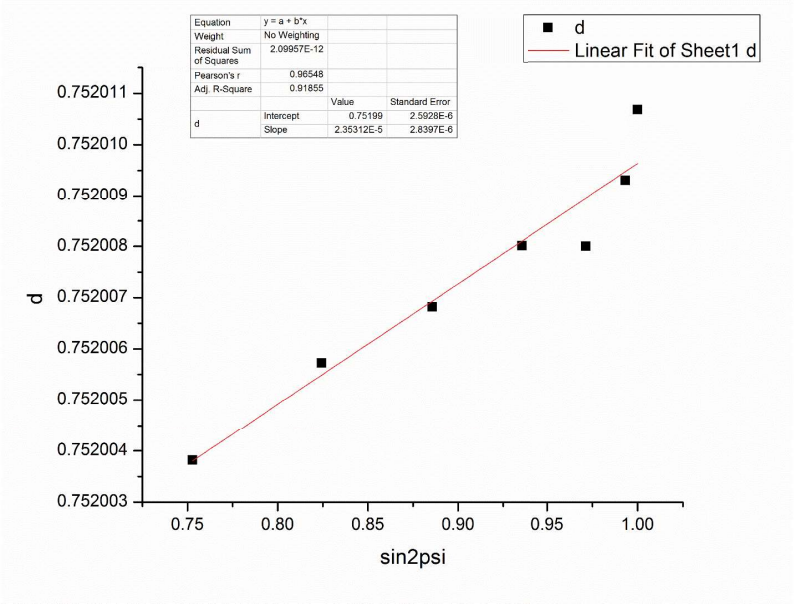

Figure 5.77: d-spacing vs $\sin^2\psi$ plot for sample 96

Residual Stress (Pa)	E (Pa)	ν	Slope
3.75E+06	2.12E+11	0.33	2.35E-05

Table 5.27: Residual Stress Measurements for surface alloyed layer of sample 95

As can be seen from the above graphs, the nature of residual stress is compressive but the magnitude of 3.7 MPa is not high enough to cause any issues during mechanical processing. One of the major reasons for sample or tool damage is residual stress. A compressive residual stress can lead to the sample clamping on to the cutting blade leading to failure of the blade and improper sectioning of the sample. The graph in figure 5.76 does not show linear trend as compared to figure 5.77. One of the primary reasons was the noise in the data due to fluorescence produced due to the use of a Cu anode. This can be reduced further using a Ni filter and can lead to some improvement. Another factor for such trend can be due to effect of surface roughness of the sample.

The data obtained from the measurements was fitted using a Gaussian Fit for identifying the peak. As mentioned above, fluorescence produced on account of Cu anode lead to noise in the data. The peak obtained from the Gaussian fit was chosen as the highest intensity and the corresponding 2θ was obtained. This was then used with ψ by the relation of ψ being subtracted from half of 2θ which is ω. The ψ offsets can be as high as 40° (Fitzpatrick, Fry, Holdway, et al., 2005).

5.6 Hardness Measurements

5.6.1 Nano-indentation

The nanoindentation test was performed on the surface alloyed layer and the base metal to compare the hardness of the as-cast base metal and as-cast surface alloyed layer. There was an increase in the hardness of the surface alloyed layer on account of enrichment of the surface alloyed layer by Ni and Cr. Ni leads to solid solution strengthening while Cr helps as a carbide former. R series samples which were cast at the UWM Foundry Lab were also enriched with Mo, Si, and Mn which lead to solid solution strengthening of the alloy. Additionally, the affinity of formation of carbides is high on account of the carbon alloying from the base metal into the melt with alloying powders.

Sample	Average Hardness of Base Metal (GPa)	Average Hardness of Surface Alloyed Layer (GPa)	Percent Increase
R1	12.02	22.01	45.38
R2	6.83	7.52	9.17
R3	7.69	8.22	6.44

Table 5.28: Average hardness comparison of base metal and surface alloyed layer after nanoindentation tests for UWM R-series samples.

A similar trend can be observed in the samples made at Maynard Steel that underwent normalizing and tempering heat treatment. The normalized grain structure lead to consistent readings of hardness in the base metal but there is increase in hardness in the surface alloyed layer on account of increase in alloying elements in the surface alloyed layer. The highest increase in hardness is almost twice the value of the base metal. In case of nanoindentation, the indents were made in an array of 4X4 readings per average value on the alloyed layer and base metal to understand the variation in hardness on account of microstructure. The Maynard Steel samples contained only Ni and Cr as alloying elements targeted to reach a composition similar to 316L stainless steel in surface alloyed layer. An attempt was made to indent the interface but this was not possible due to difficulty in selecting the area as indent would come in contact with surface alloyed layer or the base metal thus nullifying the results. The examples of the 4X4

indents array on the surface alloyed layer and the base metal are shown below:

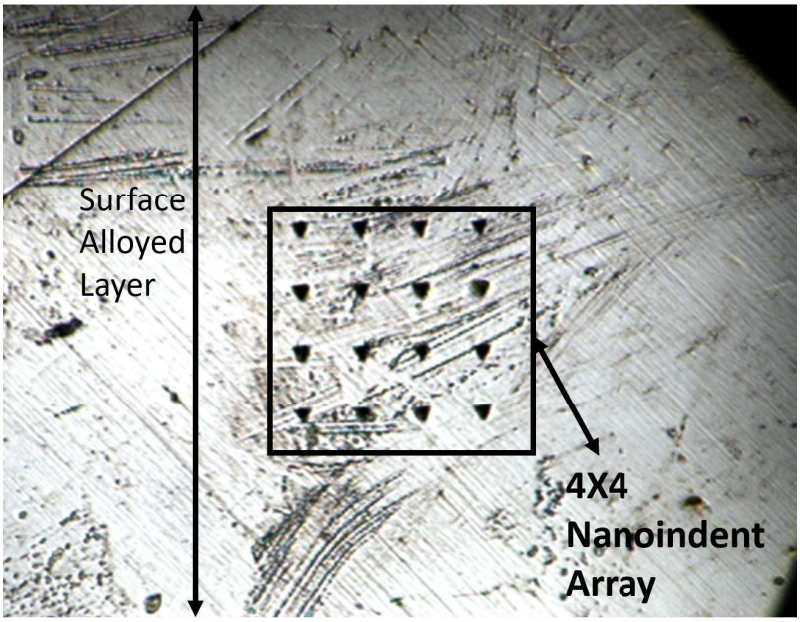

Figure 5.78: Indents in the surface alloyed layer of sample R2.

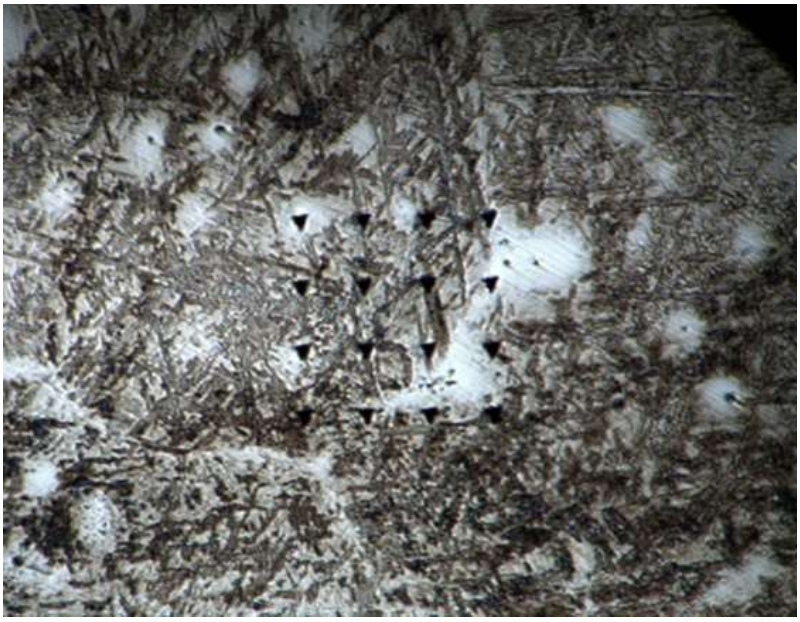

Figure 5.79: Indents in the base metal of sample R2.

Sample	Average Hardness of Base Metal (GPa)	Average Hardness of Surface Alloyed Layer (GPa)	Percent increase
112	4.28	6.78	36.8
110	3.9	5.34	26.9
111	4.2	5.5	23.6
74	4.2	5.1	17.6
96	4.5	8.78	48.7
95	3.7	6.9	46.3
97	4.9	9.89	50.45

Table 5.29: Average hardness comparison of base metal and surface alloyed layer after nanoindentation tests for Maynard Steel samples.

5.6.2 Vicker's Microhardness

Vicker's microhardness confirms the results obtained using nanoindentation in terms of an increase in the hardness in the surface alloyed layer compared to base metal. There is an average increase of 28.1% in the hardness of the surface alloyed layer with a maximum increase of 54%, a minimum increase of 7.1%, and a standard deviation of 13.48. Each average value was measured after 4 indents on the surface alloyed layer as well as the base metal. The indents on the surface alloyed layer were spaced through the length and not formed in an array to get an overall measurement. An example of an indent on the surface alloyed layer and the base metal are shown below:

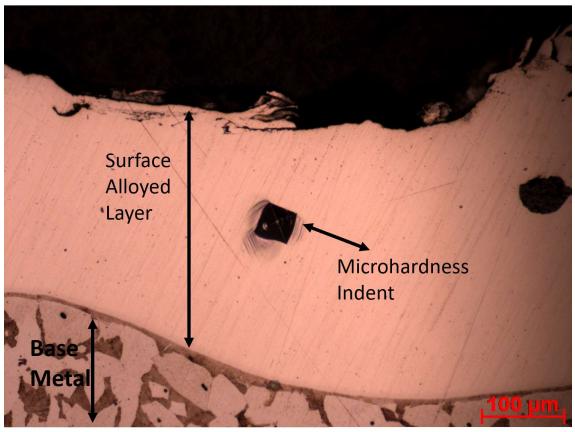

Figure 5.80: Vicker's Microhardness test indent on the surface alloyed layer.

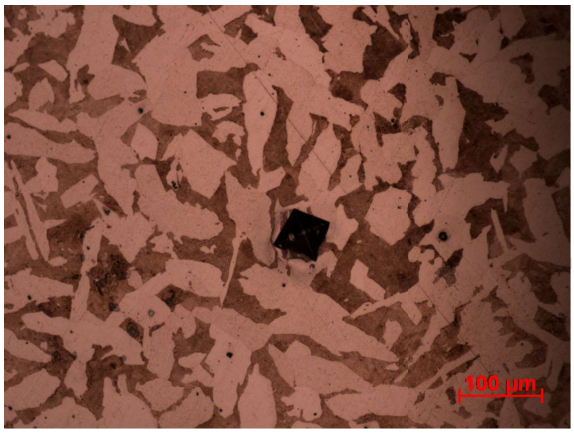

Figure 5.81: Vicker's Microhardness test indent on the base metal.

Sample	Average Vicker's Microhardness of Base Metal (HV)	Average Vicker's Microhardness of Surface Alloyed Layer (HV)	Percent Increase
301	195.5	304	54
303	244.3	320.2	31.1
304	266.9	346.2	29.7
305	298.6	322.3	7.9
306	259.6	351.6	35.4
307	249.6	290.4	16.3
308	261.95	342.4	30.7
309	280.8	346.2	23.3
310	260.8	342.8	31.4
311	254.6	356.1	39.9
312	198	299.4	51.1
313	305.5	367	20.2
314	267.4	337.4	26.2
315	282.8	352.7	24.8
316	264.8	343.5	29.7
317	307.7	329.8	7.2
318	223.1	238.9	7.1
319	210.2	294.5	40.1

Table 5.30: Average microhardness comparison of the base metal and surface alloyed layer measured using Vicker's Microhardness Test of 316L stainless steel alloying powder.

Sample	Average Vicker's Microhardness of Base Metal (HV)	Average Vicker's Microhardness of Surface Alloyed Layer (HV)	Percent Increase
R1	292.8	510.2	42.61
R2	316.1	502.8	37.13
R3	382.1	433.9	11.93
R4	418	540.1	22.6
R5	301.4	553.8	43.53
R6	301.2	589.4	48.89
R7	350.7	498.9	29.7
R9	312.7	514.6	39.23
R10	285.4	503.7	43.33

Table 5.31: Average microhardness comparison of the base metal and surface alloyed layer measured using Vicker's Microhardness Test for UWM R series samples.

Chapter 6

Conclusion

Maynard Steel Trial 1 - Ni and Cr powders

1. The consistency of the surface alloyed layer was impaired due to the alloying powders not adhering to the alcohol based binder.

2. There was an increase in the hardness of the surface alloyed layer as compared to the base metal by a maximum of 58% which was confirmed by nanoindentation and Vicker's Microhardness tests.

3. The primary phase observed during this set of trials was austenite which was confirmed using XRD analysis.

Maynard Steel Trial 2 - 316L Stainless Steel powder

1. The surface alloying process was successful but the weight percentage of Ni and Cr present in 316L stainless steel was lower than the required 18 weight% Cr and 8 weight% Ni.

2. The hardness of the surface alloyed layer increased by a maximum of 54% as compared to the base metal.

3. The primary phase observed in these trials was ferrite which was confirmed using XRD analysis.

Badger Alloys Trials - Ni, Cr and 316L Stainless Steel powder

1. The pour at Badger Alloys was an industrial trial to test the viability of the process for casting a surface alloyed water industry component.

2. Ni and Cr were the alloying elements selected for the process but the powders were 95% pure and not lab grade 99.9999% pure.

3. The surface alloyed layer had higher quantities of Cr and Ni weight percentages up to 20 weight % and 10 weight % respectively as compared to the previous heats of Maynard Steel.

4. The concentration of alloying powders (grams) per square inch was 1 gram/in^2.

5. The hardness of the surface alloyed layer increased as compared to the base metal by 50%.

6. The primary phases identified during these trials were austentie and ferrite in varying volume percentages.

UWM Foundry Lab Trials - Ni, Cr, Fe-Mn and Fe-Si

1. The measurement of the alloying elements required to surface alloyed a selected depth of WCB steel was performed using only a selected mass of WCB steel that was to be alloyed which allowed for the control of depth of the surface alloyed layer.

2. From the EDS data, it can be observed that using the water based binder gave better results in terms of controlling the weight percentages of alloying elements in the surface alloyed layer as well as controlling the depth of the surface alloyed layer.

3. The use of both water based binder and alcohol based binder led to the formation of a surface alloyed layer thus confirming that both can be feasible in an industrial environment.

4. The highest depth of surface alloyed observed using stereo-spectroscopy was 4000 μm.

5. The samples made during these trials had higher hardness of surface alloyed layer by 45% at its maximum as compared with base metal.

6. The primary phases observed during this set of trials were austenite and ferrite.

Overall Conclusions

1. As the trials were conducted with two different purity levels of alloying powders, viz. 99.9999% and 95%, the successful forming of the surface alloyed layer indicates that the alloying powders in the above range of purity can be used for alloying WCB steel.

2. Using a smaller particle size for the alloying powders leads to a surface alloyed layer without defects, smooth interface layer and weight percentages in the range of targeted comositions. A higher particle size leads to an uneven surface alloyed layer.

3. Residual stress analysis using X-Ray Diffraction concluded that the maximum residual stress in the surface alloyed layer is 3.75 MPa while the average residual stress is 3.65 MPa.

4. The highest enrichment levels observed in the surface alloyed layer through all of the trials are as follows: Ni - 17.87 weight%, Cr - 26.67 weight %, Mn - 10.46 weight %, and Si - 3 weight %.

5. Both alcohol based and water based binders can be used for preparing the slurry which is used to apply the alloying powders to the mold cavity.

Bibliography

Alloy c-276 (uns n10276 / w.nr. 2.4819). (n.d.). Retrieved from `https://www.corrosionmaterials.com/alloys/alloy-c276/`

Amirsadeghi, A., & Sohi, M. H. (2008). Comparison of the influence of molybdenum and chromium tig surface alloying on the microstructure, hardness and wear resistance of adi. *Journal of materials processing technology*, *201*(1-3), 673–677.

ASTM, S. (2008). Standard test method for determining residual stresses by the hole-drilling strain-gage method. In *Astm, e* (pp. 837–95).

Badji, R., Bouabdallah, M., Bacroix, B., Kahloun, C., Belkessa, B., & Maza, H. (2008). Phase transformation and mechanical behavior in annealed 2205 duplex stainless steel welds. *Materials Characterization*, *59*(4), 447–453.

Bali, S., Kain, V., & Raja, V. (2009). Effect of low-temperature sensitization on intergranular stress corrosion cracking behavior of austenitic stainless steels in simulated boiling water reactor environment. *Corrosion*, *65*(11), 726–740.

Chen, X., Li, J., Cheng, X., Wang, H., & Huang, Z. (2018). Effect of heat treatment on microstructure, mechanical and corrosion properties of austenitic stainless steel 316l using arc additive manufacturing. *Materials Science and Engineering: A*, *715*, 307–314.

Cheng, X., Feng, Z., Li, C., Dong, C., & Li, X. (2011). Investigation of oxide film formation on 316l stainless steel in high-temperature aqueous environments. *Electrochimica Acta*, *56*(17), 5860–5865.

Chun, E. J., Baba, H., Terashima, K., Nishimoto, K., & Saida, K. (2013). Prediction of σ phase precipitation in type 316fr stainless steel weld metal. *QUARTERLY JOURNAL OF THE JAPAN WELDING SOCIETY*, *31*(4), 168s–172s.

Cullity, B. D., & Stock, S. R. (2001). *Elements of x-ray diffraction* (Vol. 3). Prentice hall New Jersey.

Davis, J. R., et al. (1994). *Stainless steels*. ASM international.

De Keyzer, J., Cacciamani, G., Dupin, N., & Wollants, P. (2009). Thermodynamic modeling and optimization of the fe–ni–ti system. *Calphad*, *33*(1), 109–123.

Elhamid, M. H. A., & Dadheech, G. V. (2014, September 16). *Surface alloying of stainless steel*. Google Patents. (US Patent 8,834,734)

Fernández-Domene, R. M., Blasco-Tamarit, E., García-García, D. M., & García-Antón, J. (2014). Effect of alloying elements on the electronic properties of thin passive films formed on carbon steel, ferritic and austenitic stainless steels in a highly concentrated libr solution. *Thin Solid Films*, *558*, 252–258.

Fitzpatrick, M., Fry, T., Holdway, P., et al. (2005). Npl good practice guide no. 52: determination of residual stresses by x-ray diffraction—issue 2. *NPL, Great Britain*.

Flemings, M. C. (1974). Solidification processing. *Metallurgical transactions*, *5*(10), 2121–2134.

Fuzuli, R., & Agil, B. (2018). Surface alloying of the casting in the casting mold. *Engineering and Applied Sciences*, *3*(3), 64.

Gebril, M. A. M. (n.d.). Heat treatment of duplex stainless steel 2205 by inserting nano nd2feb14 in hip manifolds under the scope of category theory.

Hammood, A. S., Noor, A. F., & Alkhafagy, M. T. (2017). Effect of heat treatment on corrosion behavior of duplex stainless steel in orthodontic applications. *Materials Research Express*, *4*(12), 126506.

Jinlong, L., Tongxiang, L., & Chen, W. (2016). Surface enriched molybdenum enhancing the corrosion resistance of 316l stainless steel. *Materials Letters*, *171*, 38–41.

Kashiwar, A., Vennela, N. P., Kamath, S., & Khatirkar, R. (2012). Effect of solution annealing temperature on precipitation in 2205 duplex stainless steel. *Materials Characterization*, *74*, 55–63.

Kim, C. K., Kim, Y. C., Park, J. I., Lee, S., Kim, N. J., & Yang, J. S. (2005). Effects of alloying elements on microstructure, hardness, and fracture toughness of centrifugally cast high-speed steel rolls. *Metallurgical and Materials Transactions A*, *36*(1), 87–97.

Kolařík, K., Pala, Z., Ganev, N., & Fojtik, F. (2014). Combining xrd with hole-drilling method in residual stress gradient analysis of laser hardened c45 steel. In *Advanced materials research* (Vol. 996, pp. 277–282).

Kopyciński, D., & Guzik, E. (2007). The kinetics of zinc coating growth on hyper-sandelin steels and ductile cast iron. *Archives of Foundry Engineering*, *7*(4), 105–110.

Korsunsky, A. M., Wells, K. E., & Withers, P. J. (1998). Mapping two-dimensional state of strain using synchroton x-ray diffraction. *Scripta Materialia*, *39*(12), 1705–1712.

Krakhmalev, P., Yadroitsava, I., Fredriksson, G., & Yadroitsev, I. (2015). In situ heat treatment in selective laser melted martensitic aisi 420 stainless steels. *Materials & Design*, *87*, 380–385.

Krauss, G. (2015). *Steels: processing, structure, and performance.* Asm International.

LaFontaine, W., Paszkiet, C., Korhonen, M., & Li, C.-Y. (1991). Residual stress measurements of thin aluminum metallizations by continuous indentation and x-ray stress measurement techniques. *Journal of materials research*, *6*(10), 2084–2090.

Luo, H., Li, X., Dong, C., & Xiao, K. (2017). Effect of solution treatment on pitting behavior of 2205 duplex stainless steel. *Arabian Journal of Chemistry*, *10*, S90–S94.

Luyckx, S., & Love, A. (2004). The relationship between the abrasion resistance and the hardness of wc-co alloys. *Journal of the South African Institute of Mining and Metallurgy*, *104*(10), 579–582.

Macdonald, D. F. (1969, June 17). *Process of coating metal castings.* Google Patents. (US Patent 3,450,189)

Martin, M., Weber, S., Theisen, W., Michler, T., & Naumann, J. (2011). Effect of alloying elements on hydrogen environment embrittlement of aisi type 304 austenitic stainless steel. *International Journal of Hydrogen Energy*, *36*(24), 15888–15898.

Martinez, S., Sathish, S., Blodgett, M., & Shepard, M. (2003). Residual stress distribution on surface-treated ti-6al-4v by x-ray diffraction. *Experimental Mechanics*, *43*(2), 141–147.

Mazumder, J., & Singh, J. (1986). Laser surface alloying and cladding for corrosion and wear. *High Temperature Materials and Processes*, *7*(2-3), 101–106.

Metzger, D., New, K. J., & Dantzig, J. (2001). A sand surface element for efficient modeling of residual stress in castings. *Applied Mathematical Modelling*, *25*(10), 825–842.

Montero Sistiaga, M., Nardone, S., Hautfenne, C., & Van Humbeeck, J. (2016). Effect of heat treatment of 316l stainless steel produced by selective laser melting (slm). In *Proceedings of the 27th annual international solid freeform fabrication symposium-an additive manufacturing conference* (pp. 558–565).

Nicard, C., Allély, C., & Volovitch, P. (2019). Effect of zn and mg alloying on microstructure and anticorrosion mechanisms of al-si based coatings for high strength steel. *Corrosion Science*, *146*, 192–201.

Ohkubo, N., Miyakusu, K., Uematsu, Y., & Kimura, H. (1994). Effect of alloying elements on the mechanical properties of the stable austenitic stainless steel. *ISIJ international*, *34*(9), 764–772.

Okamoto, H., Kacprzak, L., & Subramanian, P. (1996). *Binary alloy phase diagrams*. ASM international Materials Park, OH.

Prevey, P. S. (1976). A method of determining the elastic properties of alloys in selected crystallographic directions for x-ray diffraction residual stress measurement. *Advances in X-ray Analysis*, *20*, 345–354.

Prevey, P. S., et al. (1986). X-ray diffraction residual stress techniques. *ASM International, ASM Handbook., 10*, 380–392.

Radziszewska, A., & Kusiński, J. (2008). Laser alloying of the plain carbon steel surface layer. *Archives of foundry Engineering*, *8*(2), 175–179.

Rendler, N., & Vigness, I. (1966). Hole-drilling strain-gage method of measuring residual stresses. *Experimental mechanics*, *6*(12), 577–586.

Revankar, G. S. (1999, March 9). *Method for hardfacing a metal surface.* Google Patents. (US Patent 5,879,743)

Shamanian, M., Abarghouie, S. M., & Pour, S. M. (2010). Effects of surface alloying on microstructure and wear behavior of ductile iron. *Materials & design*, *31*(6), 2760–2766.

Sieurin, H., & Sandström, R. (2007). Sigma phase precipitation in duplex stainless steel 2205. *Materials Science and Engineering: A*, *444*(1-2), 271–276.

Sohi, M. H., Ebrahimi, M., Ghasemi, H., & Shahripour, A. (2012). Microstructural study of surface melted and chromium surface alloyed ductile iron. *Applied Surface Science*, *258*(19), 7348–7353.

Sriram, R., & Tromans, D. (1989). Pitting corrosion of duplex stainless steels. *Corrosion*, *45*(10), 804–810.

Suzuki, N., Bando, S., Ikeda, S., Tsuda, T., Yakawa, A., & Yoshikawa, Y. (1994, July 19). *Corrosion-resistant surface-coated steel sheet.* Google Patents. (US Patent 5,330,850)

Szajnar, J., Dulska, A., Wróbel, T., & Baron, C. (2015). Description of alloy layer formation on a cast steel substrate. *Archives of Metallurgy and Materials*, *60*(3), 2367–2372.

Szajnar, J., Wróbel, P., & Wróbel, T. (2007). Enrichment of casting surface in founding process. *Archives of Foundry Engineering*, *7*(3), 153–156.

Takano, H., Tsutsui, H., Kifune, M., & Miyoshi, K. (1971, November 2). *Method of measuring stress with x-rays.* Google Patents. (US Patent 3,617,705)

Tan, H., Jiang, Y., Deng, B., Sun, T., Xu, J., & Li, J. (2009). Effect of annealing temperature on the pitting corrosion resistance of super duplex stainless steel uns s32750. *Materials Characterization*, *60*(9), 1049–1054.

Tomlinson, W., & Bransden, A. (1990). Laser surface alloying grey iron with cr, ni, co, and co–cr coatings. *Surface Engineering*, *6*(4), 281–286.

Townsend, H. (2001). Effects of alloying elements on the corrosion of steel in industrial atmospheres. *Corrosion*, *57*(6), 497–501.

Uchida, H., Kiguchi, T., Saiki, A., Wakiya, N., Ishizawa, N., Shinozaki, K., & Mizutani, N. (1999). Measurement technique for the evaluation of residual stress in epitaxial thin film by asymmetric x-ray diffraction. *Journal of the Ceramic Society of Japan*, *107*(1247), 606–610.

Yoshiwara, S., & Kawanami, T. (1988, June 14). *Method for surface-alloying metal with a high-density energy beam and an alloy metal.* Google Patents. (US Patent 4,750,947)

Zhang, S., Wu, C., Zhang, C., Guan, M., & Tan, J. (2016). Laser surface alloying of fecocralni high-entropy alloy on 304 stainless steel to enhance corrosion and cavitation erosion resistance. *Optics & Laser Technology*, *84*, 23–31.

Zhong, M., Liu, W., & Zhang, H. (2006). Corrosion and wear resistance characteristics of nicr coating by laser alloying with powder feeding on grey iron liner. *Wear*, *260*(11-12), 1349–1355.

Chapter 7

Appendix

7.1 Appendix A - Maynard Steel - Trial 1

Sample	Ni (grams)	Cr (grams)
95	1.64	1.64
97	2	2
96	1.9	2
111	15	15
112	15	15

Table 7.1: Composition of the alloying powders for the Maynard Steel - Trial 1 samples. Purity of alloying powders was 99.9999%. The particle size of Ni was -50+100 mesh and Cr was -60 mesh. Area coated = 20.27 cm^2. REFCOTEC REFCOHOL 1010 was used as binder.

Sample	Average Hardness of Base Metal (GPa)	Average Hardness of Surface Alloyed Layer (GPa)	Percent Increase
112	4.28	6.78	36.8
110	3.9	5.34	26.9
111	4.2	5.5	23.6
74	4.2	5.1	17.6
96	4.5	8.78	48.7
95	3.7	6.9	46.3
97	4.9	9.89	50.45

Table 7.2: Average hardness comparison of base metal and surface alloyed layer after nanoindentation tests for Maynard Steel samples.

Residual Stress (Pa)	E (Pa)	ν	Slope
3.65E+06	2.77E+11	0.33	1.75E-05

Table 7.3: Residual Stress Measurements for Sample 95

Residual Stress (Pa)	E (Pa)	ν	Slope
3.75E+06	2.12E+11	0.33	2.35E-05

Table 7.4: Residual Stress Measurements for surface alloyed layer of sample 95

Element	Weight%
Ni	6.216
Cr	8.77
Fe	Balance

Table 7.5: Average elemental composition of the surface alloyed layer obtained using EDS considering the sample size of all samples made in the Maynard Steel trials.

7.2 Appendix B - Maynard Steel - Trial 2

Sample	Particle Size (μm)	Weight (grams)
305	1000	4
309	800	2
317	600	2
319	600	2
321	600	4
322	600	4

Table 7.6: List of castings made at Maynard Steel using 316L Stainless Steel powder as alloying powder. The purity of the alloying powder was 95%. Area coated = 20.27 cm^2. REFCOTEC REFCOHOL 1010 was used as binder.

Sample	Average Vicker's Microhardness of Base Metal (HV)	Average Vicker's Microhardness of Surface Alloyed Layer (HV)	Percent Increase
301	195.5	304	54
303	244.3	320.2	31.1
304	266.9	346.2	29.7
305	298.6	322.3	7.9
306	259.6	351.6	35.4
307	249.6	290.4	16.3
308	261.95	342.4	30.7
309	280.8	346.2	23.3
310	260.8	342.8	31.4
311	254.6	356.1	39.9
312	198	299.4	51.1
313	305.5	367	20.2
314	267.4	337.4	26.2
315	282.8	352.7	24.8
316	264.8	343.5	29.7
317	307.7	329.8	7.2
318	223.1	238.9	7.1
319	210.2	294.5	40.1

Table 7.7: Average microhardness comparison of the base metal and surface alloyed layer measured using Vicker's Microhardness Test of 316L stainless steel alloying powder.

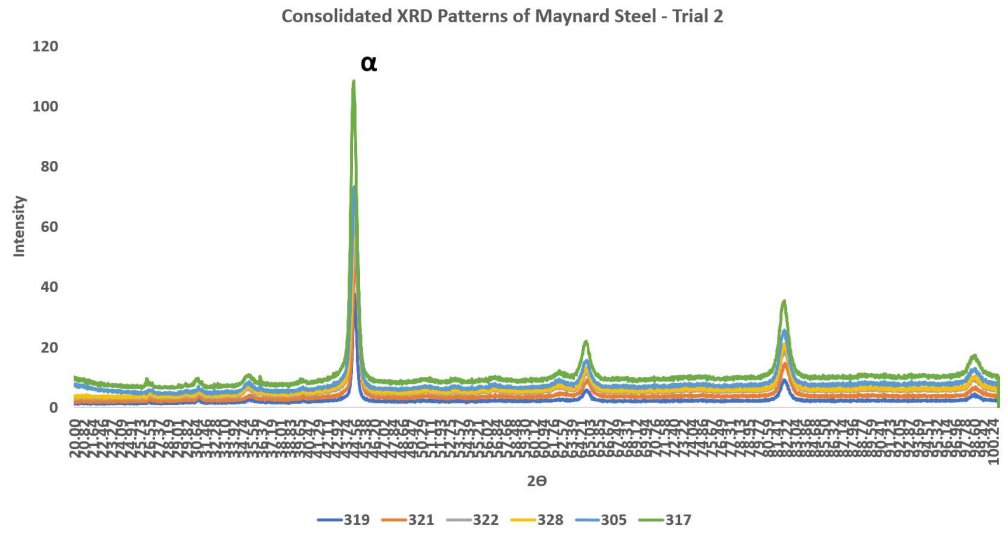

Figure 7.1: Consolidated XRD pattern of all samples analyzed during the study and cast at Maynard Steel using the 316L stainless steel powder as alloying compositions as specified above.

Element	Weight%
Ni	5.31
Cr	4.81
Fe	Balance

Table 7.8: Average elemental composition of the surface alloyed layer obtained using EDS considering the sample size of all samples made in the Maynard Steel trial 2 using 316L stainless steel powder as the alloying powder. The particle size of the powders was 1000 μ, 800 μ and 600 μ.

7.3 Appendix C - Badger Alloys Trials

Alloying Elements	Particle Size μ	Ni (grams)	Cr (grams)	Total Wight (grams)
Ni and Cr	40	0.8	1.84	2.64
Ni and Cr	80	0.51	1.19	1.7
316L SS	200			2.192

Table 7.9: Composition of the alloying powders for the Badger Alloys Trials samples cast at Badger Alloys using Ni, Cr and 316L powders as alloying elements. The purity level of alloying powders was 95%. Area coated = 201.06 cm^2. REFCOTEC REFCOHOL 1010 was used as binder.

Element	Weight%
Ni	6.78
Cr	13.71
Fe	Balance

Table 7.10: Average elemental composition of the surface alloyed layer obtained using EDS considering the sample size of all samples made in the Badger Alloys trials using Ni, Cr, and 316L stainless steel powder as the alloying powders.

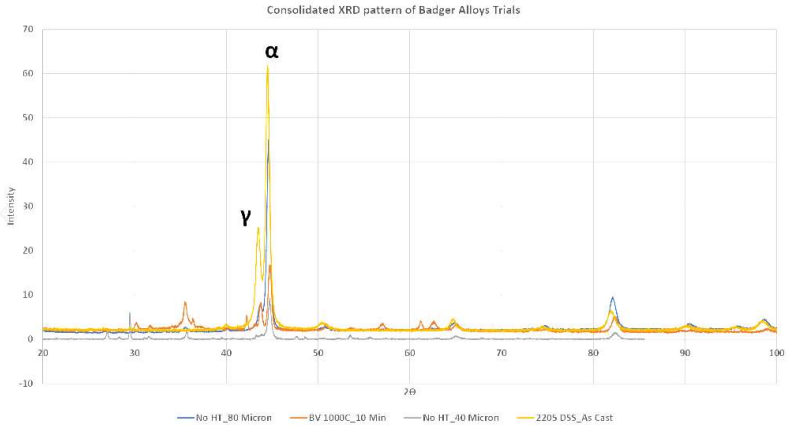

Figure 7.2: Consolidated XRD pattern of all samples analyzed during the study and cast at Badger Alloys using the compositions specified above.

7.4 Appendix D - UWM R-Series Samples

Sample	Ni (grams)	Cr (grams)	Fe-Mn (grams)	Fe-Si (grams)
R1	0.76	1.38		
R2	1.45	2.62		
R3	2.05	3.71		
R4	2.97	5.37		
R5	0.62	1.72	0.38	0.02
R6	0.82	2.27	0.51	0.03
R7	5.85	16.26	3.64	0.23
R8	2.92	8.13	1.82	0.11
R9	2.92	8.13	1.82	0.11
R10	1.95	5.42	1.21	0.07
R12	3.9	10.84	2.42	0.156

Table 7.11: Composition of the alloying powders for the R series samples cast at the UWM Foundry Lab with WCB as the base metal. The purity of alloying powders was 95%. The particle size of Ni was 40 micron, Cr was 40 micron, Fe-Mn was 44 micron, and Fe-Si was 149 micron. Area coated (R1-R5) = 10.75 cm^2. Area coated (R6-R7) = 25.5 cm^2. Area coated (R8-R12) = 75 cm^2. REFCOTEC REFCOBAR Gel was used as binder.

Sample	Average Hardness of Base Metal (GPa)	Average Hardness of Surface Alloyed Layer (GPa)	Percent Increase
R1	12.02	22.01	45.38
R2	6.83	7.52	9.17
R3	7.69	8.22	6.44

Table 7.12: Average hardness comparison of base metal and surface alloyed layer after nanoindentation tests for UWM R-series samples.

Sample	Average Vicker's Microhardness of Base Metal (HV)	Average Vicker's Microhardness of Surface Alloyed Layer (HV)	Percent Increase
R1	292.8	510.2	42.61
R2	316.1	502.8	37.13
R3	382.1	433.9	11.93
R4	418	540.1	22.6
R5	301.4	553.8	43.53
R6	301.2	589.4	48.89
R7	350.7	498.9	29.7
R9	312.7	514.6	39.23
R10	285.4	503.7	43.33

Table 7.13: Average microhardness comparison of the base metal and surface alloyed layer measured using Vicker's Microhardness Test for UWM R series samples.

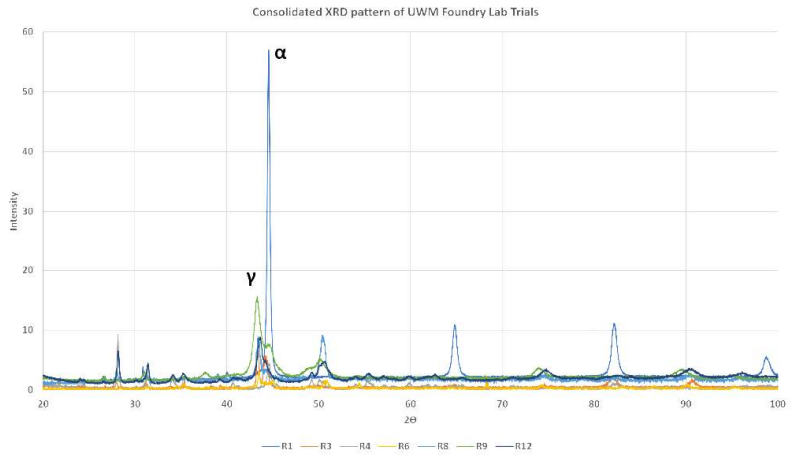

Figure 7.3: Consolidated XRD pattern of all samples analyzed during the study and cast at UWM Foundry Lab using the compositions specified above.